ROMA TRE
UNIVERSITA' DEGLI STUDI

DEPARTMENT OF MECHANICAL AND INDUSTRIAL ENGINEERING

PHD IN MECHANICAL AND INDUSTRIAL ENGINEERING
XXVI CYCLE

Phd Candidate:

ARTAN NDOKAJ

Thesis Title:

POWER QUALITY IN POWER DRIVE SYSTEMS

Supervisor:

PROF. AUGUSTO DI NAPOLI

Coordinator:

PROF. EDOARDO BEMPORAD

INDEX

INTRODUCTION 10

1. POWER QUALITY 15

1.1 Power Quality definition 15
1.2 Power quality progression 16
1.3 Power Quality terminology 18
1.4 Power Quality Issues 24
1.5 Role of Power Electronics in Improving Quality of AC Grid Power 27
1.5.1 Flexible AC Transmission Systems (FACTS) Operating Principle 28
1.5.2 Shunt-Connected Controllers 29
1.5.3 Series-Connected Controllers 30

2. ULTRACAPACITORS STORAGE SYSTEM 33

2.1 Introduction 34
2.1.1 Ultracapacitors construction 35
2.1.2 Typical Applications 36
2.2 The Gantry Crane System 39
2.3 The Ultracapacitors Storage System 39
2.4 Gantry Crane System 41
2.5 Electrical system layout 47
2.6 Ultracapacitors model 50
2.7 Ultracapacitors Sizing 52
2.7 System modeling 55
2.8 Power Flow regulation strategy 59
2.8.1 K parameter definition 59
2.8.2 H and H1 definition 60
2.8.3 H_1 and K regulation 60
2.9 Gantry crane model wilth UC storage 62
2.10 Experimental validation of the model 64
2.12.1 Light load cycle 68
2.12.2 Heavy load cycle 72
2.13 Simulation Results 76

2.14 Economic Evaluation of the simulation results ... 92
2.14.1 Cost of Investment ... 93
2.14.2 Cost of the electric energy ... 95
2.14.3 Payback period ... 96
3. ACTIVE FRONT-END CONVERTER ... 99
3.1 Introduction ... 99
3.2 Active Front End operating principle ... 101
3.3 Key Features of Active Front-End Inverters ... 106
3.3.1 Comparison between Traditional Drives and Active Front-End Drives ... 108
3.4 System configuration ... 111
3.5 Compensation Characteristics of an Active Drive ... 112
3.6 Steady-State Control ... 113
3.7 The *d-q* theory ... 116
3.8 Deriving the d-q model ... 122
3.9 Selecting the Rotating Coordinate System ... 125
3.10 Power Definitions in d-q Coordinate System ... 128
3.11 Dynamic Equations for an Active Front-End Converter ... 131
3.12 Control of the Active Drive ... 133
3.12.1 Feed-Back Control ... 134
3.12.2 Estimating Angular Frequency of Source Voltages ... 136
3.12.3 Input-Output Linearization Control ... 137
3.12.4 Feed-Forward Compensation ... 139
3.12.5 Complete Control Scheme for Active Front-End Converter ... 141
3.13 Simulation Model ... 143
3.14 Simulation Results ... 145
3.14.1 Normal Condition mode ... 145
3.14.2 AFE in presence of voltge sags ... 149
3.14.2.1 Single phase voltage sag ... 151
3.14.2.2 Double phase voltage Sags ... 154
3.14.3 AFE in presence of voltge notches ... 156
3.14.3.1 Single phase voltage notches ... 158
3.14.3.2 Double phase voltage notches ... 162
4. APPENDIX I - DIRECT TORQUE CONTROL TECHNIQUE. 166

5. APPENDIX II – EMC MEASUREMENTS 176
5.1 Introduction 176
5.2 Apparatus Conformity Assestement 177
5.3 EMC Testing 179
5.4 Test Set-Up 180
5.5 Experimental results 183
CONCLUSIONS 189
REFERENCES 191
PUBLICATIONS 196

List of Figures

Fig. 1.1: Crest factor for sinusoidal waves 19
Fig. 1.2: Distorted waveform 20
Fig. 1.3: Power Quality issues 25
Fig. 2.1: Ultracapacitor charge separation 36
Fig. 2.2: Bridge crane operation 39
Fig. 2.3: Absorbed/Delivered power of the lifting motor 40
Fig. 2.4: Circuit diagram of the bridge crane drive with recovery capabilities 40
Fig. 2.5: Geometry of the system 42
Fig. 2.6: Load speed, trajectory and Acceleration during the lifting/descending process. 43
Fig. 2.7: Lifting/descending motor torque, energy, power during the lifting/descending process 43
Fig. 2.8: Load speed, trajectory and Acceleration during the rotation process. 44
Fig. 2.9: Rotation motor torque, energy, power during the rotation process. 45
Fig. 2.10: Load speed, trajectory and Acceleration during the translation process. 45
Fig. 2.11: Translation motor torque, energy, power during the translation process. 46
Fig. 2.12: Load speed, trajectory and Acceleration during the scroll process 46
Fig. 2.13: Scroll motor torque, energy, power during the scroll process. 47
Fig. 2.14: Blocks scheme of the electrical drive 48
Fig. 2.15: Bidirectional dc-dc converter for UCs management 48
Fig. 2.16: Simplified model of the ultracapacitors 51
Fig. 2.17: Wiring diagram of the ultracapacitors 54
Fig. 2.18: Load lifting – UCs discharge 56
Fig. 2.19: Load descending – UCs recharge 56
Fig. 2.20: Implemented simulation model 57
Fig. 2.21: Drive simulation model 58
Fig. 2.22: Regulation strategy flow chart 62
Fig. 2.23: Drive diagram 63
Fig. 2.24: Lifting prototype of Ultracapacitors Storage system 65
Fig. 2.25: Motor speed and torque in function of time 67
Fig. 2.26: Motor drive power in function of time 68
Fig. 2.27: Light load cycle measured voltages vs time 68
Fig. 2.28: Light load cycle measured currents vs time 69
Fig. 2.29: Light load cycle measured motor power demand vs time 69
Fig. 2.30: Light load cycle SIMULATED motor power demand vs time 70
Fig. 2.31: Light load cycle SIMULATED speed vs time 70
Fig. 2.32: Light load cycle SIMULATED torque vs time 70
Fig. 2.33: Light load cycle SIMULATED voltages vs time 71
Fig. 2.34: Light load cycle SIMULATED currents vs time 71
Fig. 2.35: Light load cycle – comparison between simulated and measured I_{link} 72
Fig. 2.36: Heavy load cycle measured voltages vs time 72
Fig. 2.37: Heavy load cycle measured currents vs time 73
Fig. 2.38: Heavy load cycle measured motor power demand vs time 73

Fig. 2.39: Heavy load cycle SIMULATED motor power demand vs time 74
Fig. 2.40: Heavy load cycle SIMULATED torque vs time 74
Fig. 2.41: Heavy load cycle SIMULATED voltages vs time 75
Fig. 2.42: Heavy load cycle SIMULATED currents vs time 75
Fig. 2.43: Heavy load cycle – comparison between simulated and measured I_{link} 75
Fig. 2.44: DC-link Voltage vs time for K = 0, C = 63F, H = 0; H_1 = 1. 77
Fig. 2.45: Traction motor simulated power demanded vs time for K = 0, C = 63F, H = 0; H_1 = 1. 77
Fig. 2.46: Grid current Igid vs time for K = 0, C = 63F, H = 0; H_1 = 1 78
Fig. 2.47: Traction motor shaft speed vs time for K = 0, C = 63F, H = 0; H_1 = 1 78
Fig. 2.48: Motor Reference and current Torque vs time for K = 0, C = 63F, H=0; H_1=1. 79
Fig. 2.49: Energy flow for K = 0, C = 63F, H=0; H_1=1 79
Fig. 2.50: Simulated voltages for K=0, C=63F, H=0.6, H_1=1.3 80
Fig. 2.51: Simulated currents for K=0, C=63F, H=0.6, H_1=1.3. 80
Fig. 2.52: Simulated voltages for K=0.5, C=63F, H=0.6, H_1=1.3 81
Fig. 2.53: Simulated currents for K=0.5, C=63F, H=0.6, H_1=1.3. 81
Fig. 2.54: Simulated voltages for K=1, C=63F, H=0.8, H_1=1.3 82
Fig. 2.55: Simulated currents for K=1, C=63F, H=0.8, H_1=1.3. 82
Fig. 2.56: Simulated voltages for K=1, C=75.78F, H=0.8, H_1=1.3. 83
Fig. 2.57: Simulated currents for K=1, C=75.78F, H=0.8, H_1=1.3. 84
Fig. 2.58: Simulated power grid for K=0, C=63F, H=0, H_1=1 85
Fig. 2.59: Simulated energy grid for K=0, C=63F, H=0, H_1=1 85
Fig. 2.60: Simulated power grid for K=0, C=63F, H=0.6, H_1=1 86
Fig. 2.61: Simulated energy grid for K=0, C=63F, H=0.6, H_1=1 86
Fig. 2.62: Simulated power grid for K=0.5, C=63F, H=0.6, H_1=1.3 87
Fig. 2.63: Simulated energy grid for K=0.5, C=63F, H=0.6, H_1=1.3 87
Fig. 2.64: Simulated power grid for K=1, C=63F, H=0.8, H_1=1.3 88
Fig. 2.65: Simulated energy grid for K=1, C=63F, H=0.8, H_1=1.3 88
Fig. 2.66: Simulated power grid for K=1, C=75.78F, H=0.8, H_1=1.3 89
Fig. 2.67: Simulated energy grid for K=1, C=75.78F, H=0.8, H_1=1.3 89
Fig. 2.68: Delta T vs I for duty cycle = 50% 91
Fig. 2.69: Specific Cost/Wh for different types of cells and voltages. 94
Fig. 2.70: Payback period – Case 2 97
Fig. 2.71: Payback period – Case 3 97
Fig. 2.72: Payback period – Case 4 98
Fig. 2.73: Payback period – Case 5 98
Fig. 3.1: Active front-end induction motor drive system 102
Fig. 3.2: Per-phase equivalent circuit 103
Fig. 3.3: PF=1 during motor mode 104
Fig. 3.4: PF=1 during regenerative mode 104
Fig. 3.5: Leading PF during motor mode 105
Fig. 3.6: Distributed energy source and utility interface 108
Fig. 3.7: Comparison between phase-controlled and active front-end rectifiers 109
Fig. 3.8: A simplified power system 111

Fig. 3.9: A voltage source rectifier 114
Fig. 3.10: Steady-state control of PWM rectifier 115
Fig. 3.11: Balanced, 3-phase, Y-connected system 117
Fig. 3.12: 3-phase system superponed to a 2-phase d-q system 117
Fig. 3.13: Three-phase to two-phase transformation 120
Fig. 3.14: Stationary to rotary reference frame, Park's transformation 120
Fig. 3.15: Circuit representation of system mathematical model 122
Fig. 3.16: Tracking θ_e 126
Fig. 3.17: DC-link dynamics controlled by line-side converter 132
Fig. 3.18: AC-side per-phase equivalent circuit 132
Fig. 3.19: DC-side equivalent circuit of an active drive 132
Fig. 3.20: High-gain feedback controller for line-side converter 135
Fig. 3.21: Supply voltage frequency estimation 137
Fig. 3.22: Feed-forward compensation for input-output linearization controller 140
Fig. 3.23: Complete control scheme for front-end converter 141
Fig. 3.24: Simulation model of the AFE 144
Fig. 3.25: AFE Normal Mode simulation results 146
Fig. 3.26: Grid i_{qe} and i_{de} 147
Fig. 3.27: DC-link voltage over time 147
Fig. 3.28: Phase displacement between E_1 voltage and I_1 current of phase 1 148
Fig. 3.29: Phase displacement between E1 and I1 at 0.2s instant load step change 149
Fig. 3.30: Parameters simulation at PCC point Voltage Sag in Phase A at t=0.046s 152
Fig. 3.31: Phase displacement between voltage and current in Phase A 153
Fig. 3.32: Active Power and Reactive Power Flows, single Voltage Sag 153
Fig. 3.33: Parameters simulation at PCC point Voltage Sag in Phase A and B at t=0.046s 154
Fig. 3.34: Phase displacement between voltage and current in Phase B 155
Fig. 3.35: Active Power and Reactive Power Flows, Double Voltage Sag 156
Fig. 3.36: Voltage Notches 157
Fig. 3.37: Single phase Notches Parameters simulation at PCC point Voltage notches occurred in Phase A from t=0.046.s to t=0.1262 158
Fig. 3.38: Phase displacement between voltage and current in Phase A Single Phase Notches event. 159
Fig. 3.39: Active Power and Reactive Power flows, single phase Voltage Notches event.. 160
Fig. 3.40: Active and Reactive Currents in the rotary reference frame, single phase notches event. 161
Fig. 3.41: Parameters simulation at PCC point for voltage notches in Phase A and Phase B at time interval [0.046s 0.1262s]. 162
Fig. 3.42: Phase displacement between voltage and current in Phase B. 163
Fig. 3.43: Active and Reactive Power , Double phase Voltage Notches Event. 164
Fig. 3.44: Active Currents and Reactive Currents in the rotary reference frame. 164
Fig. 4.1: Inverter 166
Fig. 4.2: inverter feeding an induction motor 169
Fig. 4.3: Current flow during braking 170

Fig. 4.4: Vector representation of the inverter voltages and the corresponding flux variation in a time interval ΔT. 172
Fig. 4.5: Block diagram of DTC 174
Fig. 5.1: Conducted emission testing set-up (current probe method) scheme (top view): 1 EMI receiver 2 ground plane, 3 EUT, 4 non-conductive supports, 5 current probe, 6 power lines, 7 LISN, 8 DC power supply. 180
Fig. 5.2: Radiated emission testing set-up scheme (top view): 1 EUT, 2 cables, 3 LISN (Line Impedance Stabilization Network), 4 ground plane, 5 non-conductive supports, 6antenna, 7 EMI receiver. 181
Fig. 5.3: architetture of the vehicle system 181
Fig. 5.4: Electric wheelchair 182
Fig. 5.5: Semi-anechoic chamber with ferrite tiles 183
Fig. 5.6: Frequency characteristics of ferrite tiles and pyramidal polystyrene ferrite 183
Fig. 5.7: Conducted emissions 150kHz-30MHz. No Emi filter 184
Fig. 5.8: Conducted emissions 500kHz-5MHz. No Emi filter 184
Fig. 5.9: Radiated Emissions, horizontal polarization 185
Fig. 5.10: Radiated Emissions, vertical polarization 185
Fig. 5.11: EMI filter 186
Fig. 5.12: EMI filter Bode plot 187
Fig. 5.13: Conducted emissions 150kHz-30MHz. No EMI filter 187
Fig. 5.14: Conducted emissions 500kHz-5MHz. No EMI filter 188

List of Tables

Table 1: A summary of FACTS controllers configuratin 32
Table 2: Main features of the lifting system 42
Table 3: UCs module main characteristics 53
Table 4: Simulation Reference Parameters 59
Table 5: Test Drive parameters 65
Table 6: Simulation parameters for the Light Load cycle 69
Table 7: Simulation parameters for the Heavy Load cycle.. 73
Table 8: Simulation cases 76
Table 9: Maximum grid power and energy grid per cycle... 84
Table 10: Ultracapacitors module specifications 91
Table 11: MV consumer cost analysis... 95
Table 13: Summerized costs and saving for the considered 4 cases 96
Table 14: Normal Condition mode simulation parameters... 145
Table 15: Voltage notches simulation parameters.. 157
Table 16: Inverter switches configuration 167
Table 17: Vectors applied in various sectors depending on the errors 173
Table 18: Device under test specifications 182

Introduction

The threatened limitations of conventional electrical power sources have focused a great deal of attention on power, its application, monitoring and correction. Power economics now play a critical role in industry as never before. With the high cost of power generation, transmission, and distribution, it is of paramount concern to effectively monitor and control the use of energy.

The electric utility's primary goal is to meet the power demand of its customers at all times and under all conditions. But as the electrical demand grows in size and complexity, modifications and additions to existing electric power networks have become increasingly expensive. The measuring and monitoring of electric power have become even more critical because of down time associated with equipment breakdown and material failures.

In modern electrical power systems, electricity is produced at generating stations, transmitted through a high voltage network, and finally distributed to consumers. Due to the rapid increase in power demand, electric power systems have developed extensively during the 20th century, resulting in today's power industry probably being the largest and most complex industry in the world. Electricity is one of the key elements of any economy, industrialized society or country. A modern power system should provide reliable and uninterrupted services to its customers at a rated voltage and frequency within constrained variation limits. If the supply quality suffers a reduction and is outside those constrained limits, sensitive equipment might trip, and any motors connected on the system might stall.

The electrical system should not only be able to provide cheap, safe and secure energy to the consumer, but also to compensate for the continually changing load demand. During that process the quality of power could be distorted by faults on the system, or by the switching of heavy loads within the customers facilities. In the early days of power systems, distortion did not impose severe problems towards end-users or utilities. Engineers first raised the issue in the late 1980s when they discovered that the majority of total equipment interruptions were due to power quality disturbances. Highly interconnected transmission and distribution lines have highlighted the previously small issues in power quality due to the wide propagation of power quality disturbances in the system. The reliability of power systems has improved due to the growth of interconnections between utilities. In the modern industrial world, many electronic and electrical control devices are part of automated processes in order to increase energy efficiency and productivity. However, these control devices are characterized by extreme sensitivity in power quality variations, which has led to growing concern over the quality of the power supplied to the customer.

From the end-user point of view, is important not only the quality of power but also the quantity of power used to supply the loads, that is, the quantity of money the user has to pay for the power supply.

Thus, the work of this thesis is the characterization of a power drive system focused on :

- *Minimization of Power supplied by the Grid (Ultracapacitors)*
- *Optimiziation of Power supplied by the Grid (Active Front End).*

In the first part of the thesis a general overview of the Power Quality concept is given. Power Quality related phenomena definitions are presented together with the most common Power Quality issues. Moreover, a general overview of the role of power electronic in contrasting these issues is given together with the most used type of controllers for Power Quality improvements.

The second part of the thesis is focused on the downstream of a power drive, that is, from the rectifier to the load, so the minimization of the grid power.

It is presented a gantry crane system coupled with a storage system based on Ultracapacitors. The aim of the storage system is to minimize the usage of the Grid power, thus, to improve, from the economical point of view, the usage of the power drive, especially if the utilization frequency is relevant.

First an overview of the Ultracapacitors tecnology is given together with the ultracapacitors model used to perform the simulation model.

Afterwards, an overview of the power drive system is given together with the assumed work cycle. The phase which is considered as the Ultracapacitors recovery phase (energy recovery) is the descending phase, in which the energy of the ultracapacitors is recovered and then released during the lifting phase.

All the data related to the gantry crane, such as power, torque, energy, load speed, load acceleration and load trajectory are technical real data which are used as input data for the simulation model. So, what was done was to take real data as a reference for the simulation model.

Once the model of the gantry crane coupled with the ultracapacitors storage system is obtained, a procedure of sizing the ultracapacitors based on the energy related to the descending of the load (for the sizing it is considered the maximum of the load = 50 tons).

Aftwards a power flow regulatin strategy control strategy is developed. The aim of this regulation strategy is to have different degrees of freedom in choosing the appropriate ammount of Grid Power, that is, to have balanced or unbalanced grid power flow during the entire process.

Experimental measurements for two different load conditions performed on a scaled experimental set up are presented and used to validate the simulation model. Afterwards simulation results are presented for different regulation strategy parameters.

At the end of the second part an economic evaluation is done in order to investigate the payback time of the investment for different simulation cases.

The third part of the thesis is mainly focused in the upstream of the power drive, that is, the optimization of grid power utilization (second main point of the thesis).

In this part it is presented the simulation model of an Active Front End with Reactive Power compensation capabilities, which provides, too, the Active Power to the own load.

First an overview of the Active Front End concept is given, together with the operating principle. Main keyfeatures of Active Fron End are presented both with a comparison between Active Front Ends drives and traditionals drives.

The AFE is used to compensate the Reactive power in such a way that the Power Factor is unity.

The steady state characteristics as well as differential equations describing the dynamics of the front-end rectifier are shown.

The dynamic equations describing the dynamic model of the system are obtained based on the d-q theory. The Control model is obtained and implemented in Matlab-Simulink platform. Feed-forward compensation was used to achieve a better dynamic response.

Different Resistive-inductive loads are connected in the PCC point to simulate the other user of the Grid, which contribute in the pollution of the network and, thus, in the phase shift between the phase voltage and the phase current of the grid, resulting in a non-unity Power Factor. Different conditions of the PCC point connected loads where considered to simulate variable conditions of the Grid. It will be seen that the AFE compensates the Reactive Power introduced by the R-L loads, bringing the Power factor back to unity (phase displacement between phase voltage and phase current = 1).

Afterwards, the AFE behavior is studied in presence of voltage sags and voltage notches in one phase or in two phases.

EMC is a great issue of the Power Quality. Every Electronic device has to comply with the EMC standards Appendix 1 provides some theoretical and experimental discussions on conducted electromagnetic interference (EMI) emissions in the automotive applications. Conducted and radiated emission tests have been carried out in the frequency range between 150 kHz and 1GHz and presented, relative to an electric wheelchair with a traction power of 205W.

1. Power Quality

Development of technology in all its areas is progressing at a faster rate. Power scenario has changed a lot. With the increase of size and capacity, power systems have become complex leading to reduced reliability. But, the development of electronics, electrical device and appliances have become more and more sophisticated and they demand uninterrupted and conditioned power. These have pushed the present complex electricity network and market in a strong competition resulting in the concept of deregulation. In this ever changing power scenario, quality assurance of electric power has also been affected. It demands a deep research and study on the subject ‘Electric Power Quality’.

In this chapter an overview of Power Quality will be given, together with most common issues related to this concept.

An overview of most used Power Quality Improve devices will be given too.

1.1 Power Quality definition

Power quality is a term that means different things to different people. Institute of Electrical and Electronic Engineers (IEEE) Standard IEEE1100 defines power quality as “the concept of powering and grounding sensitive electronic equipment in a manner suitable for the equipment.” As appropriate as this description might seem, the limitation of power quality to “sensitive electronic equipment” might be subject to disagreement. Electrical equipment susceptible to power quality or more appropriately to lack of power quality would fall within a seemingly boundless domain. All electrical devices are prone to failure or malfunction when exposed to one or more power quality problems. The electrical device might be an electric motor, a transformer, a generator, a computer, a printer, communication equipment, or a household appliance.

All of these devices and others react adversely to power quality issues, depending on the severity of problems. A simpler and perhaps more concise definition might state: “Power quality is a set of electrical boundaries that allows a piece of equipment to function in its intended manner without significant loss of performance or life expectancy.” This definition embraces two things that we demand from an electrical device: performance and life expectancy. Any power-related problem that compromises either attribute is a power quality concern.

1.2 Power quality progression

Since the discovery of electricity 400 years ago, the generation, distribution, and use of electricity have steadily evolved. New and innovative means to generate and use electricity fueled the industrial revolution, and since then scientists, engineers, and hobbyists have contributed to its continuing evolution. In the beginning, electrical machines and devices were crude at best but nonetheless very utilitarian. They consumed large amounts of electricity and performed quite well. The machines were conservatively designed with cost concerns only secondary to performance considerations. They were probably susceptible to whatever power quality anomalies existed at the time, but the effects were not readily discernible, due partly to the robustness of the machines and partly to the lack of effective ways to measure power quality parameters. However, in the last 50 years or so, the industrial age led to the need for products to be economically competitive, which meant that electrical machines were becoming smaller and more efficient and were designed without performance margins. At the same time, other factors were coming into play. Increased demands for electricity created extensive power generation and distribution grids. Industries demanded larger and larger shares of the generated power, which, along with the growing use of electricity in the residential sector, stretched electricity generation to the limit. Today, electrical utilities are no longer independently operated entities; they are part of a large network of utilities tied together in a complex grid. The combination of these factors has created electrical systems requiring power quality.

The difficulty in quantifying power quality concerns is explained by the nature of the interaction between power quality and susceptible equipment. What is “good” power for one piece of equipment could be “bad” power for another one. Two identical devices or pieces of equipment might react differently to the same power quality parameters due to differences in their manufacturing or component tolerance. Electrical devices are becoming smaller and more sensitive to power quality aberrations due to the proliferation of electronics. For example, an electronic controller about the size of a shoebox can efficiently control the performance of a 1000-hp motor; while the motor might be somewhat immune to power quality problems, the controller is not. The net effect is that we have a motor system that is very sensitive to power quality. Another factor that makes power quality issues difficult to grasp is that in some instances electrical equipment causes its own power quality problems. Such a problem might not be apparent at the manufacturing plant; however, once the equipment is installed in an unfriendly electrical environment the problem could surface and performance suffers. Given the nature of the electrical operating boundaries and the need for electrical equipment to perform satisfactorily in such an environment, it is increasingly necessary for engineers, technicians, and facility operators to become familiar with power quality issues. It is hoped that this book will help in this direction.

1.3 Power Quality terminology

More commonly used power quality terms are defined and explained below:

- **Bonding —**Intentional electrical-interconnecting of conductive parts to ensure common electrical potential between the bonded parts. Bonding is done primarily for two reasons. Conductive parts, when bonded using low impedance connections, would tend to be at the same electrical potential, meaning that the voltage difference between the bonded parts would be minimal or negligible. Bonding also ensures that any fault current likely imposed on a metal part will be safely conducted to ground or other grid systems serving as ground.
- **Capacitance —**Property of a circuit element characterized by an insulating medium contained between two conductive parts. The unit of capacitance is a farad (F), named for the English scientist Michael Faraday. Capacitance values are more commonly expressed in microfarad (μF), which is 10^{-6} of a farad. Capacitance is one means by which energy or electrical noise can couple from one electrical circuit to another. Capacitance between two conductive parts can be made infinitesimally small but may not be completely eliminated.

- **Coupling —**Process by which energy or electrical noise in one circuit can be transferred to another circuit that may or may not be electrically connected to it.
- **Crest factor —**Ratio between the peak value and the root mean square (RMS) value of a periodic waveform. Fig. 1.1 indicates the crest factor of a sinusoidal waveform. Crest factor is one indication of the distortion of a periodic waveform from its ideal characteristics.

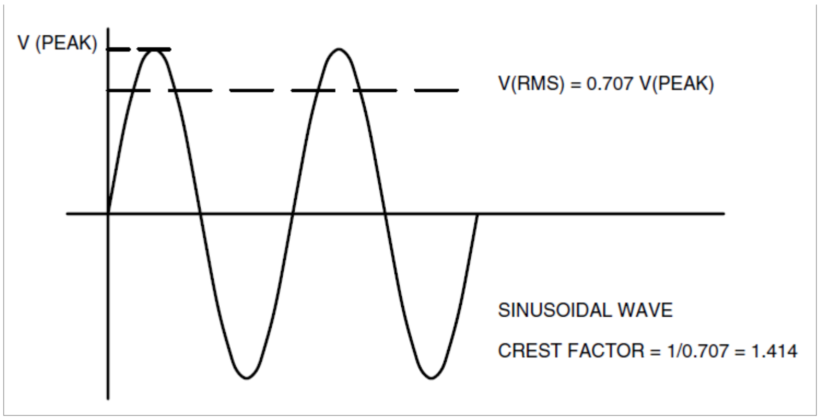

Fig. 1.1: Crest factor for sinusoidal waves

- **Distortion —** Qualitative term indicating the deviation of a periodic wave from its ideal waveform characteristics. Fig. 1.2 contains an ideal sinusoidal wave along with a distorted wave. The distortion introduced in a wave can create waveform deformity as well as phase shift.

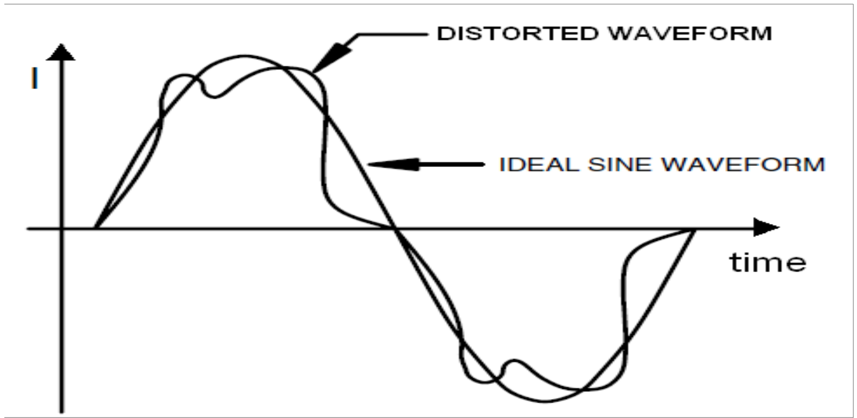

Fig. 1.2: Distorted waveform

- **Distortion factor —** Ratio of the RMS of the harmonic content of a periodic wave to the RMS of the fundamental content of the wave, expressed as a percent. This is also known as the total harmonic distortion (THD).
- **Flicker** —Variation of input voltage sufficient in duration to allow visual observation of a change in electric light source intensity. Quantitatively, flicker may be expressed as the change in voltage over nominal expressed as a percent.
- **Form factor** — Ratio between the RMS value and the average value of a periodic waveform. Form factor is another indicator of the deviation of a periodic waveform from the ideal characteristics.
- **Frequency** —Number of complete cycles of a periodic wave in a unit time, usually 1 sec. The frequency of electrical quantities such as voltage and current is expressed in hertz (Hz).
- **Ground electrode** — Conductor or a body of conductors in intimate contact with earth for the purpose of providing a connection with the ground.

- **Ground grid** — System of interconnected bare conductors arranged in a pattern over a specified area and buried below the surface of the earth.
- **Ground loop** — Potentially detrimental loop formed when two or more points in an electrical system that are nominally at ground potential are connected by a conducting path such that either or both points are not at the same ground potential.
- **Ground ring —** Ring encircling the building or structure in direct contact with the earth.
- **Grounding —** Conducting connection by which an electrical circuit or equipment is connected to the earth or to some conducting body of relatively large extent that serves in place of the earth.
- **Harmonic —** Sinusoidal component of a periodic wave having a frequency that is an integral multiple of the fundamental frequency.
- **Harmonic distortion —** Quantitative representation of the distortion from a pure sinusoidal waveform.
- **Impulse —** Traditionally used to indicate a short duration overvoltage event with certain rise and fall characteristics. Standards have moved toward including the term *impulse* in the category of transients.
- **Inductance —** Inductance is the relationship between the magnetic lines of flux (Ø) linking a circuit due to the current (I) producing the flux. If I is the current in a wire that produces a magnetic flux of Ø lines, then the self-inductance of the wire, L, is equal to Ø/I. Mutual inductance (M) is the relationship between

the magnetic flux $Ø_2$ linking an adjacent circuit 2 due to current I_1 in circuit 1. This can be stated as $M = Ø_2/I_1$.

- **Inrush —** Large current that a load draws when initially turned on.
- **Interruption —** Complete loss of voltage or current for a time period.
- **Isolation —** Means by which energized electrical circuits are uncoupled from each other. Two-winding transformers with primary and secondary windings are one example of isolation between circuits. In actuality, some coupling still exists in a two-winding transformer due to capacitance between the primary and the secondary windings.
- **Linear loads —** Electrical load which in steady-state operation presents essentially constant impedance to the power source throughout the cycle of applied voltage. A purely linear load has only the fundamental component of the current present.
- **Noise —** Electrical noise is unwanted electrical signals that produce undesirable effects in the circuits of control systems in which they occur.
- **Nonlinear load —** Electrical load that draws currents discontinuously or whose impedance varies during each cycle of the input AC voltage waveform.
- **Notch —** Disturbance of the normal power voltage waveform lasting less than a half cycle; the disturbance is initially of opposite polarity than the waveform and, thus, subtracts from the waveform.
- **Periodic —** A voltage or current is periodic if the value of the function at time t is equal to the value at time $t + T$, where T is the

period of the function. In this book, function refers to a periodic time-varying quantity such as AC voltage or current.

- **Power disturbance —** Any deviation from the nominal value of the input AC characteristics.
- **Power factor (displacement) —** Ratio between the Active Power (Watt) of the fundamental wave to the Apparent Power (VA) of the fundamental wave. For a pure sinusoidal waveform, only the fundamental component exists. The power factor, therefore, is the cosine of the displacement angle between the voltage and the current waveforms.
- **Power factor (total) —** Ratio of the total Active Power (Watt) to the total Apparent Power (VA) of the composite wave, including all harmonic frequency components. Due to harmonic frequency components, the total power factor is less than the displacement power factor, as the presence of harmonics tends to increase the displacement between the composite voltage and current waveforms.
- **Recovery time —** Interval required for output voltage or current to return to a value within specifications after step load or line changes.
- **Ride through —** Measure of the ability of control devices to sustain operation when subjected to partial or total loss of power of a specified duration.
- **Sag —** RMS reduction in the AC voltage at power frequency from 1ms to a few seconds duration.
- **Surge —** Electrical transient characterized by a sharp increase in voltage or current.

- **Swell —** RMS increase in AC voltage at power frequency from half of a cycle to a few seconds duration.
- **Transient —** Sub-cycle disturbance in the AC waveform evidenced by a sharp, brief discontinuity of the waveform. This may be of either polarity and may be additive or subtractive from the nominal waveform. Transients occur when there is a sudden change in the voltage or the current in a power system. Transients are short-duration events, the characteristics of which are predominantly determined by the resistance, inductance, and capacitance of the power system network at the point of interest. The primary characteristics that define a transient are the peak amplitude, the rise time, the fall time, and the frequency of oscillation.

1.4 Power Quality Issues

Power quality is a simple term, yet it describes a multitude of issues that are found in any electrical power system and is a subjective term. The concept of good and bad power depends on the end user. If a piece of equipment functions satisfactorily, the user feels that the power is good. If the equipment does not function as intended or fails prematurely, there is a feeling that the power is bad. In between these limits, several grades or layers of power quality may exist, depending on the perspective of the power user. Understanding power quality issues is a good starting point for solving any power quality problem. Fig. 1.3 provides an overview of the power quality issues.

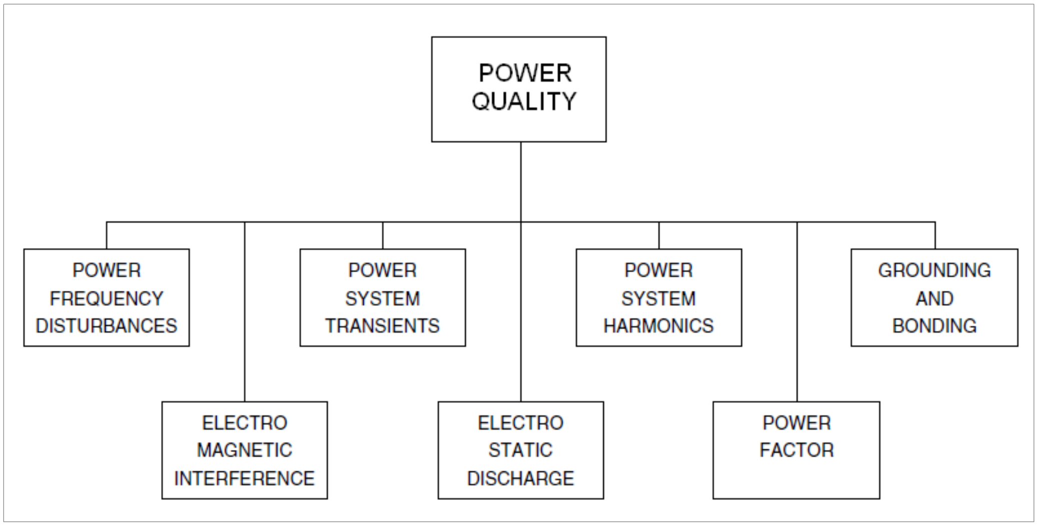

Fig. 1.3: Power Quality issues.

Power frequency disturbances are low-frequency phenomena that result in voltage sags or swells. These may be source or load generated due to faults or switching operations in a power system. The end results are the same as far as the susceptibility of electrical equipment is concerned.

Power system transients are fast, short-duration events that produce distortions such as notching, ringing, and impulse. The mechanisms by which transient energy is propagated in power lines, transferred to other electrical circuits, and eventually dissipated are different from the factors that affect power frequency disturbances.

Power system harmonics are low-frequency phenomena characterized by waveform distortion, which introduces harmonic frequency components. Voltage and current harmonics have undesirable effects on power system operation and power system components. In some instances, interaction between the harmonics and the power system parameters (R–L–C) can cause harmonics to multiply with severe consequences.

Grounding and bonding is one of the more critical issues in power quality studies. Grounding is done for three reasons. The fundamental objective of grounding is safety, and nothing that is done in an electrical system should compromise the safety of people who work in the environment. The second objective of grounding and bonding is to provide a low-impedance path for the flow of fault current in case of a ground fault so that the protective device could isolate the faulted circuit from the power source. The third use of grounding is to create a ground reference plane for sensitive electrical equipment. This is known as the signal reference ground (SRG). The configuration of the SRG may vary from user to user and from facility to facility. The SRG cannot be an isolated entity. It must be bonded to the safety ground of the facility to create a total ground system.

Electromagnetic interference (EMI) refers to the interaction between electric and magnetic fields and sensitive electronic circuits and devices. EMI is predominantly a high-frequency phenomenon. The mechanism of coupling EMI to sensitive devices is different from that for power frequency disturbances and electrical transients. The mitigation of the effects of EMI requires special techniques.

Radio frequency interference (RFI) is the interaction between conducted or radiated radio frequency fields and sensitive data and communication equipment. It is convenient to include RFI in the category of EMI, but the two phenomena are distinct.

Electrostatic discharge (ESD) is a very familiar and unpleasant occurrence. In our day-to-day lives, ESD is an uncomfortable nuisance we are subjected to when we open the door of a car or the refrigerated case in the supermarket. But, at high levels, ESD is harmful to electronic equipment, causing malfunction and damage.

Power factor is included for the sake of completing the power quality discussion. In some cases, low power factor is responsible for equipment damage due to component overload. For the most part, power factor is an economic issue in the operation of a power system. As utilities are increasingly faced with power demands that exceed generation capability, the penalty for low power factor is expected to increase. An understanding of the power factor and how to remedy low power factor conditions is not any less important than understanding other factors that determine the health of a power system.

1.5 Role of Power Electronics in Improving Quality of AC Grid Power

Power electronics, which is the major contributor to the troublesome line-side interactions in the form of reactive currents and harmonics, can also provide solution for removing such effects. The prospects of using power electronics based system to address the power quality issues promise to change the landscape of future power systems in terms of generation, transmission and distribution, operation and control. The ever increasing interest in these applications can be attributed to the several factors as listed below:

- Availability of power semiconductor devices with high power ratings capable of switching fast lead to better conversion efficiency and high power density.
- Growing awareness of power quality issues and stricter norms set forth by the utility companies and regulatory authorities to control harmonic pollution and EMC effects.

- Continual use of existing transmission system capacity for increased power transfer without compromising transmission system stability and reliability.
- Need for effective control of power flow in a deregulated environment.
- Increased emphasis on decentralized generation with renewable energy sources to avoid transmission line congestion.

Many types of utility applications based on power electronics controllers are being envisaged. These include active and reactive power flow control, system stability, improving power quality by eliminating harmonics, improving transmission efficiency, and protection.

Thus, power quality solutions comprising reactive compensation, compensation for the non-active currents, harmonic compensation, or active filtering is one of the many significant areas of utility applications for these controllers, summarily referred to as flexible ac transmission system (FACTS) controllers. The different types of FACTS controllers and the principle of operation is reviewed briefly in the following subsections.

1.5.1 Flexible AC Transmission Systems (FACTS) Operating Principle

In existing ac transmission networks, limitations on constructing new power lines has led to several ways to increase power transmission capability without sacrificing the stability requirements. Power flow on a transmission line connecting two ac systems is given by:

$$P = \frac{E_1 E_2}{X} \sin \delta$$

Where E_1 and E_2 are magnitudes at the two ends of transmission line, X is the line reactance, and δ is the angle between the two bus voltages. Equation above shows that power flow on a transmission line depends on the voltage magnitude E_1 and E_2, the line reactance X, and the power angle δ. FACTS devices based on phase-controlled thyristors or active switches such as IGBTs can be used to rapidly control one or more of above three quantities.

The term, FACTS devices, can be formally defined as a collection of power converters and controllers that can be applied individually or in coordination with others to control – series impedance, shunt impedance, current, voltage, phase angle, oscillation damping. By controlling one or all these quantities, FACTS devices enable transmission system to be operated closer to its thermal limit without decreasing the system's reliability in addition to providing improved quality power. Depending on whether they are connected in shunt or series, the FACTS devices can be categorized as shunt-connected and series-connected controllers.

1.5.2 Shunt-Connected Controllers

Typically, the shunt-connected controllers draw or supply reactive power from a bus, thus causing the bus voltage to change due to the internal system reactance. Some of the popular shunt controllers are described below.

Static synchronous compensator (STATCOM) is a shunt-connected static VAR compensator, which can control its output current (inductive/capacitive) independent of the ac system voltage variations. It uses self-commutated (active) switches like IGBTs, GTOs, or IGCTs. It may or may not need large energy storage capacity depending on what active and/or reactive power compensation is desired.

Static VAR compensator (SVC) is another type of power compensator, whose output is adjusted to exchange capacitive or inductive current so as to maintain bus voltage constant. SVC is based on devices without turn-off capability, like thyristors. SVC functions as a shunt-connected controlled reactive admittance. Some popular SVC configurations are thyristor controlled reactor (TCR), thyristor switched reactor (TSR), and thyristor switched capacitor (TSC). The TCR has an effective inductive reactance which is varied by firing angle control of the thyristor valve. The effective inductive reactance of a TSR, on the other hand, is varied in step-wise manner by full or zero conduction of the thyristor vale. In case of a TSC, the effective capacitive reactance is varied in a step-wise manner by full or full conduction of the thyristor valve.

1.5.3 Series-Connected Controllers

These types of devices are connected in series with a transmission line, thereby, changing the effective transmission line reactance. This feature allows series-connected controllers to control the flow of power through the transmission line. Various forms of such devices include static synchronous series compensator (SSSC), thyristor controlled or switched series capacitor (TCSC/TSSC), and thyristor controlled or switched series inductor (TCSR/TSSR). The output of SSSC is in quadrature with the line current, and is controlled independently of the line current. The SSSC decreases the overall reactive voltage drop across the transmission line and controls flow of electric power. The SSSC may include transiently rated energy storage to compensate temporarily an additional real power component. The TCSC varies its effective capacitive reactance smoothly by firing angle control of the thyristor valve. Alternately, the effective capacitive reactance of a TSSC is varied in step-wise manner, by full or zero conduction of the thyristor vale. Similarly in case of a TCSR and TSSR, the effective reactance is varied smoothly and in a step-wise manner respectively.

Table 1 summarizes the above discussion on different types of controllers, their respective circuit schematic, system functions, and control principle. The active frontend induction motor drive analyzed in this thesis work falls under the category of static synchronous compensator (STATCOM). From power quality point of view, it is basically a shunt-connected static VAR compensator which can control its output current (inductive/capacitive) independent of the ac system voltage variations or load. It needs a temporary energy storage element in the form of a dc-link capacitor to effectively supply the desired power compensation while driving the mechanical load connected to the induction motor.

After establishing different methods of compensation, it will be worthwhile to know exactly how much and which component of the source power needs to be compensated. In other words we need to establish the reference commands for the power controllers discussed above. The instantaneous power definitions presented in the next section explain how to choose compensation references.

Table 1: A summary of FACTS controllers configuratin

Controller	Circuit configuration	System functions	Control principle
TCR/TSC - Thyristor Controlled or Switched Reactor	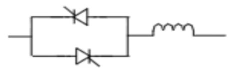	• Regulate voltage • Improve stability	VAR control by varying L in the shunt connection
TCC/TSC – Thyristor Controlled or Switched Capacitor	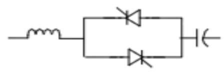	• Regulate voltage & compensate VAR • Improve stability	VAR control by varying C in the shunt connection
TSSC – Thyristor Switched Series Capacitor	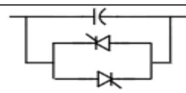	• Control power flow • Improve stability	Power and VAR control through varying C.
TCSR – Thyristor Controlled Series Capacitor	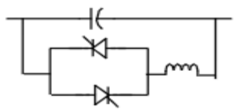	• Control power flow • Improve stability • Limit fault current	Power and VAR control through varying C & L in shunt connection
TCSR – Thyristor Controlled Series Reactor	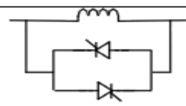	• Limit fault current	Current control by inserting L in series.
STATCOM Static Synchronous Compensator	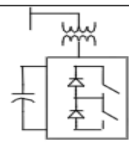	• Regulate voltage & compensate VAR • Improve stability	VAR control through current control in shunt connection
Active Filter (Shunt Connected)	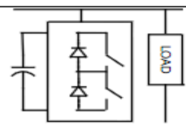	• Harmonic current filtering	Inject canceling harmonic current into the source
SSSC – Static Series Synchronous Compensator	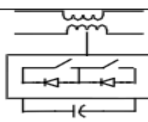	• Control power flow • Improve stability	VAR control through series voltage control.

The use of power supply conditioning systems through the use of technologies for electrical storage (batteries and ultracapacitors) can be very interesting in all applications that require peak powers with respect to the nominal average power, such as the power required for load lifting, which is characterized by high value of required power but short duration in time. In this case, moreover, possibility of energy recovery during the descending of loads is interesting too.

2. Ultracapacitors storage system

In this chapter an energy storage system based on ultracapacitors for the recovery of energy dissipated during braking and the movement of loads in a logistics node (bridge cranes, gantry cranes, small locomotives, etc.). In these situations, the insertion of electric storage systems can reduce the commitment power required by the distributor, with lower costs and lower losses, and to reduce the net energy consumption, in an amount proportional to the frequency of use energy recovery feature.

An application example is developed, which refers to a gantry crane, for the Bertolotti company which has already issued a very detailed technical specification concerning the basic version without energy recovery, which is the technical specification main input data of the presented project. The project is configured as an improved version of the original project, which correspond to higher investment costs and lower operating costs by reducing the consumption of energy that introduced system allows.

Is is presented, for a system consisting of a gantry crane, the sizing of an Ultracapacitor (UC) based storage system, and its performance test using a simulated model of the system considered as a multi-axis drive.

Preliminary examination of different operating processes has been done. For each proccess were considered the different drives refered to the toughest conditions, and the diagrams of torque, power and energy were built for each of them.

Two different approaches were used for the UCs sizing. The first approach consists on considering the peak power during each operating proccess and consequently the energy furnished by the system during these power peaks. The second approach consists on considering the energy of the lifting process (UCs recharge). Experimental data have been presented and compared with the simulation results.

Moreover, a regulation strategy for the management of the overall power flow is presented and discussed.

2.1 Introduction

Electrochemical double layer capacitors (EDLCs) are similarly known as supercapacitors or ultracapacitors. An ultracapacitor stores energy electrostatically by polarizing an electrolytic solution. Though it is an electrochemical device there are no chemical reactions involved in its energy storage mechanism. This mechanism is highly reversible, allowing the ultracapacitor to be charged and discharged hundreds of thousands to even millions of times.

An ultracapacitor can be viewed as two non-reactive porous plates suspended within an electrolyte with an applied voltage across the plates. The applied potential on the positive plate attracts the negative ions in the electrolyte, while the potential on the negative plate attracts the positive ions. This effectively creates two layers of capacitive storage, one where the charges are separated at the positive plate, and another at the negative plate.

Conventional electrolytic capacitors storage area is derived from thin plates of flat, conductive material. High capacitance is achieved by winding great lengths of material. Further increases are possible through texturing on its surface, increasing its surface area. A conventional capacitor separates its charged plates with a dielectric material: plastic, paper or ceramic films. The thinner the dielectric the more area can be created within a specified volume. The limitations of the thickness of the dielectric define the surface area achievable.

An ultracapacitor derives its area from a porous carbon-based electrode material. The porous structure of this material allows its surface area to approach 2000 square meters per gram, much greater than can be accomplished using flat or textured films and plates. An ultracapacitor charge separation distance is determined by the size of the ions in the electrolyte, which are attracted to the charged electrode. This charge separation (less than 10 angstroms) is much smaller than can be accomplished using conventional dielectric materials.

The combination of enormous surface area and extremely small charge separation gives the ultracapacitor its outstanding capacitance relative to conventional capacitors.

2.1.1 Ultracapacitors construction

The specifics of ultracapacitor construction are dependent on the application and use of the ultracapacitor. The materials may differ slightly from manufacturer or due to specific application needs. The commonality among all ultracapacitors is that they consist of a positive electrode, a negative electrode, a separator between these two electrodes, and an electrolyte filling the porosities of the two electrodes and separator (Fig. 2.1).

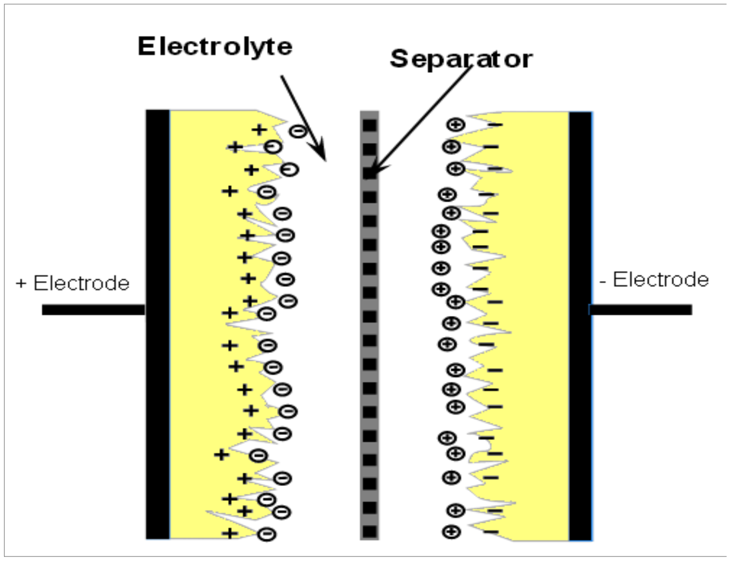

Fig. 2.1: Ultracapacitor charge separation

The assembly of the ultracapacitors can vary from product to product. This is due in part to the geometry of the ultracapacitor packaging. For products having a prismatic or square packaging arrangement, the internal construction is based upon a stacking assembly arrangement with internal collector paddles extruding from each electrode stack. These current collector paddles are then welded to the terminals to enable a current path outside the capacitor.

For products with round or cylindrical packaging, the electrodes are wound into a jellyroll configuration. The electrodes have foil extensions that are then welded to the terminals to enable a current path outside the capacitor.

2.1.2 Typical Applications

The ultracapacitors can be used in a variety of industries for many power requirement needs. These applications span from mA current or mW power to several hundred amps current or several hundred kilowatts power needs. Industries employing ultracapacitors have included: consumer electronics, traction, automotive, and industrial. Examples within each industry are numerous.

- **Automotive** – vehicle supply networks, power steering, electromagnetic valve controls, starter generators, electrical door opening, regenerative braking, hybrid electric drive, active seat belt restraints.
- **Transportation** – Diesel engine starting, train tilting, security door opening, tram power supply, voltage drop compensation, regenerative braking, hybrid electric drive.
- **Industrial** – uninterrupted power supply (UPS), wind turbine pitch systems, power transient buffering, automated meter reading (AMR), elevator micro-controller power backup, security doors, forklifts, cranes, and telecommunications.
- **Consumer** – digital cameras, lap top computers, PDA's, GPS, hand held devices, toys, flashlights, solar accent lighting, and restaurant paging devices.

Consideration for the various industries listed, and for many others, is typically attributed to the specific needs of the application the ultracapacitor technology can satisfy. Applications ideally suited for ultracapacitors include:

- **Pulse Power -** Ultracapacitors are ideally suited for pulse power applications. As mentioned in the theory section, due to the fact the energy storage is not a chemical reaction, the charge/discharge behavior of the capacitors is efficient. Since ultracapacitors have low internal impedance they are capable of delivering high currents and are often times placed in parallel with batteries to load level the batteries, extending battery life. The ultracapacitor buffers the battery from seeing the high peak currents experienced in the application. This methodology is employed for devices such as digital cameras, hybrid drive systems and regenerative braking (for energy recovery).

- **Bridge Power -** Ultracapacitors are utilized as temporary energy sources in many applications where immediate power availability may be difficult. This includes UPS systems utilizing generators, fuel cells or flywheels as the main power backup. All of these systems require short start up times enabling momentary power interruptions. Ultracapacitor systems are sized to provide the appropriate amount of ride through time until the primary backup power source becomes available.
- **Main Power -** For applications requiring power for only short periods of time or is acceptable to allow short charging time before use, ultracapacitors can be used as the primary power source. Examples of this utilization include toys, emergency flashlights, restaurant paging devices, solar charged accent lighting, and emergency door power.
- **Memory Backup -** When an application has an available power source to keep the ultracapacitors trickle charged they may be suited for memory backup, system shut down operations, or event notification. The ultracapacitors can be maintained at its full charged state and act as a power reserve to perform critical functions in the event of power loss. This may include AMR for reporting power outage, micro-controllers and board memory.

2.2 The Gantry Crane System

Consider in the next figure the operation of an bridge crane, reported schematically:

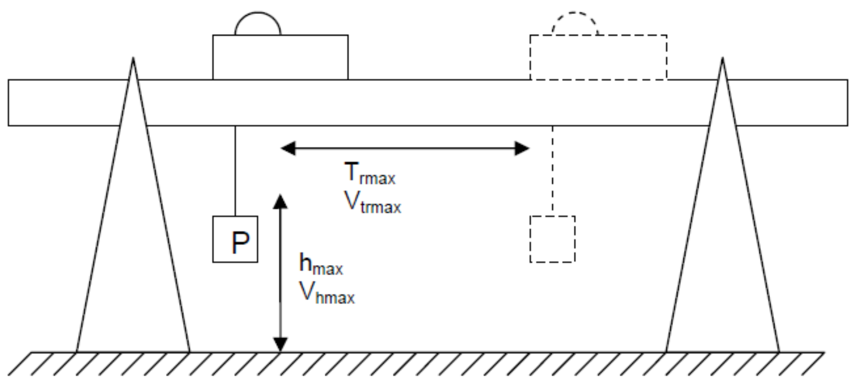

Fig. 2.2: Bridge crane operation

It is assumed that the weight is lifted from the ground and carried as high as possible h_{max} at the maximum speed allowed by the lifting engine V_{hmax}, subsequently, is traversed at the maximum distance T_{rmax} at the maximum travel speed V_{trmax} and placed on the ground at the same height of departure. Usually, the energy generated is dissipated through resistors or returned to the grid.

2.3 The Ultracapacitors Storage System

The problems of interfacing with the network are overcome, totally or partially, adding to the supply circuit of the motor a storage system capable of storing the energy during the descent of the load, and then reuse it in traction phase. By doing so it is therefore possible to reduce the power and energy required to the network, up to a lower limit at which the network will have to compensate losses due to the efficiencies of the storage system, the converters, mechanical transmissions etc..

The trend of the power absorbed / generated by the lifting motor is the following:

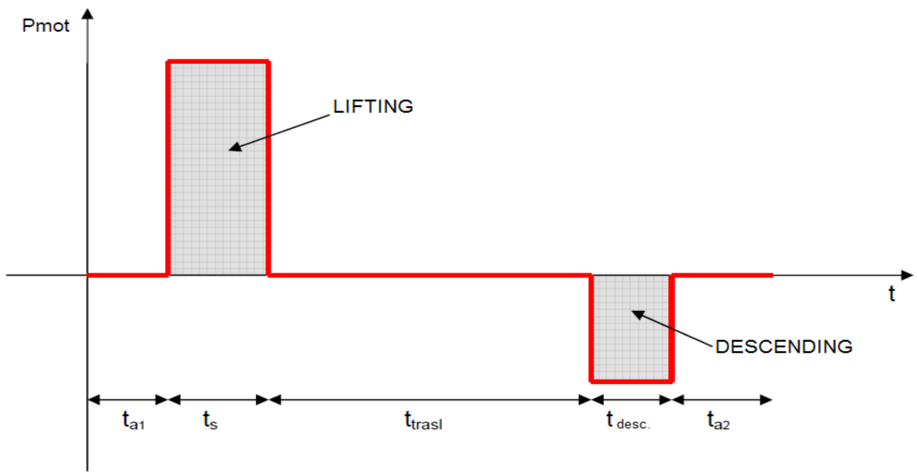

Fig. 2.3: Absorbed/Delivered power of the lifting motor

In Fig. 2.3 is presented the circuit that makes the system reversible and able to accumulate energy.

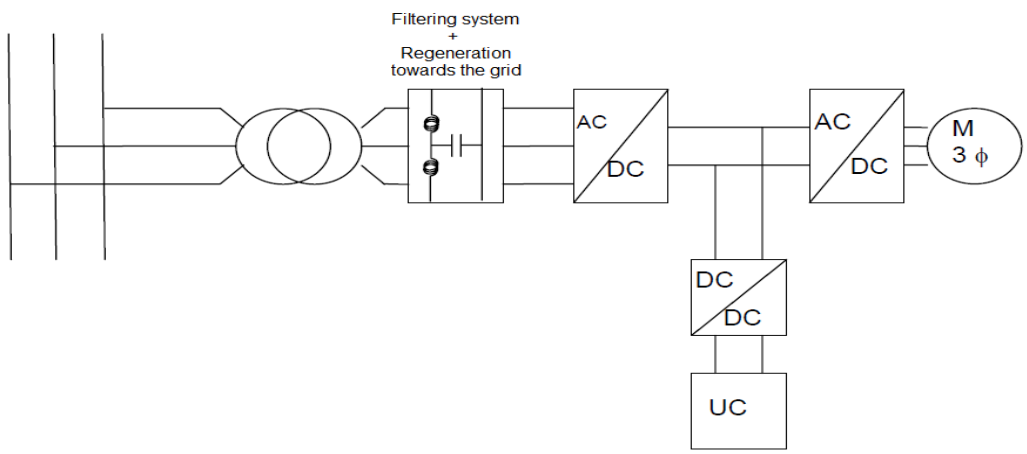

Fig. 2.4: Circuit diagram of the bridge crane drive with recovery capabilities

With this scheme the energy accumulated during the phases in which the loads behave generators (descending) can be returned at a later time with the dual benefit of energy saving and leveling of peak power consumption.

Starting from the three-phase grid, the power of the system is obtained by a bridge three-phase diode rectifier with capacitor on the dc-link that ensures a DC voltage on the dc-link. The presence of appropriate filters in the input of the bridge rectifier ensures compliance with regulatory limits at the point of interconnection to the electricity distribution network.

The drive electric responsible for movement of the bridge crane consists of a three-phase induction motor with field oriented control, and a three-phase inverter.

The accumulation system, in this case a bank of ultracapacitors (UC: Ultracapacitor), supplies power to the electric drive during the lifting phase of the load (resulting in discharge of the UC)and recovers the energy that is available during the descending phase of the load (resulting in charging of the UC).

To interface the storage system with the dc-link a bidirectional dc-dc step-up/step-down converter is required, which shall govern the storage and the return of power according to the logic of control that depend on the practical employment.

2.4 Gantry Crane System

The lifting system under consideration consists of a gantry crane with a capacity of 50 tons. In table 1 the main specifications are listed and in Fig. 4 the geometry of the gantry crane is presented.

Table 2: Main features of the lifting system

Maximum lift height (m)	15
Maximum Weight (tons) (including the container)	67
Grid voltage (Vac)	1500 Vac, 3-Phase, 50Hz
Induction motor supply	400 Vdc / 400 Vac
Dc-link (Vdc)	500 Vdc

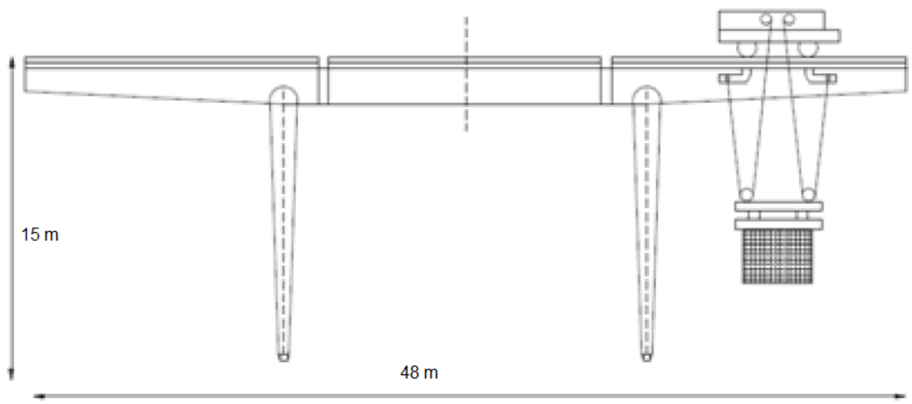

Fig. 2.5: Geometry of the system

The working cycle of the crane examined is composed of the working phases listed below:

1. Load lifting;
2. Load Rotation;
3. Load Translation;
4. Load Descending;
5. Gantry Crane Scroll (if necessary);
6. Return Path.

At the end of these work phases, the gantry crane returns back to the starting point (without container) and repeats the process. The maximum mass of the container is estimated at 50 t, so the mass of the crane without the load at the point of return is much lower than this value. If it is needed to move the crane from the starting point to another point, the entire complex of the crane can be moved for a maximum distance of 500m. In Fig 5 and Fig.6 are shown the working phases of lifting and descending in terms of speed, acceleration, space (Fig. 5) and in terms of power, torque and energy (Fig.6). The total weight in the descending phase is 67t (including load).

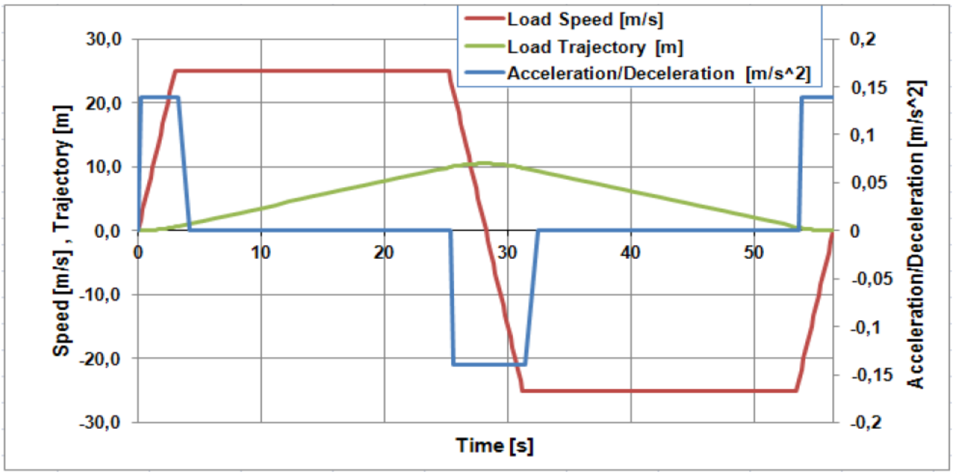

Fig. 2.6: Load speed, trajectory and Acceleration during the lifting/descending process.

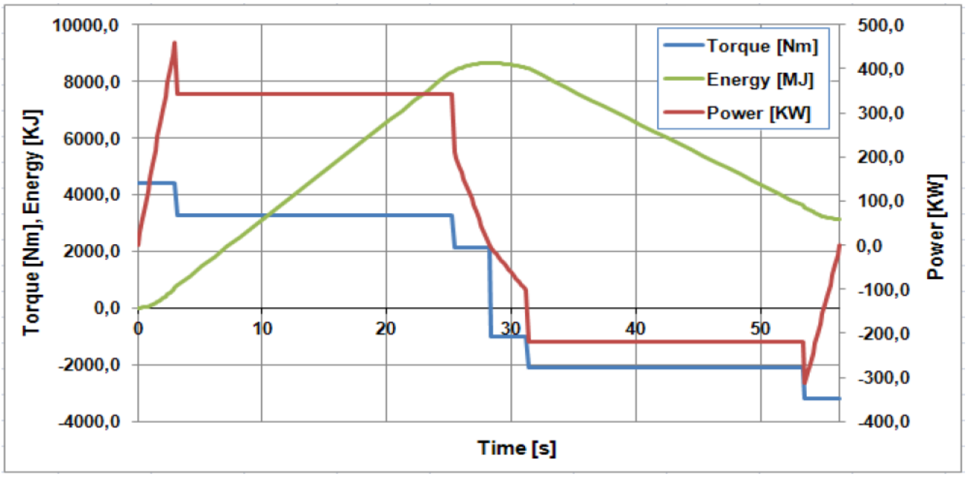

Fig. 2.7: Lifting/descending motor torque, energy, power during the lifting/descending process

The lifting-descending process lasts a total of 56 sec. A time pause between the two phases is not considered in the model. This comes at advantage of safety, because the presence of a pause improves the thermal behavior of the equipment.

As it can be seen, there is a power peak during the transition between the acceleration/deceleration phase and the regime phase. During the lifting process the expended energy is about 8650 kJ, while during the descending of the load the energy lost by the system is 5498kJ (Peak Energy – Final Energy). For the lifting process the peak power is about 459 kW.

In Fig.7 and Fig.8 is shown the work cycle referred to the rotation process of the load. The overall weight of the rotation set is 115t.

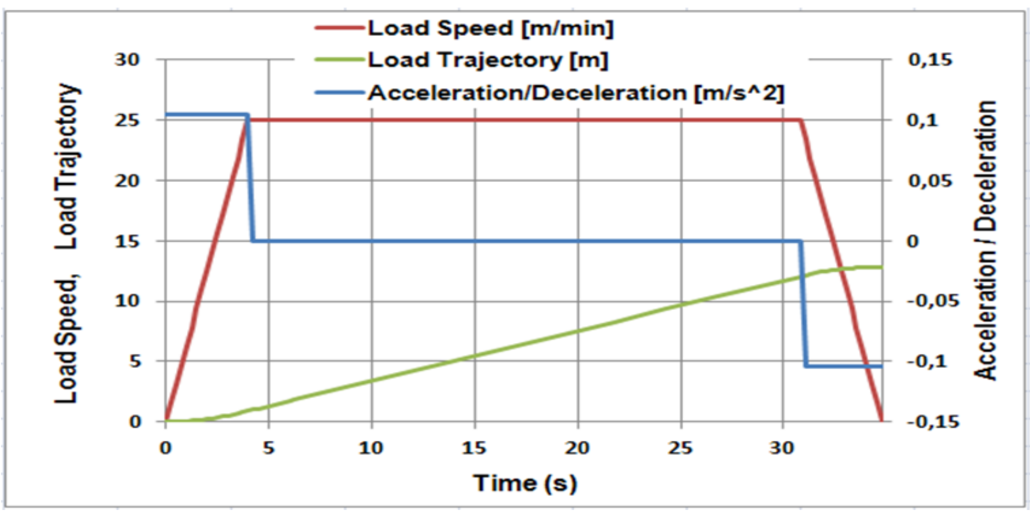

Fig. 2.8: Load speed, trajectory and Acceleration during the rotation process.

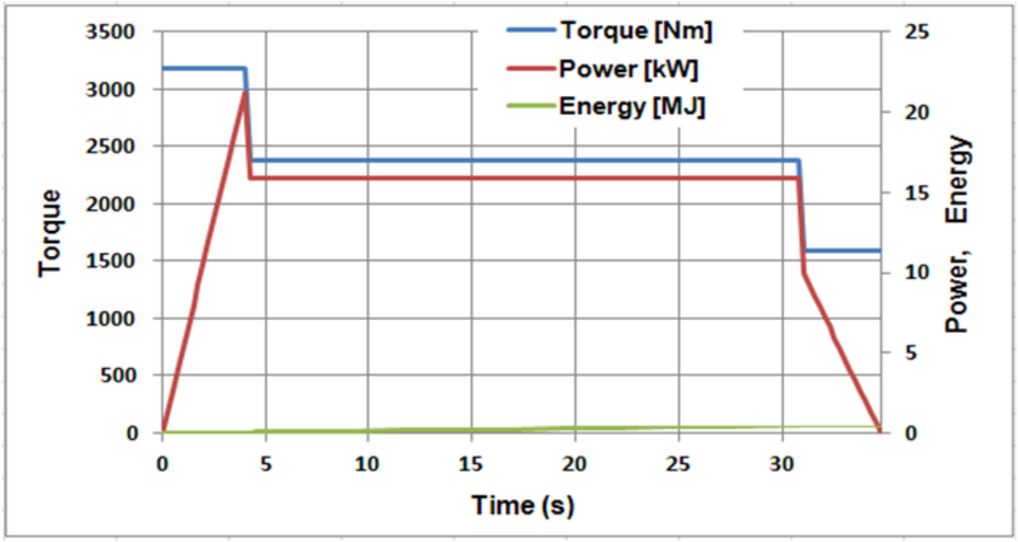

Fig. 2.9: Rotation motor torque, energy, power during the rotation process.

It was considered a maximum rotation of 180°. The rotation process endures maximum for 35s (180°). It has a peak power of 21 kW. The energy spent by the system during this process is about 490kJ.

In Fig. 2.10 and Fig. 2.11 is shown the work cycle referred to the translation process of the load. This set has a total weight of 146t.

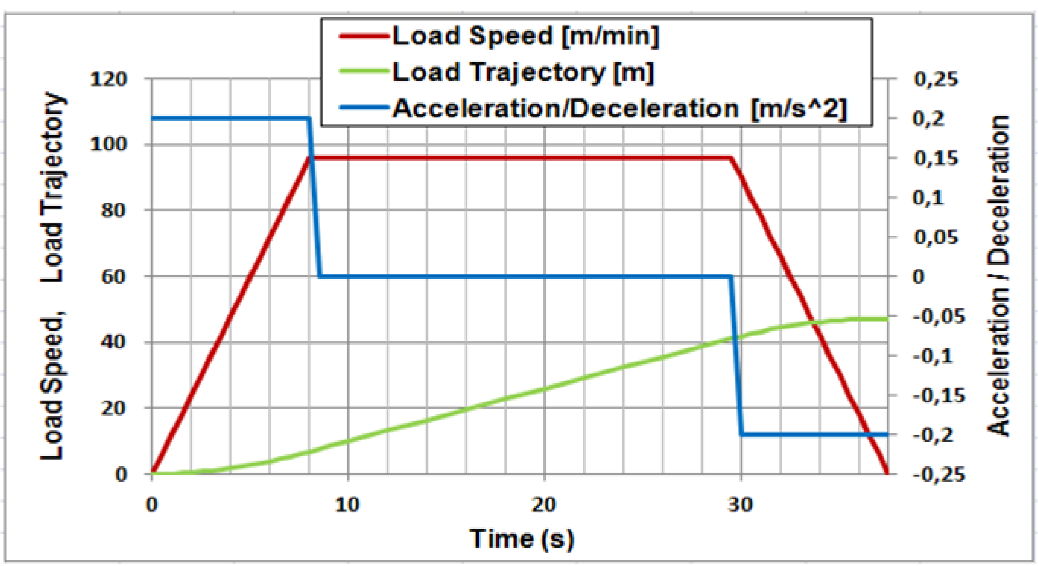

Fig. 2.10: Load speed, trajectory and Acceleration during the translation process.

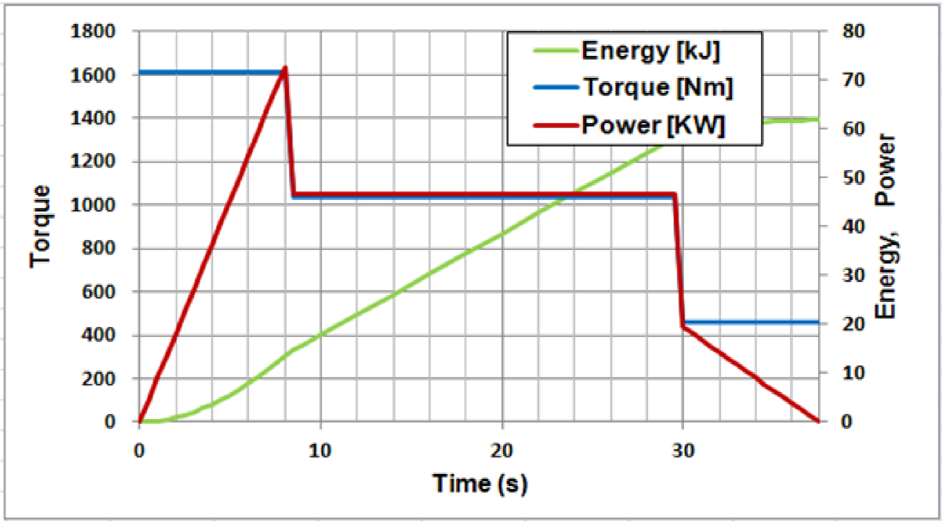

Fig. 2.11: Translation motor torque, energy, power during the translation process.

The maximum translation of the load is 48m, the peak power is 72 kW and the energy spent by the system during this process is 1391kJ.

In Fig. 2.12 and in Fig. 2.13 is shown the work cycle referred to the scroll process of the entire crane with an overall weight of 198t.

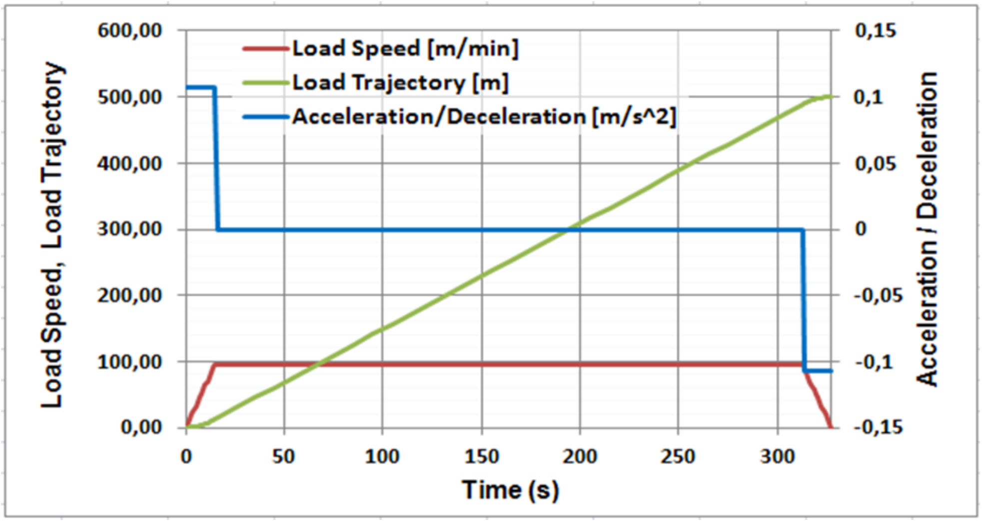

Fig. 2.12: Load speed, trajectory and Acceleration during the scroll process.

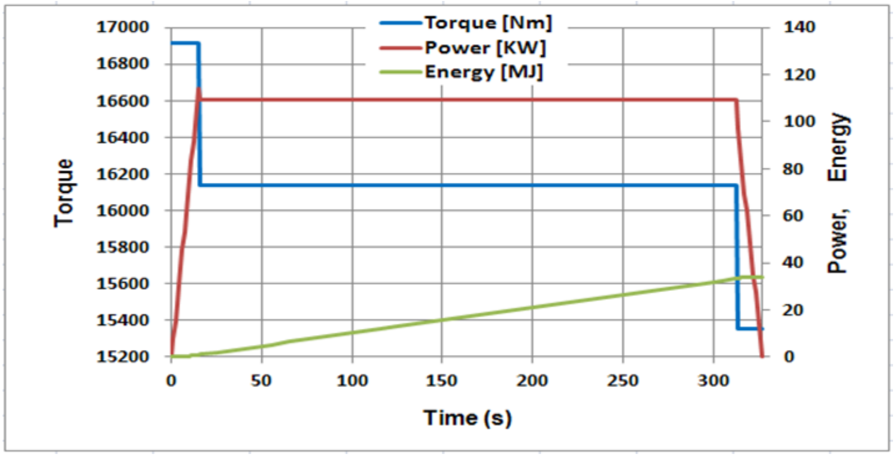

Fig. 2.13: Scroll motor torque, energy, power during the scroll process.

The maximum scroll of the crane is 500m, the peak power is 114 kW and the energy spent by the system during this process is 34MJ.

The return procceses of rotation, translation and scroll were not shown in this paper because the return process is the same as the graphs that have been shown above. In this case the speed has to be considered negative and the weight with 50t less. That means the energy involved is lower.

2.5 Electrical system layout

Ultracapacitors (UC) show high power density and low energy density; they provide a cost-effective solution at medium power levels. UCs are widely used in applications that require high power peaks, in addition to an average energy consumption. In fact, by smoothing the power demand, it is possible an energy saving; this is particularly true in applications (like materials handling or hoisting machines) that allow to recover energy during braking or load descending. In Fig. 2.14 is shown the general block scheme of the electrical drive interfaced with UCs.

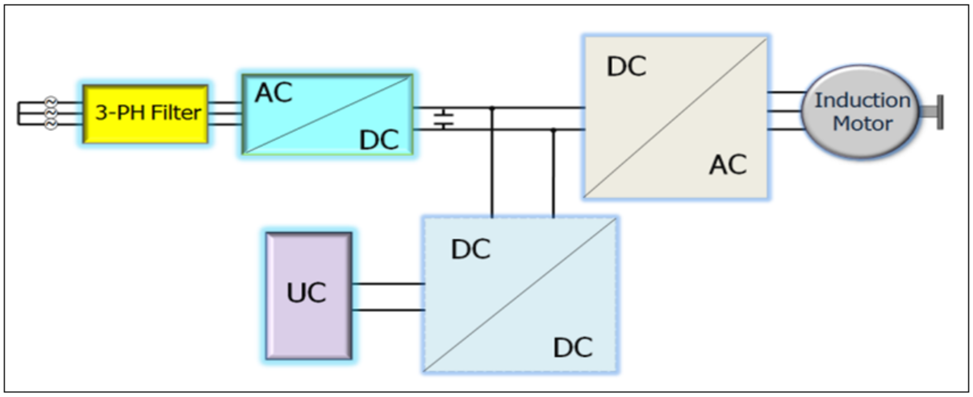

Fig. 2.14: Blocks scheme of the electrical drive

The UCs tank provides peak power supply to the electric motor, while it recovers (UCs recharge) the energy furnished by the traction drive itself during the descending of loads (regenerative braking).

A dc-dc converter is the interface between the storage unit and the dc-link; it has to be bidirectional in order to allow the current flows in both directions, according to UCs discharge or recharge cycle. The electrical scheme for the UCs bidirectional dc-dc converter is shown in Fig. 2.15.

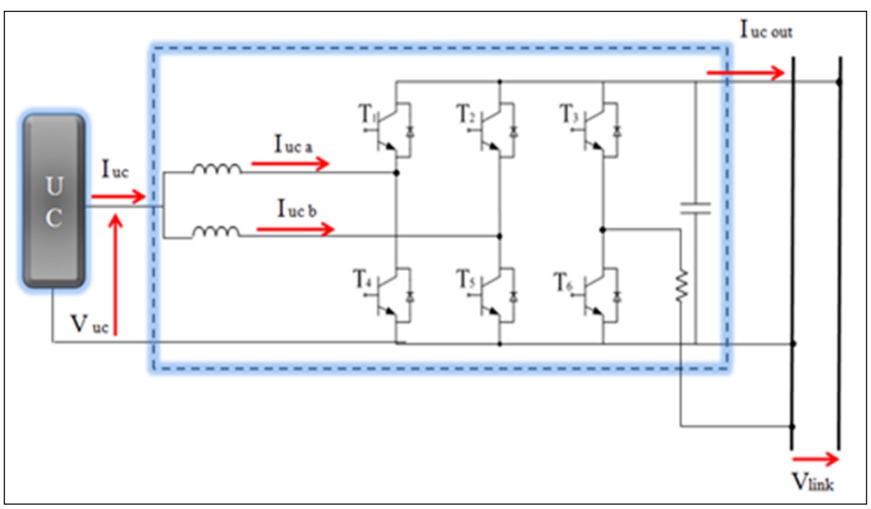

Fig. 2.15: Bidirectional dc-dc converter for UCs management

The dc-dc converter for the management of the storage system must be capable to adapt the level of the ultracapacitors voltage (variable) with that of the dc-link voltage (constant). It has to be necessarily bi-directional converter in configuration boost / buck (or step-up/step-down), which allows operation on two quadrants of the plane VI (voltage always positive and current positive or negative) and allows the possibility of energy recovery in the descending phase of the load (charging of ultracapacitors).

The DC-link voltage is imposed by the ac-grid voltage, as an uncontrolled diode rectifier is used:

$$V_{DC\_link} = \frac{3\sqrt{2}}{\pi} V_{rms\_grid} = \frac{3\sqrt{2}}{\pi} 380 = 513.17V$$

It is possible to determine the range of variation of the duty cycle of the dc-dc converter recalling the maximum and minimum voltage values of the ultracapacitors (V_{UC_max} = 500V, V_{UC_min} =250V) and the dc-linkvoltage (V_{DC_link} = 513V).

$$\delta = 1 - \frac{V_{UC}}{V_{DC\_link}}$$

The result is that the duty cycle has to be between 0.02 and 0.5.

To calculate the maximum current I_{UC_max} that can be supplied by the ultracapacitors, must be taken into account the worst case, when these are called to deliver the peak power in correspondence of their minimum state of charge. Known the I_{UC_max}, given the architecture of the dc-dc converter (two branches in parallel - Fig. 2.15), the current that circulates in each inductor is $I_L = 1/2\ I_{UC\_max}$. Having imposed the maximum current ripple as around 20% of the the nominal value, it can be written $\Delta I_L = 0.2\ I_L$.

To size the inductor and the capacitor of the bi-directional dc-dc converter, it has to be considered the operation of the dc-dc converter in the lifting phase (higher power condition). It is then possible to calculate the minimum inductance value of each branch of the dc-dc converter using the following equation:

$$L_{\min} = \frac{(1-\delta_{\max})\delta_{\max} V_{DC\_link}}{\Delta I_L \, f_{SW}}$$

where f_{SW} is the switching frequency.

Regarding the output capacitor of the dc-dc converter, the following equation has to be used:

$$C_{out\_\min} = \frac{\delta_{\max} I_{DC\_link}}{\Delta V_{DC\_link\_\max} \, f_{SW}}$$

where I_{DC_link} is the maximum output current delivered from the ultracapacitors and $\Delta V_{DC\_link\_max}$ is the maximum allowed dc-link voltage ripple (equals to 1% of the nominal value).

2.6 Ultracapacitors model

The elementary circuit model of an ultracapacitor is similar to the model of the batteries, constituted by a open-circuit OCV generator in series with an internal resistance. In this case the charge is accumulated only electrostatically and represent the scale of the phenomena is sufficient to adopt for the ultracapacitor a RC series model, in which the values of the resistor and capacity can be considered constant, Fig. 2.16. The state of charge is at the maximum lrvrl when the open circuit voltage corresponds to the maximum allowed. The company manufacturers provide the values of the capacity, maximum voltage and internal resistance of the component and the relative tolarances too.

The EPR represents the phenomenon of self-discharge, phenomenon by which an ulracapacitor left unconnected and charged at the maximum allowed voltage in a variable time between hours and days discharge completely. The E_{PR} / E_{SR} ratio can vary between 103 and 106. For this reason is reasonable to neglect the E_{PR} under normal operating conditions.

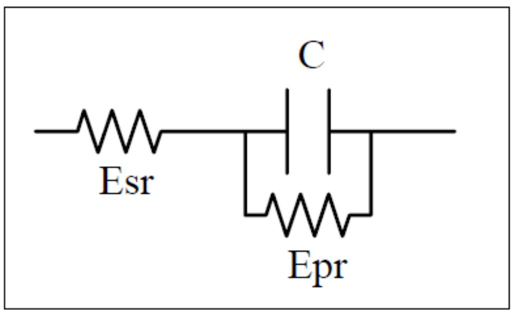

Fig. 2.16: Simplified model of the ultracapacitors

The equations used are as follows:

$$Q(t) = CV_{UC}(t)$$

$$V_{UC}(t) - I(t)R_{\text{int}} = E_{UC}(t)$$

where:

- C is the capacity of the condensator;
- Q(t) is the accumulated charge at time t;
- V_{UC} is the voltage of the ideal capacity;
- I(t) is the erogated current;

- R_{int} is the internal resistance of the device;
- E_{UC} is the voltage of the device, which equals E_{bt}.

The internal resistance of the capacitor, unlike that of the batteries, can be considered constant with the variation of the State Of Charge (SOC) , although degrades very slowly over time. Always differently from the batteries, the capacity of the capacitors does not depend on current output (or input) (Peukert Law). The current I(t) of the ultracapacitor, known the power P_{UC} to be erogated or to be absorbed, is derived from the expression:

$$I_{UC} = \frac{E_o - \sqrt{E_o^2 - 4P_{bt}R_b}}{2R_b}$$

and the looses are calculated from:

$$P = R_{\text{int}} I^2 .$$

Known the erogated power, the absorbed power and the looses, all the energetic verifications are possible. In particular it is possible to manage the system so that the final energy level of the accumulation is equal to the initial one, and then calculate the real energy consumption.

2.7 Ultracapacitors Sizing

The maximum operating voltage of the UCs (V_{UCmax}) has to be a value as near as possible to the value of the dc link (500V) in order to guarantee good performance for the UCs converter in terms of control reliability and efficiency. UCs show good performance as storage unit if used with a SOC (State of Charge) between 0.5 and 1; in fact, by further reducing the minimum SOC, discharging current grows exponentially without providing a significant increase in the available energy. In this way, even the minimum operating voltage (V_{UCmin}= V_{UCmax}/2 = 250V) is set as it corresponds to the UCs maximum discharge (minimum SOC).

Based on these two parameters (UCs maximum and minimum operating voltages) a module from Maxwell (part number: BMOD0063 P125) has been chosen. Its main characteristics are summarized in Table 3.

Table 3: UCs module main characteristics

Nominal voltage [V]	125
Nominal capacitance [F]	63
DC series resistance [mΩ]	18
Energy available [Wh]	101.7
Maximum continuous current [A]	150
Maximum current [A]	750
Weight [kg]	58
Size LxPxA [mm x mm x mm]	762 x 425 x 265

First of all, as the maximum operating voltage has been set to 500V, while the single UCs module has a nominal voltage of 125V, necessarily four modules have to be series connected. Accordingly, the resultant capacitance value (for each block made up of four series modules) is 12,6 F. In order to obtain the desired capacitance value, blocks have to be connected in a parallel configuration, as presented in Fig. 2.17.

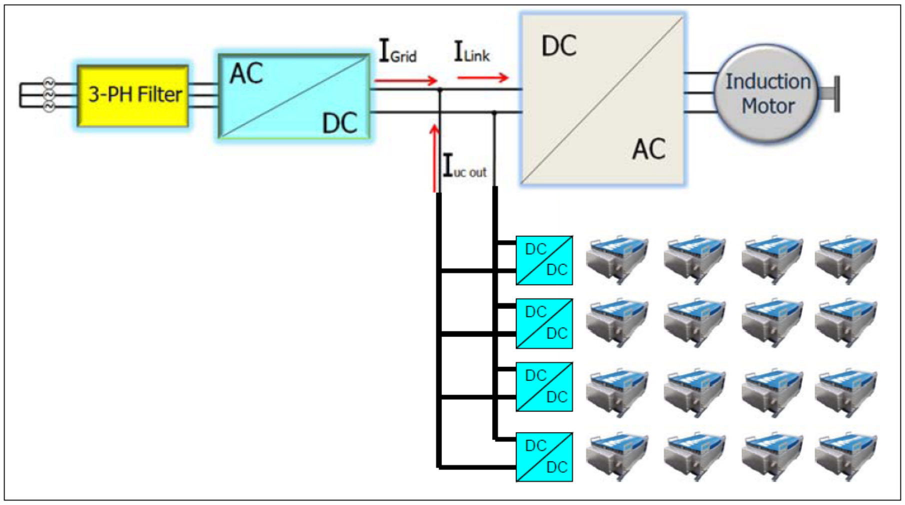

Fig. 2.17: Wiring diagram of the ultracapacitors

The maximum current that can be delivered from the single string is (Table 3) equals to 800 A, and therefore, being 250 V the minimum voltage of the bench which consists of 4 modules in series, each of the 4 required converters will have a nominal power of 200 kW. For the realization of the bi-directional dc-dc converter, IGBTs 1200V - 500A devices can be used for each of the three branches.

If ***E*** is the general energy, the corresponding UCs capacitance C is calculated accordingly to the following expression:

$$C = \frac{2\,E}{(V_{UCmax}^2 - V_{UCmin}^2)} \qquad (1)$$

Where V_{UCmax}=500Vdc and V_{UCmin} = $V_{UCmax}/2$ = 250V. To determine the capacitance C, the quantity of energy E has to be set.

Two approaches have been considered for the UCs sizing:

1. Energy during peak power ($E_1 = E_{peaks}$)
2. Energy during descending process ($E_2 = E_d$).

The first approach consists on considering only the energy spent during the power peaks of the overall proccess (lifting, rotation, translation and scroll). If the sum of the overall energy of the system dyring the power peaks is made, the value is: $E_1 = E_{peaks} = 2790$ kJ. That means:

$$C_{peak} = \frac{2\ E_{peaks}}{(V_{UCmax}^2 - V_{UCmin}^2)} = 29.75F \quad (2)$$

The second approach considers the energy related to the descending of the load (recharging process of the UCs – Fig. 2.7). In this case $E_2 = E_d = 5498$ kJ. That means:

$$C_d = \frac{2\ E_d}{(V_{UCmax}^2 - V_{UCmin}^2)} = 58.64F \qquad (3)$$

In the first case the UC modules that are to be mounted are at least 8 (two series in parallel, each serie 4 UC modules, resultant capacitance 31.5F) with an overall UC cost of 64k€.

In the second case the UC modules that are to be mounted are at least 16 (4 modules by 4 – overall capacitance 63F) with a total UC cost of at least 128k€.

By considering the first approach, the total cost of inserting the UC modules is smaller but the recovered energy amounted is smaller too comparing with the second approach, which is more expensive.

2.7 System modeling

The electric drive is speed controlled (in vectorial mode) with an inner current loop. The main control strategy considers that, by using a diode rectifier (not-controlled), the dc-link voltage is set. So, in UCs dc-dc converter, the voltage is set by the UCs state of charge (component side) and by the three-phase rectifier (DC-link side). As a result, it has to be necessarily current controlled. The current reference for the controller of UCs converter is computed as a rate of the dc-link current (provided or requested by the electric drive). Consequently, the electric grid always responds to the system by providing the difference between the dc-link current (requested or provided by the induction motor) and the UCs current (discharging or recharging UCs). In Fig. 2.18 and Fig. 2.19 is shown the system power flow, respectively, during the load lifting (UCs discharge) and during the load descending (recovering energy – UCs recharge).

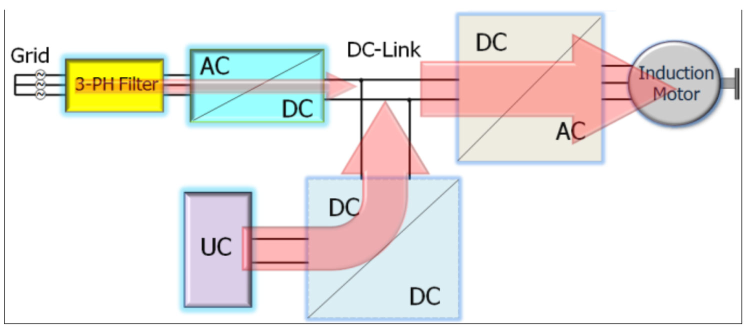

Fig. 2.18: Load lifting – UCs discharge

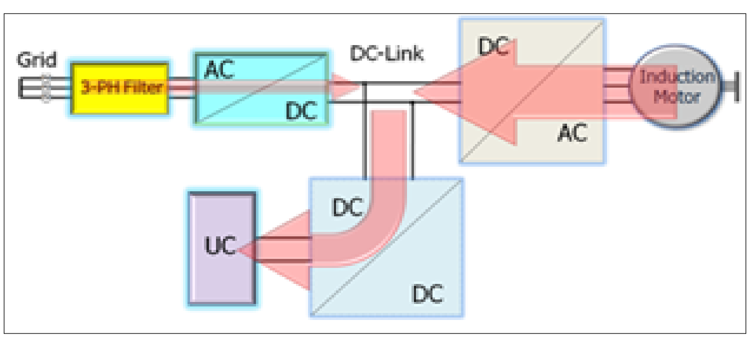

Fig. 2.19: Load descending – UCs recharge

To investigate the system behavior, a simulation model shown in Fig. **2.20** has been implemented on Simulink platform.

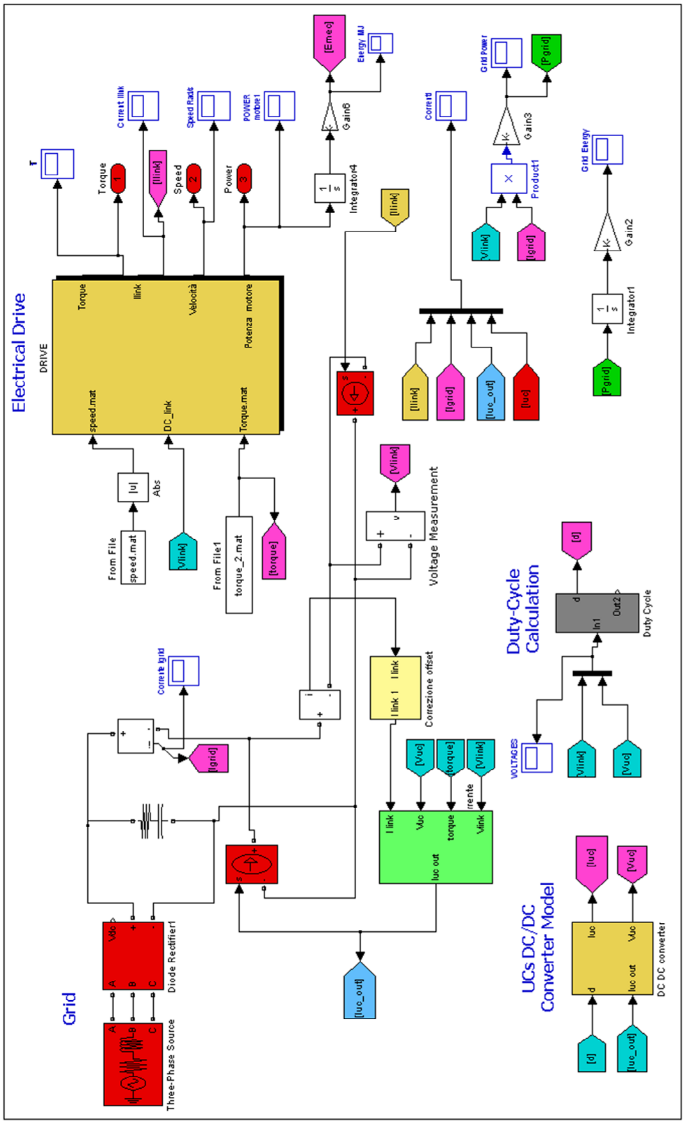

Fig. 2.20: Implemented simulation model

This simulation model includes:

- DC/DC Converter for the UCs bank.
- Converter's duty cycle calculation.

In Fig. 2.21 has been shown the control system of the crane drive, performed by PI regulators. It is made by the following subsystems:

- Crane drive, including the inverter, asynchronous motor, control algorithm performed with the DTC (Direct Torque Control) strategy to establish the commutation instants of the switching devices. For an introduction to DTC please refer to Appendix I.

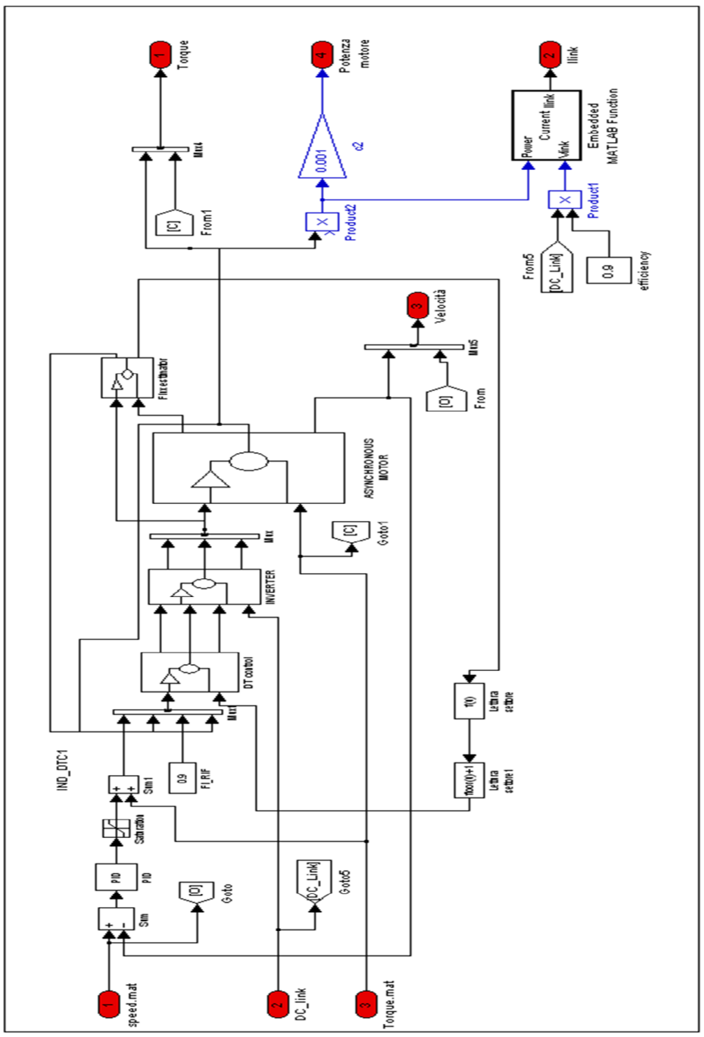

Fig. 2.21: Drive simulation model

In Table 4 are presented the simulation reference parameters.

Table 4: Simulation Reference Parameters

DC - link	500 V
UC's Max Voltage V_{uc_max}	500 V
UC's Max Voltage V_{uc_min}	250 V
Energy during Descending Process E_d	5498 kJ

2.8 Power Flow regulation strategy

For the overall characterization of the model, two different parameters have been defined. The first one is denoted with K and is called Grid Power Ratio. It indicates the Grid Power ratio between the the two processes, lifting and descending. The second parameter indicates the ratio between I_{uc_out} and I_{link}. In the lifting process it is called H, in the descending process it is called H_1.

2.8.1 K parameter definition

Let us define:

P_{Grid_L} → Grid Power during Lifting process (T_L)

P_{Grid_D} → Grid Power during Descending process (T_D)

Total time (Lifting+Descending) → $T = T_L + T_D$

Then K is defined as:

$$K = \frac{P_{Grid\_D}}{P_{Grid\_L}}$$

for $0 \leq K \leq 1$.

If K=0, it is taken power from the Grid just during the Lifting process. In this case the accumulation system (UC) has to be dimensioned to store only the energy recovered during the descending process (T_D).

If K=1, the Grid power during the total time T is constant. In this case the energy to be stored in the UCs is not only the energy recovered by the load descending but also the energy that flows from the Grid to the UC bank. This means that the energy to be stored is of a greater value compared to the case in which K=0.

The UC storage system has to be dimensioned in function of the energy that is recovered during the descending process for the case in which the Igrid that flows from the grid to the UCs is greater than zero (K>0).

2.8.2 H and H1 definition

Refering to Fig. 1, we define H and H_1 as:

$$H = \frac{I_{UC\_out}}{I_{Link}};\ 1\text{-}H = \frac{I_{Grid}}{I_{Link}}\ \text{ for } I_{Link} > 0 \ \ (\text{Lift})$$

$$H_1 = \frac{I_{UC\_out}}{I_{Link}};\ 1\text{-}H_1 = \frac{I_{Grid}}{I_{Link}}\ \text{ for } I_{Link} \le 0 \ \ (\text{Descend})$$

where I_{Link} is defined as $I_{Link} = I_{UC\_out} + I_{Grid}$, $0 \le H \le 1$ and $1 \le H_1 \le 2$.

In the following figures the parameters defined as “current” are those calculated by the simulation model, the parameters defined as “reference” are the input parameters of the simulation model.

2.8.3 H_1 and K regulation

To obtain the value of H_1 the procedure is as follows:

1. Obtain by simulation the energy $E_{tot} = E_{Link\_L}$ drawn from the Grid during the Lifting of the load for C_{UC}=0 F (the UCs do not intervene). In our case this energy equals to 2.6 kWh.

2. Calculate the energy E_{REC} that can be recovered during the descending of the load, multiplied by the mechanical efficiency.

$$E_{REC}[kWh] = \frac{m \cdot h \cdot g}{3600} \cdot \eta_{mec} \cdot \eta_{UC}$$

   where m=69T is the weight of the load, h=10m its height, g=9.81m/s^2 is the acceleration of gravity, η_{mec}=0.82 is the mechanical efficiency and η_{UC}=0.9 is the UC's DC/DC converter efficiency. So, the recovered energy available for the recharge of the UCs is 1.4 kWh.

3. Calculate the minimum energy drawn from the grid:

$$E_{Grid\_\min} = E_{tot} - E_{REC}$$

   E_{Grid_min} equals to 1.2 kWh.

4. Set K=1. We define I_{Grid_L} as I_{Grid} during the Lifting process and I_{Grid_D} as I_{Grid} during the Descending process. Set a value for H_1 and H ((2) and (3) formulas) so that $I_{Grid\_L} = I_{Grid\_D}$. Perform simulation. If the simulated $E_{Grid} < E_{Grid\_min}$, change the value of H_1 and H and reperform simulation until $E_{Grid} = E_{Grid\_min}$.
   The final values are H_1=1.3, H = 0.8.

5. Use the value of H_1 found in the previous point to perform simulation for different values of K (the value of H will change too, if the value of K changes).

6. If it is decided that the energy used to recharge the UCs is only the recovered energy during the load descending (P_{Grid_D}=0, H_1=1), that is K = 0, than the value of H must be varied so that the energy drawn from the Grid during lifting equals E_{Grid_min}.

In Fig. 2.22 is shown the flowchart which summarized the regulation strategy presented previously.

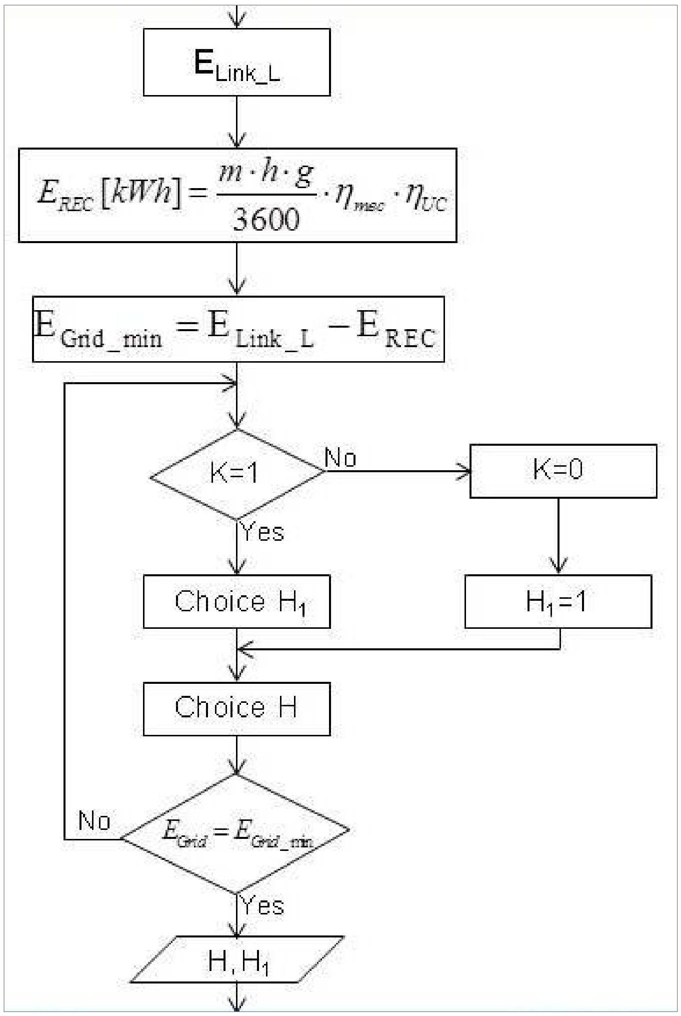

Fig. 2.22: Regulation strategy flow chart

2.9 Gantry crane model wilth UC storage

The model of the system shown in

Fig. **2.20** and Fig. 2.21 has been used to study the ultracapacitors accumulation dynamics applied to the 50 T gantry crane shown in Fig. 2.5 and in the Table 2. In Fig 36 is shown the layout of such a system, in which the electrical quantities that will be studied have been identified.

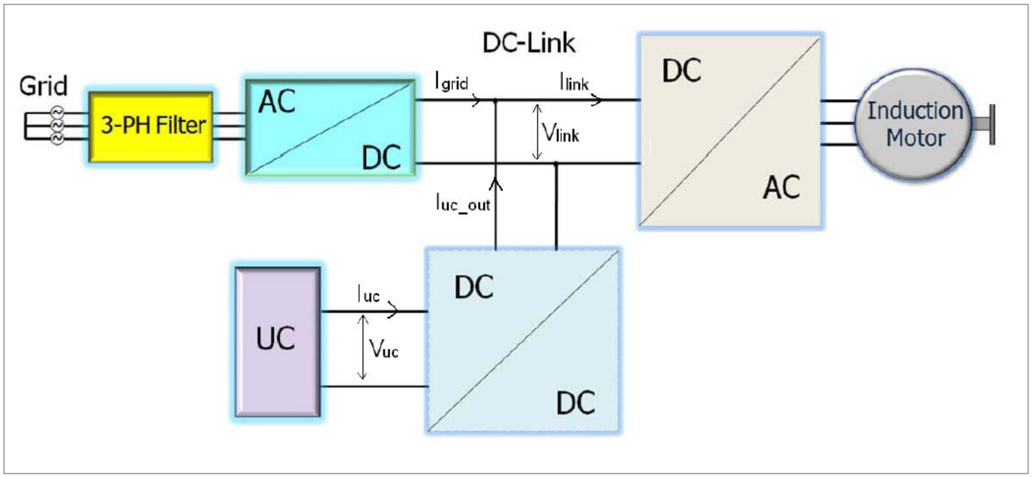

Fig. 2.23: Drive diagram

Before showing the results, some quantities and coefficients needed for the calculation program written in matlab-simulink related to the system are described.

The simulation parameters are:

- “Start Time” = 0 sec;
- “Stop Time” = 60 sec;
- “Solver Options” : “Type”= Fixed step ;
- “Solver”= Ode2;
- “Fixed Step Size” = 0.00002 sec.

Ultracapacitors model:

- Resistance = 0.018 Ω;

- Capacity = 63 F;

Speed loop PID regulator parameters:

- K_p = 10;
- K_i = 1;
- K_d = 0;

50T gantry crane drive parameters:

- Asynchronous motor nominal power P= 350 kW ;
- Asynchronous motor Moment of Inertia J = 1.3260;
- Self-inductance of the rotor windings L_r = 0.0068 H;
- Self-inductance of the stator windings L_s = 0.0069 H;
- Mutual-inductance M = 0.0066 H;
- Number of pole-pairs p = 4;
- Rotor resistance R_r = 0.0032 Ω;
- Stator resistance R_s = 0.0014 Ω;
- DC-link voltage V_{DC} = 500 V;
- Traction drive efficiency η = 82 %.

2.10 Experimental validation of the model

In order to perform the validation of the simulation model, the usage of a gantry crane with nominal power of 350kW and the consequent purchase of the UCs bank would have been very expensive. So, a bridge crane with a nominal 22kW power, coupled with a UC bank with a total capacitance of C=63F (two series in parallel, each serie two

UC modules), which is located at the ENEA laboratories (Fig. 2.24), was used as a gatry crane.

The linearity condition of the system was imposed. In this way, it is supposed that the behavior of both simulated system and real scaled system is the same. The scale ratio between the power of the simulated system (350 kW) and the real system (22kW) is 1:16.

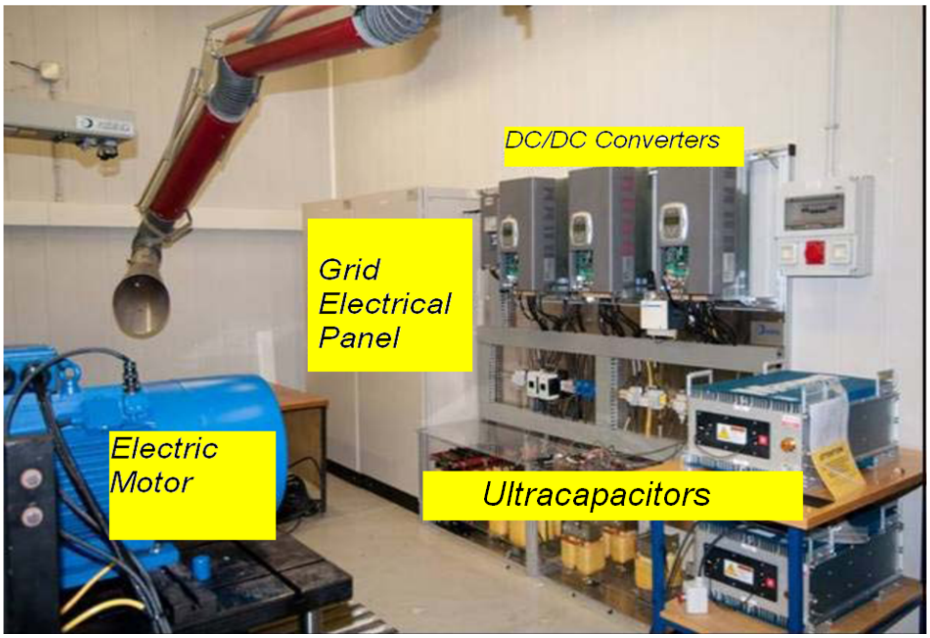

Fig. 2.24: Lifting prototype of Ultracapacitors Storage system

The drive parameters of the test nbridge crane under consideration are:

Table 5: Test Drive parameters

Induction Motor Nominal Power **P**	**22 kW**
Induction Motor Moment of Iinertia **J**	**0.096 $kg\,m^2$**
Induction Motor Nominal Speed ***v***	**152 rad/s**
Induction Motor Nominal Torque	**145 Nm**

T	
Induction motor **pole pairs**	**2**
DC link Voltage	**380 V**
Mecchanical efficiency η_{mec}	**0.9**
UCs Dc/Dc converter efficiency η_{UC}	**0.9**

Starting from the characteristics of the system, reference cycles have been developed, which would allow the available drive to operate (in reduced scale compared to the real system) both in conditions of high and low performance in order to validate with the maximum reliability the parameters to be introduced in the model of the real system.

To perform significant test, it was first created a basic cycle and then it is modified in order to highlight the behavior of the system.

It is first described the basic cycle and then the changes performed on it.

The basic cycle is made of the lifting, the translation and the descending of a 7 tons load, which is considered as the maximum capacity of the system. It corresponds to a maximum continuous power request from the traction motor shaft of 12.5 kW during lifting and 7.8 kW during descending.

Actually the power converters and motor available to us is superior to that choice (20 kW ed.). With this choice, however, all the test bench works optimal under conditions: increase of the load implies a redefinition of the control parameters, operation feasible but not important for the purposes of work. In fact working with a nominal power of 12.5 kW, the whole system works, however, with high-efficiency and performance improvements achievable by increasing the traction power are mainly in the motor, but are relative and not relevant to the real purpose of the tests.

The basic cycle is the following:

1. Minimum power phase: duration 5 sec;
2. Pause: duration 40 sec;
3. Lifting:
   - Torque = 80 Nm;
   - Motor speed = 152 rad/s;
   - Duration = 40 sec;
4. Pause: duration = 40 sec;
5. Descending:
   - Torque = -50Nm;
   - Motor speed = 152 rad/sec;
   - Duration = 40 sec;
6. Pause = 40 sec;
7. Repetition of phase 2-6.

The following graphs show the torque / speed and power profiles for the considered cycle:

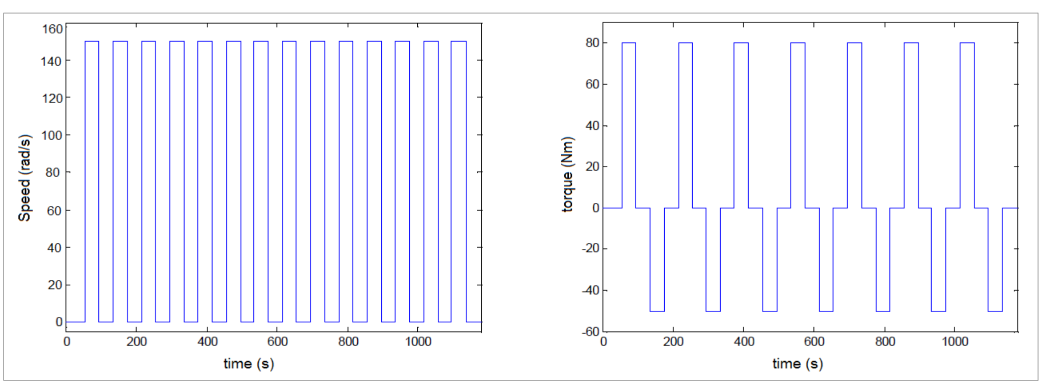

Fig. 2.25: Motor speed and torque in function of time

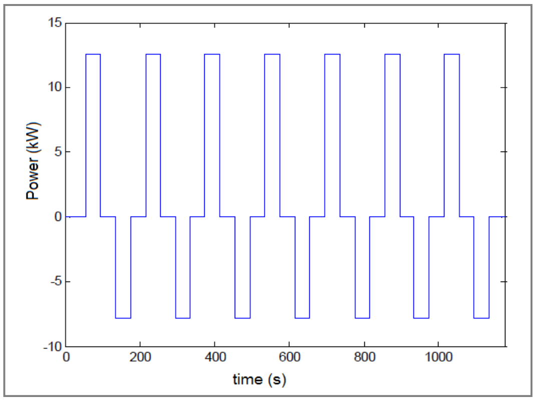

Fig. 2.26: Motor drive power in function of time

Two different work cycle will be presented.

1. "Light Load" cycle which has a running torque of 50 Nm during the lifting process.
2. "Heavy Load" cycle which has a running torque of 80 Nm during the lifting process.

The speed profile for both cycle is the same.

2.12.1 Light load cycle

From Fig. 2.27 to Fig. 2.29 are shown the measured voltages, currents and power of the motor for the Light load cycle.

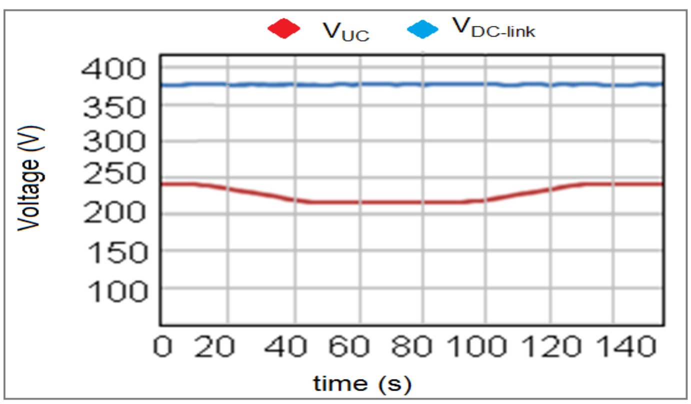

Fig. 2.27: Light load cycle measured voltages vs time

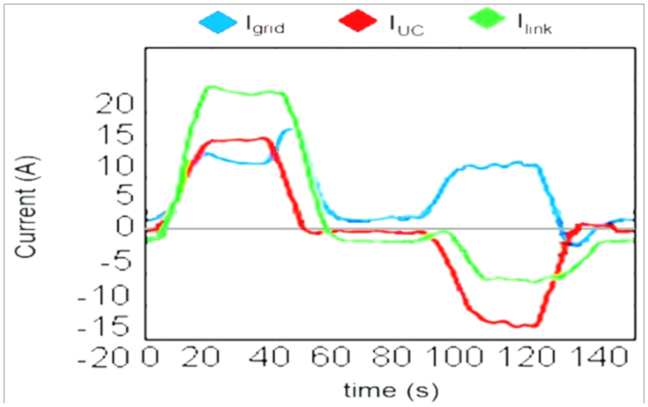

Fig. 2.28: Light load cycle measured currents vs time

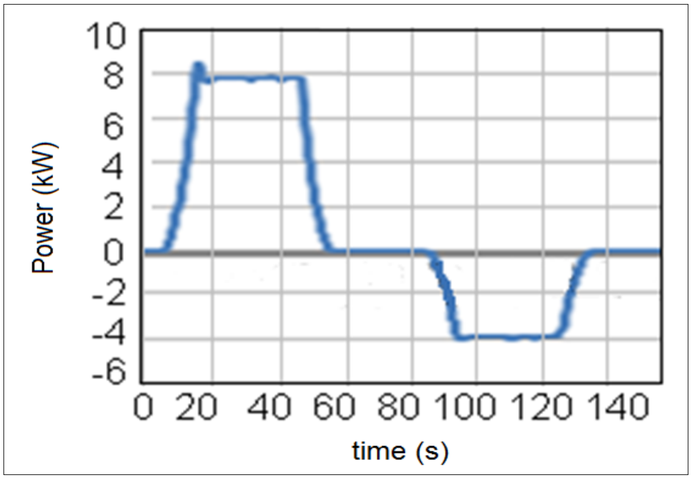

Fig. 2.29: Light load cycle measured motor power demand vs time

The Light load cycle simulation parameters are:

Table 6: Simulation parameters for the Light Load cycle

$\mathbf{V_{UCmax}}$	240 V
$\mathbf{V_{UCmin}}$	219 V
H	0.6
$\mathbf{H_1}$	1.3
K	0.8

From Fig. 2.30 to Fig. 2.31 are shown the simulated power, speed, torque, voltages and currents for the Light Load cycle.

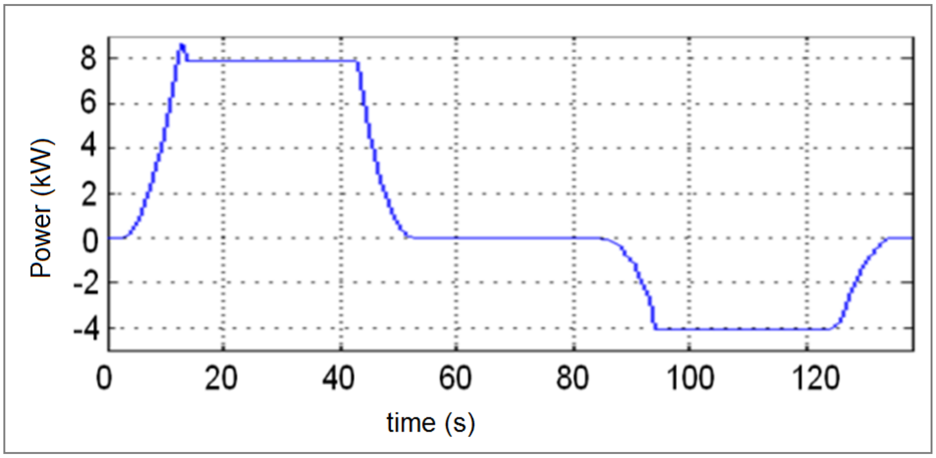

Fig. 2.30: Light load cycle SIMULATED motor power demand vs time

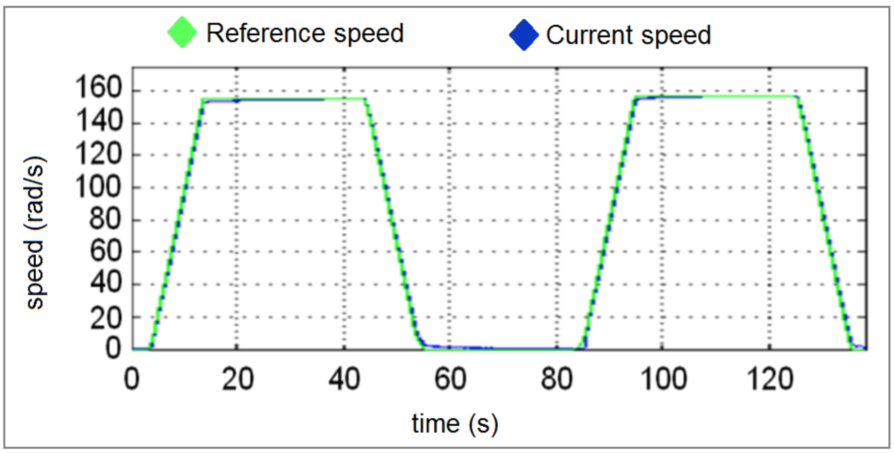

Fig. 2.31: Light load cycle SIMULATED speed vs time

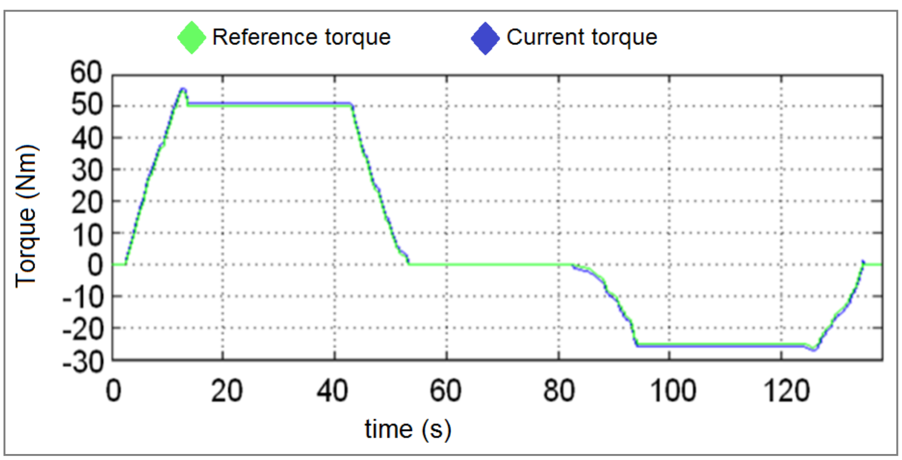

Fig. 2.32: Light load cycle SIMULATED torque vs time

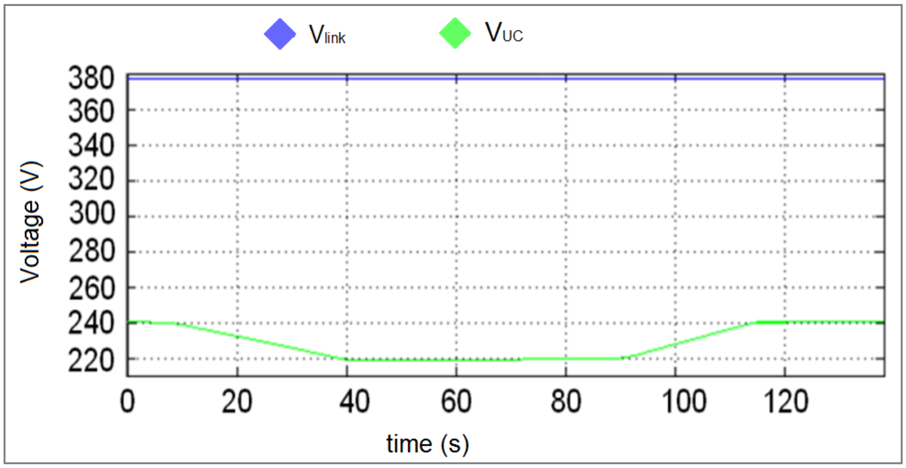

Fig. 2.33: Light load cycle SIMULATED voltages vs time

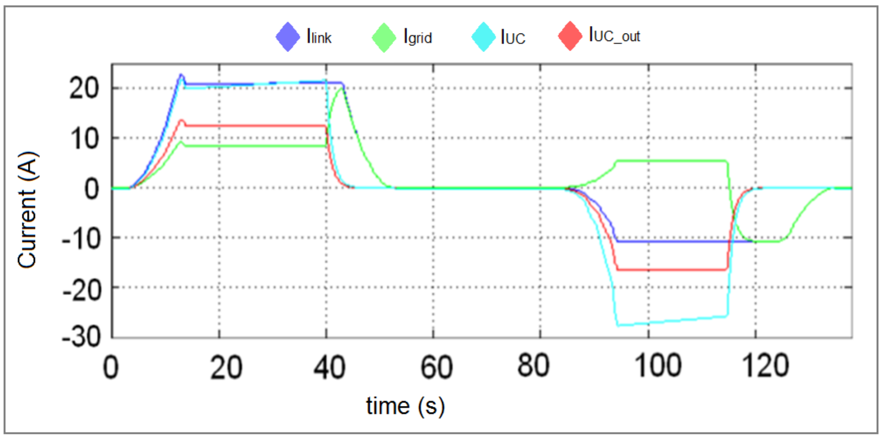

Fig. 2.34: Light load cycle SIMULATED currents vs time

I_{Grid} and I_{UC}_out quantities depends on the control parameters. The only parameter that is independent from the control parameters is I_{Link}. This is the reason why only measured and simulated I_{link} have been plotted in the same graph.

In Fig. 2.35 is shown the comparison between the measured (red trace) and the simulated (blue trace) I_{Link}. As it can be seen, there is a good match between the two quantities.

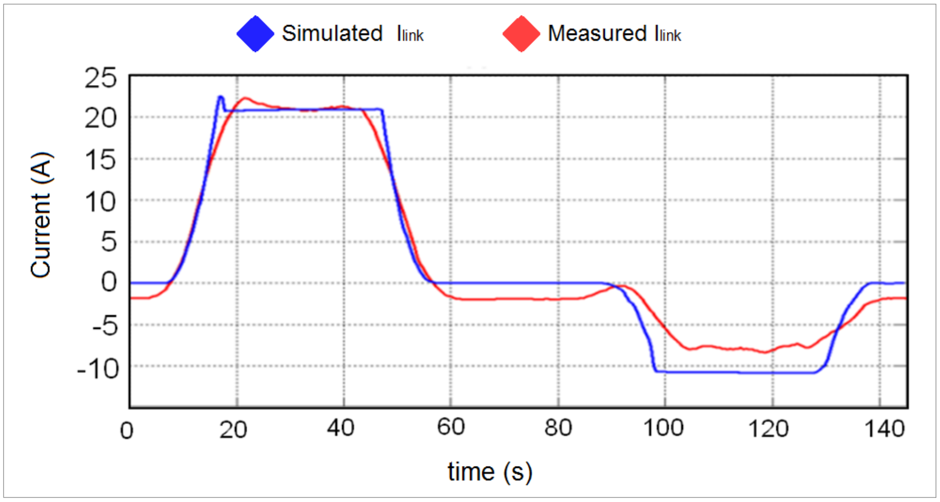

Fig. 2.35: Light load cycle – comparison between simulated and measured I_{link}

2.12.2 Heavy load cycle

From Fig. 2.36 to Fig. 2.38 are shown the measured voltages, currents and power of the motor for the Heavy load cycle.

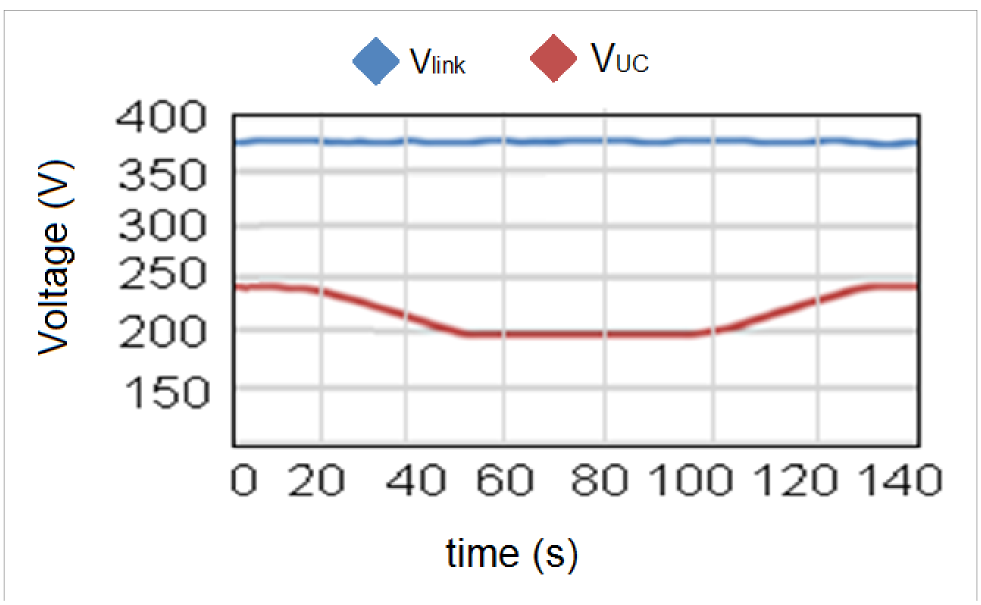

Fig. 2.36: Heavy load cycle measured voltages vs time

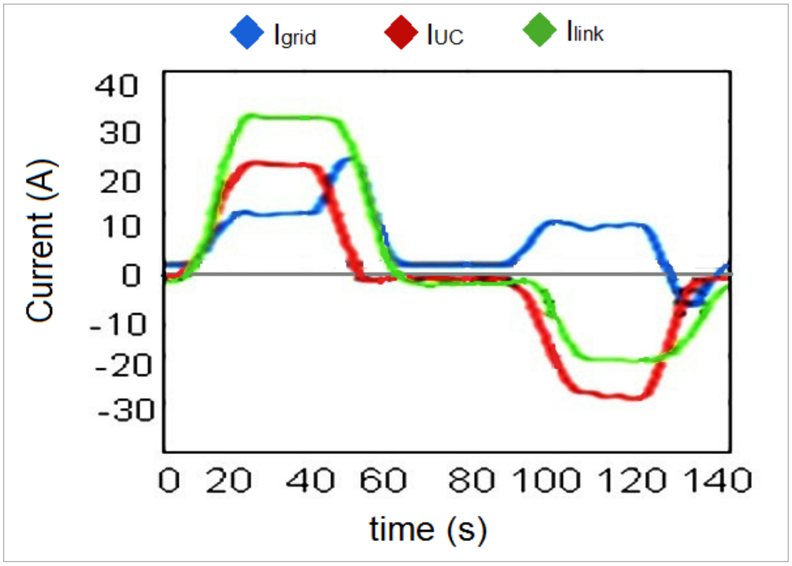

Fig. 2.37: Heavy load cycle measured currents vs time

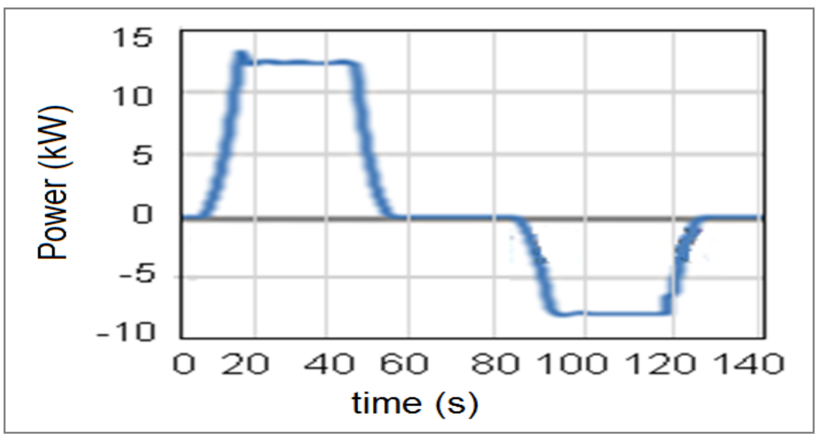

Fig. 2.38: Heavy load cycle measured motor power demand vs time

The Heavy load cycle simulation parameters are:

Table 7: Simulation parameters for the Heavy Load cycle

$\mathbf{V_{UCmax}}$	240 V
$\mathbf{V_{UCmin}}$	200 V
H	0.7
$\mathbf{H_1}$	1.3
K	0.8

From Fig. 2.39 to Fig. 2.42 are shown the simulated power, torque, voltages and currents for the Heavy Load cycle. The Speed profile is identical to that shown in Fig. 2.31.

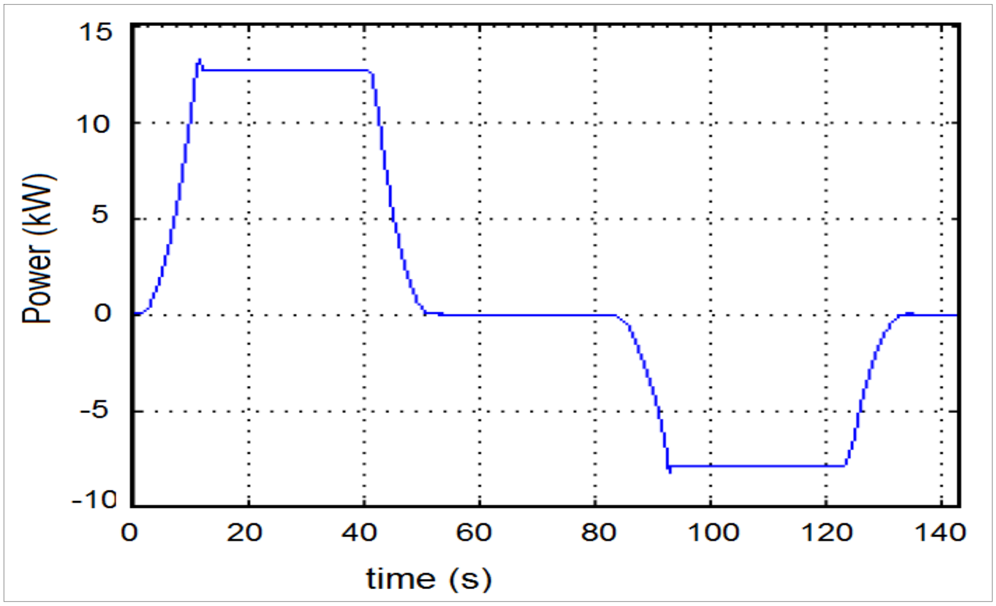

Fig. 2.39: Heavy load cycle SIMULATED motor power demand vs time

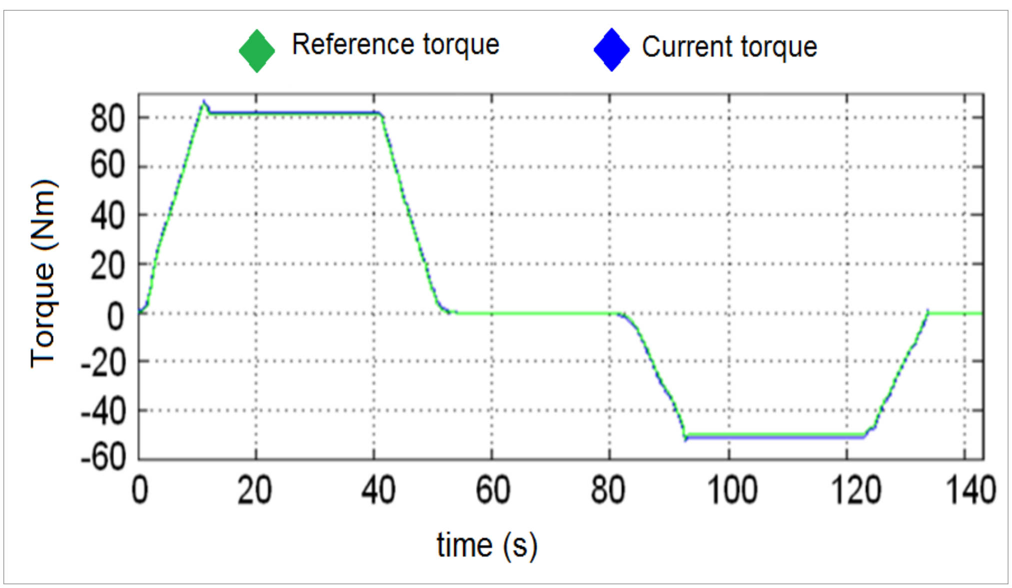

Fig. 2.40: Heavy load cycle SIMULATED torque vs time

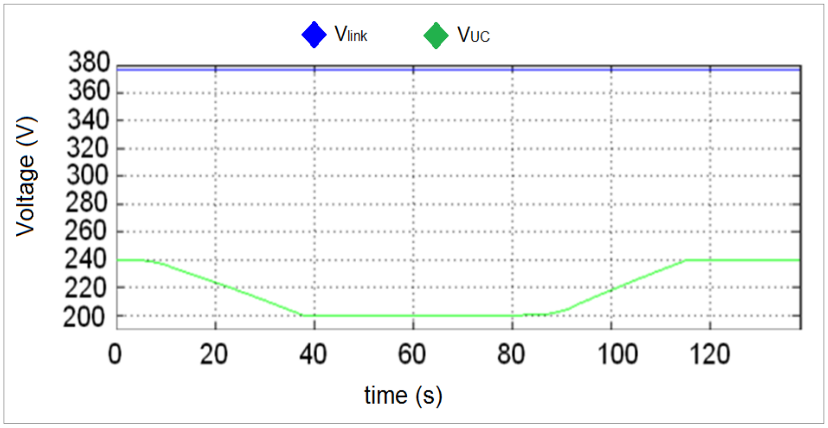

Fig. 2.41: Heavy load cycle SIMULATED voltages vs time

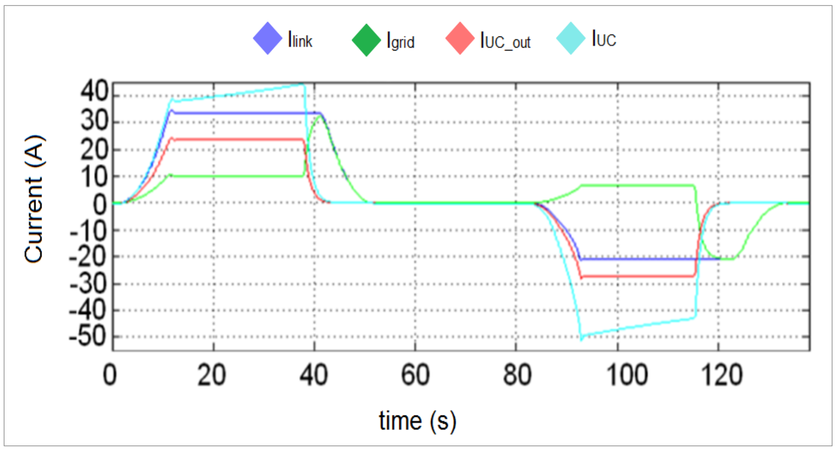

Fig. 2.42: Heavy load cycle SIMULATED currents vs time

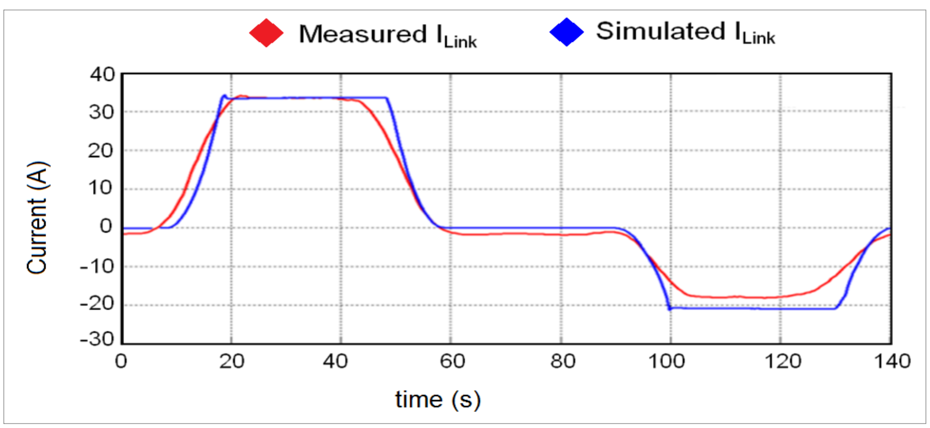

Fig. 2.43: Heavy load cycle – comparison between simulated and measured I_{link}

In Fig. 2.43 is shown the comparison between the measured (red trace) and the simulated (blue trace) I_{Link}. As it can be seen, there is a good match between the two quantities.

2.13 Simulation Results

The performed simulations are summarized in the following table:

Table 8: Simulation cases

	Parameters	***Description***
Case 1	K=0 C=63F, H=0 H_1=1	Reference case, no energy recovery
Case 2	K=0 C=63F H=0.6 H_1=1	Pgrid =0, i.e. . the grid supplies power only throughout the descending phase
Case 3	K=0.5 C=63F H=0.6 H1=1.3	The grid supplies power throughout the whole cycle
Case 4	K=1 C=63F, H=0.8 H_1=1.3	The grid supplies power throughout the whole cycle, power is constant and equal to the average requested power
Case 5	K=1 C=75.78F, H=0.8 H_1=1.3	The grid supplies power throughout the whole cycle, power is constant and equal to the average requested power. Supercapacitor capacity is increased.

For each simulation case simulation detaglied simulation results are presented.

From Fig. 2.44 to Fig. 2.49 case 1 (K=0, C=63F, H=0, H_1=1) simulation results are presented.

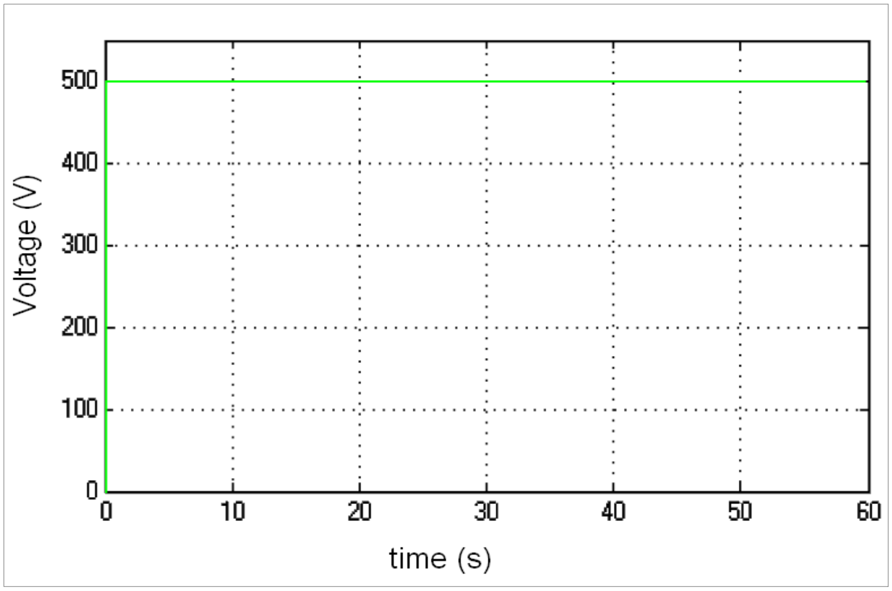

Fig. 2.44: DC-link Voltage vs time for K = 0, C = 63F, H = 0; H_1 = 1.

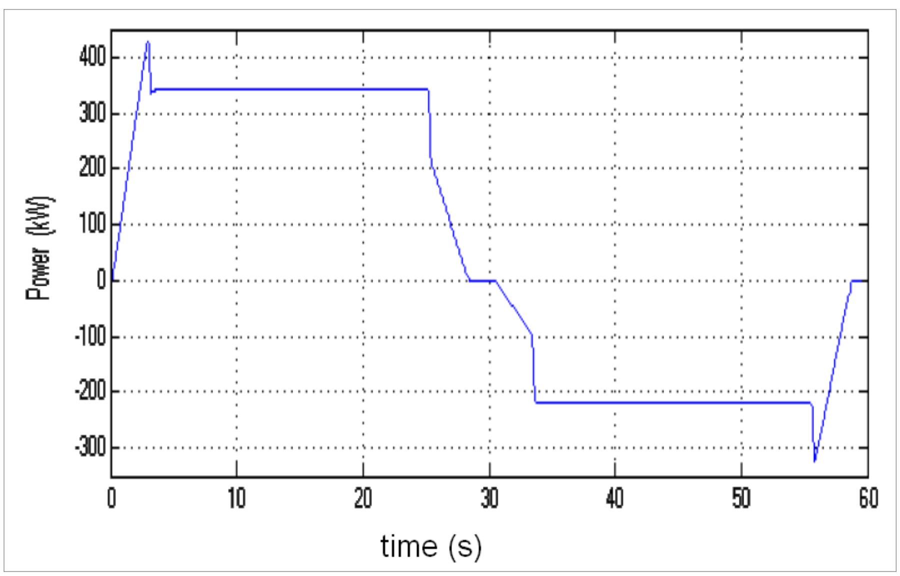

Fig. 2.45: Traction motor simulated power demanded vs time for K = 0, C = 63F, H = 0; H_1 = 1.

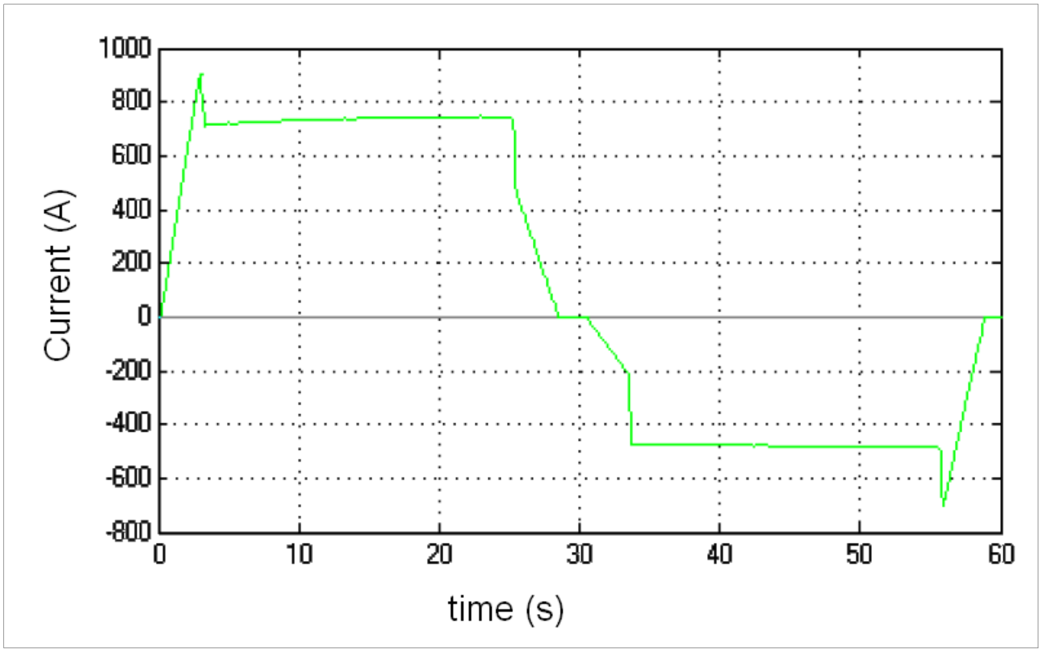

Fig. 2.46: Grid current Igid vs time for K = 0, C = 63F, H = 0; H_1 = 1.

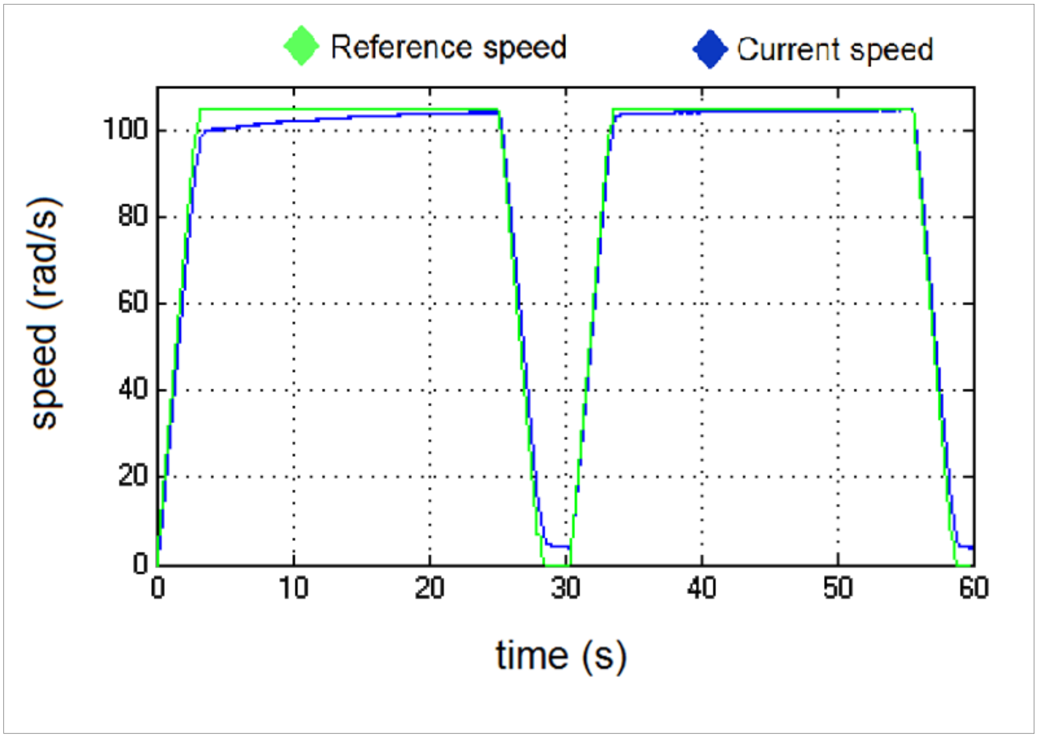

Fig. 2.47: Traction motor shaft speed vs time for K = 0, C = 63F, H = 0; H_1 = 1.

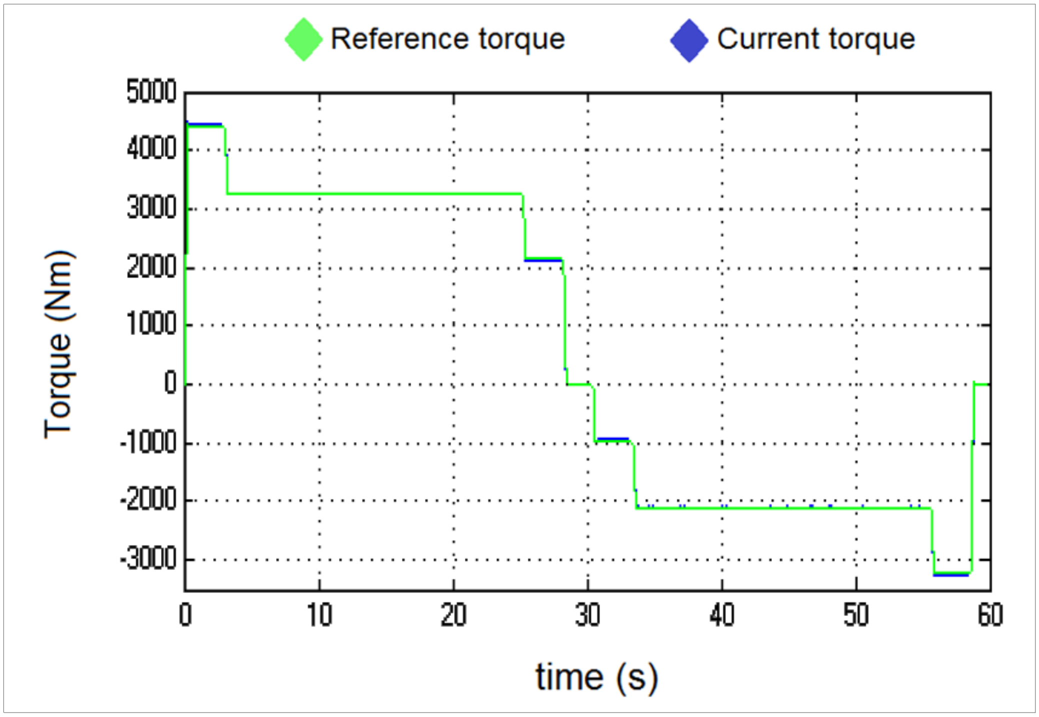

Fig. 2.48: Motor Reference and current Torque vs time for $K = 0$, $C = 63F$, $H=0$; $H_1=1$.

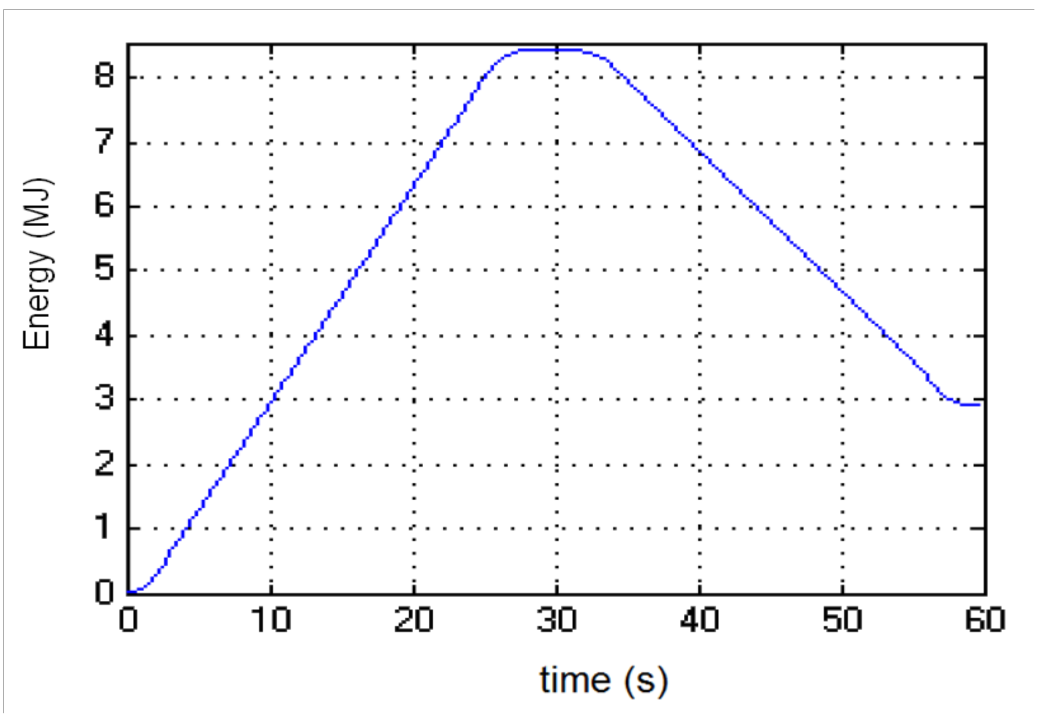

Fig. 2.49: Energy flow for $K = 0$, $C = 63F$, $H=0$; $H_1=1$

The speed, torque, power and Energy tracks are in common with all the simulated cases.

From Fig. 2.50 to Fig. 2.51 case 2 (K=0, C=63F, H=0.6, H_1=1.3) simulation results are presented.

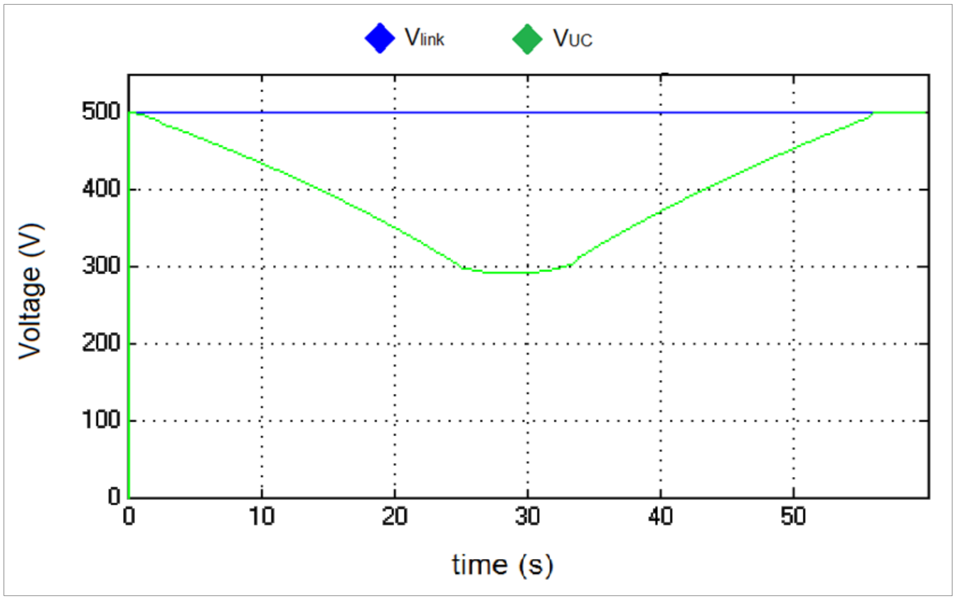

Fig. 2.50: Simulated voltages for K=0, C=63F, H=0.6, H_1=1.3.

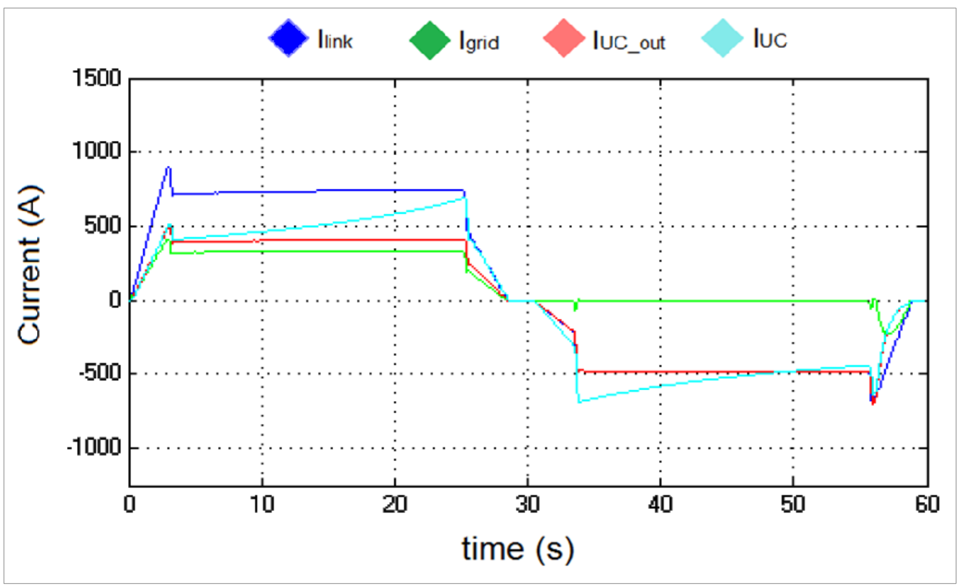

Fig. 2.51: Simulated currents for K=0, C=63F, H=0.6, H_1=1.3.

From Fig. 2.52 to Fig. 2.53 case 3 ($K=0.5$, $C=63F$, $H=0.6$, $H_1=1.3$) simulation results are presented.

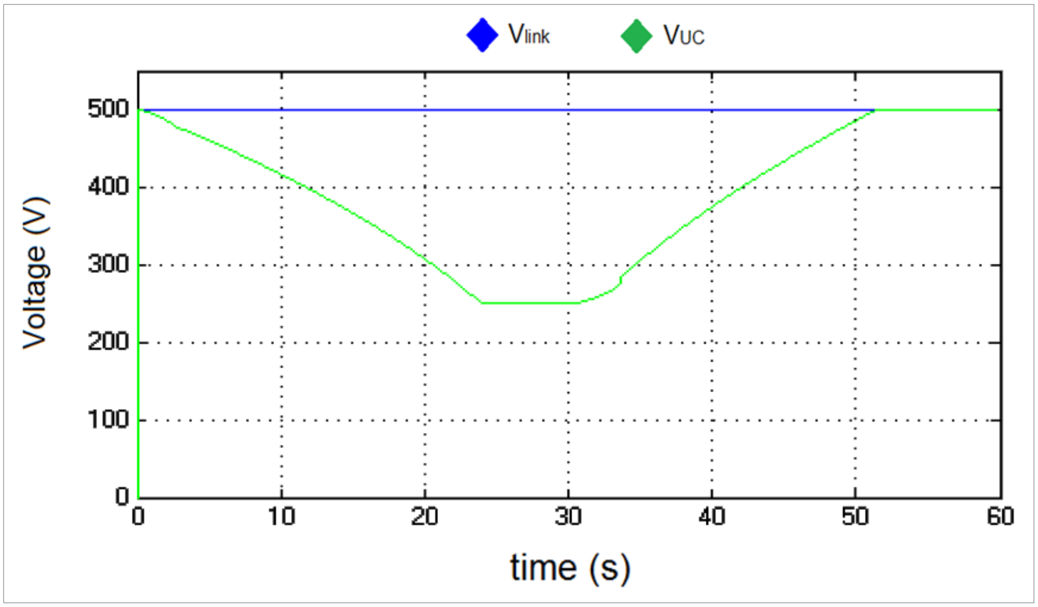

Fig. 2.52: Simulated voltages for $K=0.5$, $C=63F$, $H=0.6$, $H_1=1.3$.

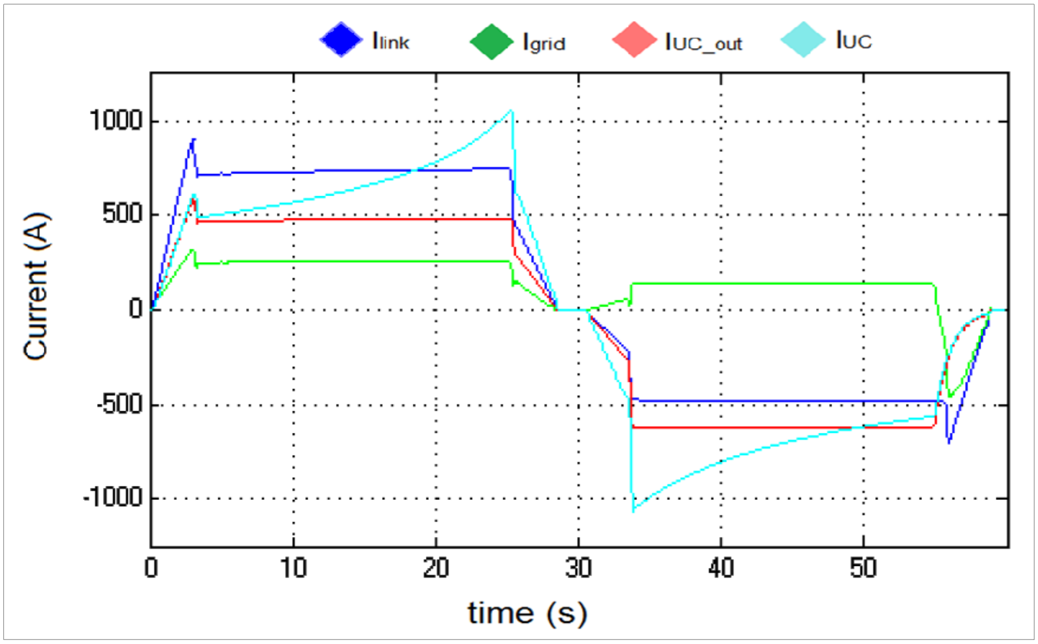

Fig. 2.53: Simulated currents for $K=0.5$, $C=63F$, $H=0.6$, $H_1=1.3$.

From Fig. 2.54 to Fig. 2.55 case 4 (K=1, C=63F, H=0.8, H_1=1.3) simulation results are presented.

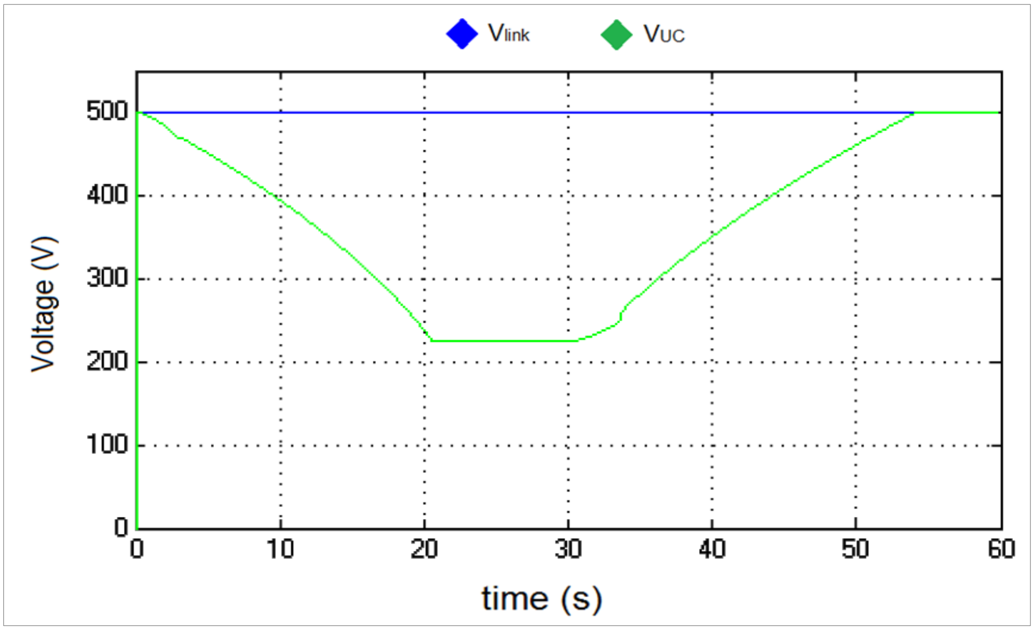

Fig. 2.54: Simulated voltages for K=1, C=63F, H=0.8, H_1=1.3.

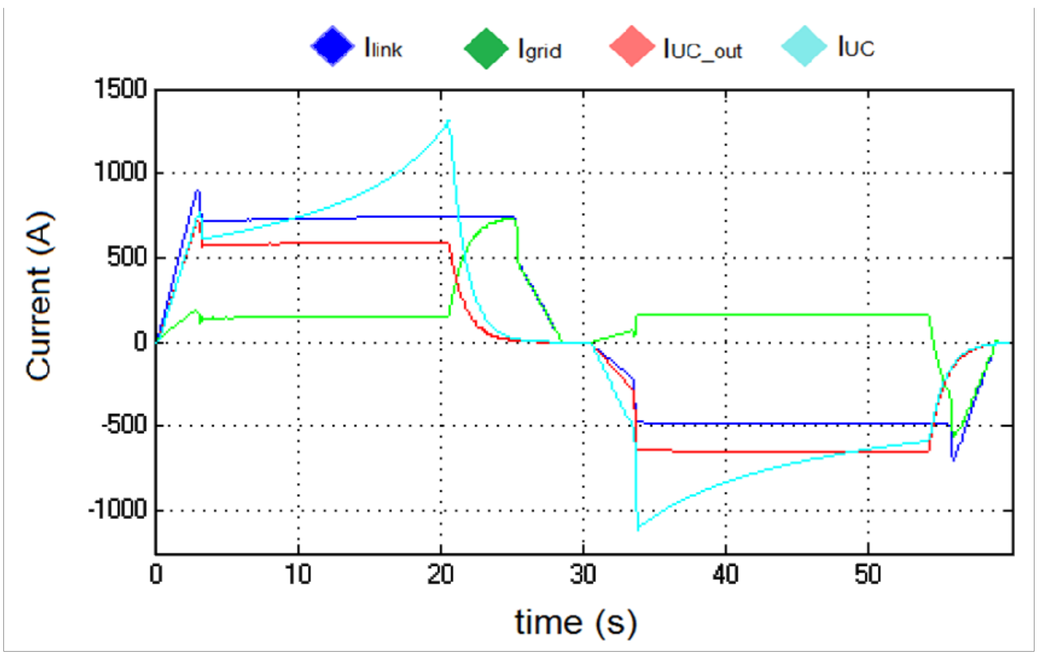

Fig. 2.55: Simulated currents for K=1, C=63F, H=0.8, H_1=1.3.

It can be observed in Fig. 2.55 that the ultracapacitors current I_{UC} is reduced to zero before the end of descending phase. This is due to the fact that the capacitor is completely charged before the descending phase finishes (Fig. 2.54), and about one-third of the energy can not be stored. If you want to store all the descending energy in the ultracapacitors storage facility, having imposed the value of K to unity, it is necessary to increase the capacity of the storage system.

Below is presented the last simulation case considered, with the capacity of the ultracapacitors increased to 75.78 F.

From Fig. 2.56 to Fig. 2.57 case 5 (K=1, C=75.78F, H=0.8, H_1=1.3) simulation results are presented.

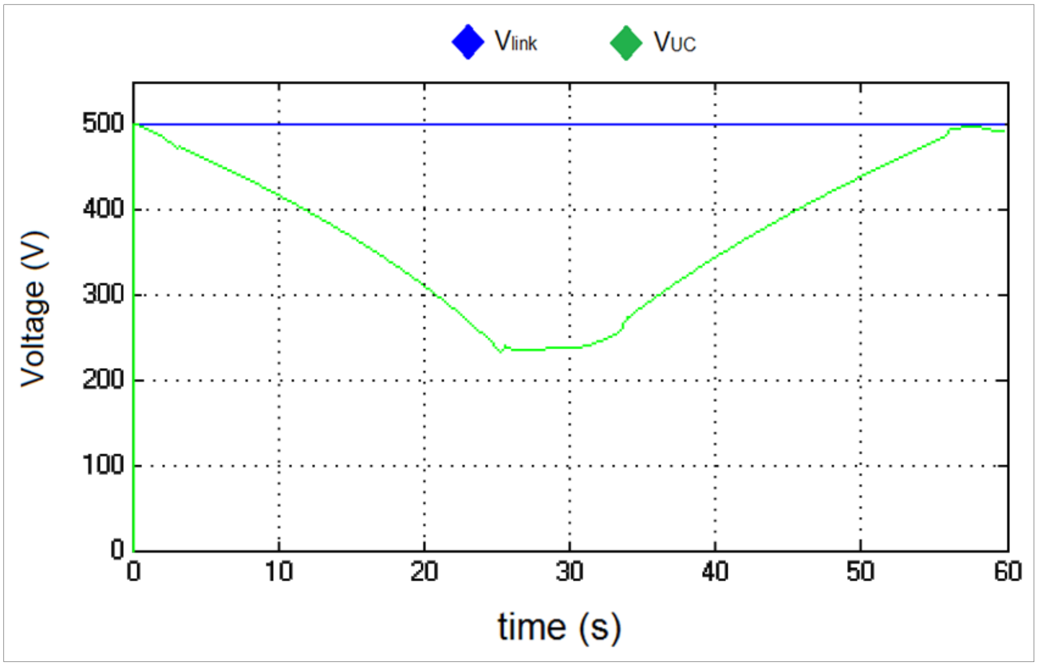

Fig. 2.56: Simulated voltages for K=1, C=75.78F, H=0.8, H_1=1.3.

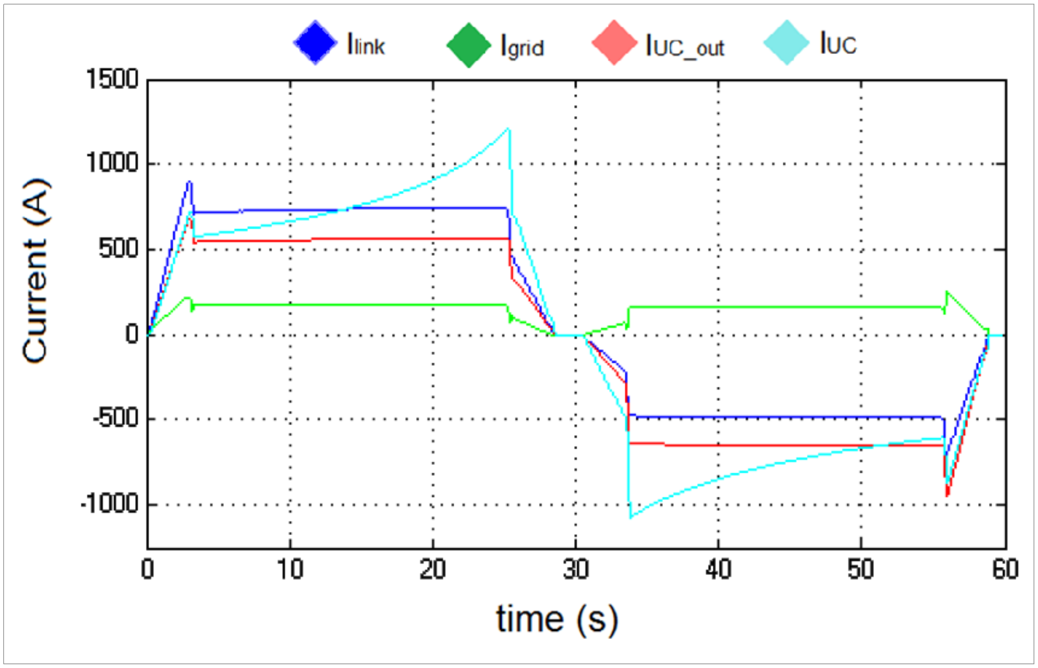

Fig. 2.57: Simulated currents for K=1, C=75.78F, H=0.8, H_1=1.3.

In the following table are shown the maximum grid power consumption P_{max_grid} and the energy per cycle E_{grid} drawn from the grid:

Table 9: Maximum grid power and energy grid per cycle

	P_{max_grid} [kW]	E_{grid} [kWh]
Case1	370	2.6
Case 2	150	1.2
Case 3	125	1.3
Case 4	70	1.4
Case 5	58	1.25

For each of the five cases considered, in the figures below are presented the profiles of power and energy drawn from the grid.

From Fig. 2.58 to Fig. 2.59 are presented the grid power and grid energy for case 1 (K=0, C=63F, H=0, H_1=1).

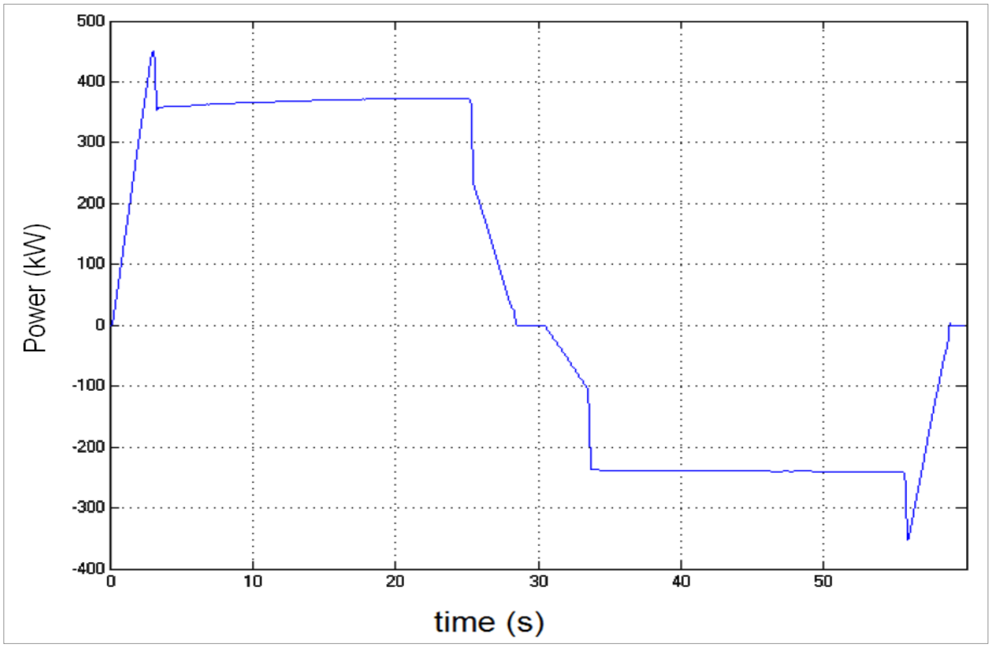

Fig. 2.58: Simulated power grid for K=0, C=63F, H=0, H_1=1

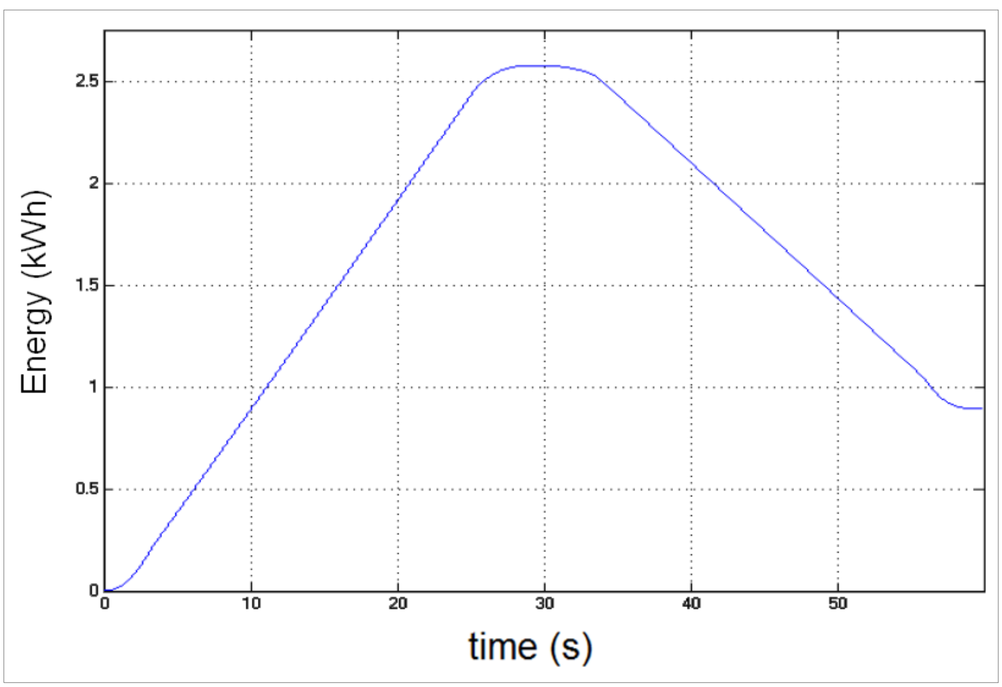

Fig. 2.59: Simulated energy grid for K=0, C=63F, H=0, H_1=1

From Fig. 2.60 to Fig. 2.61 are presented the grid power and grid energy for case 2 (K=0, C=63F, H=0.6, H_1=1).

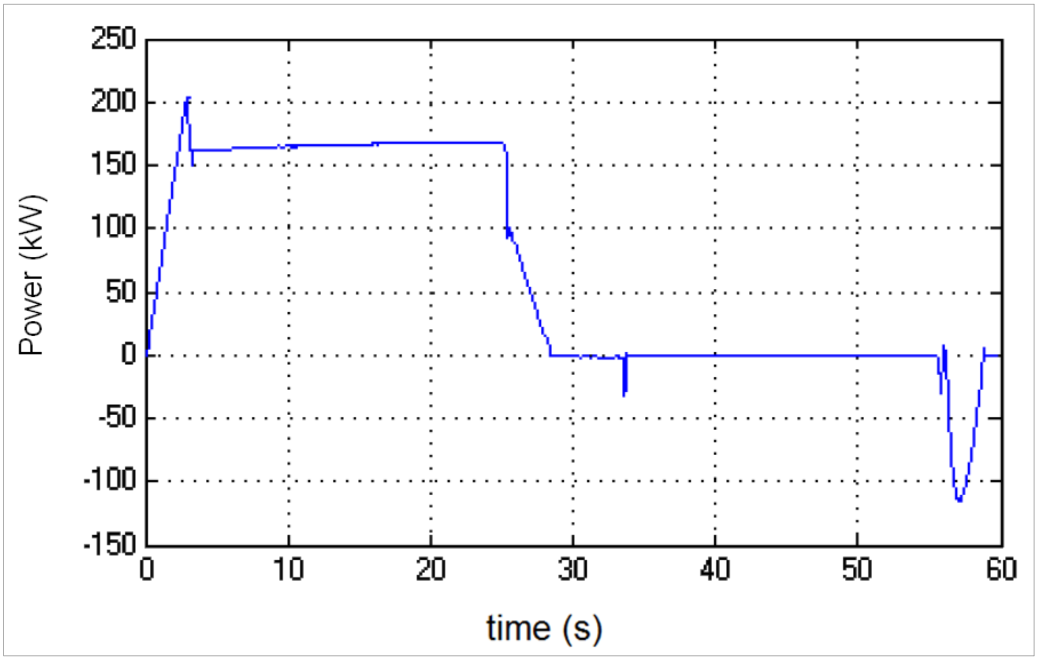

Fig. 2.60: Simulated power grid for K=0, C=63F, H=0.6, H_1=1

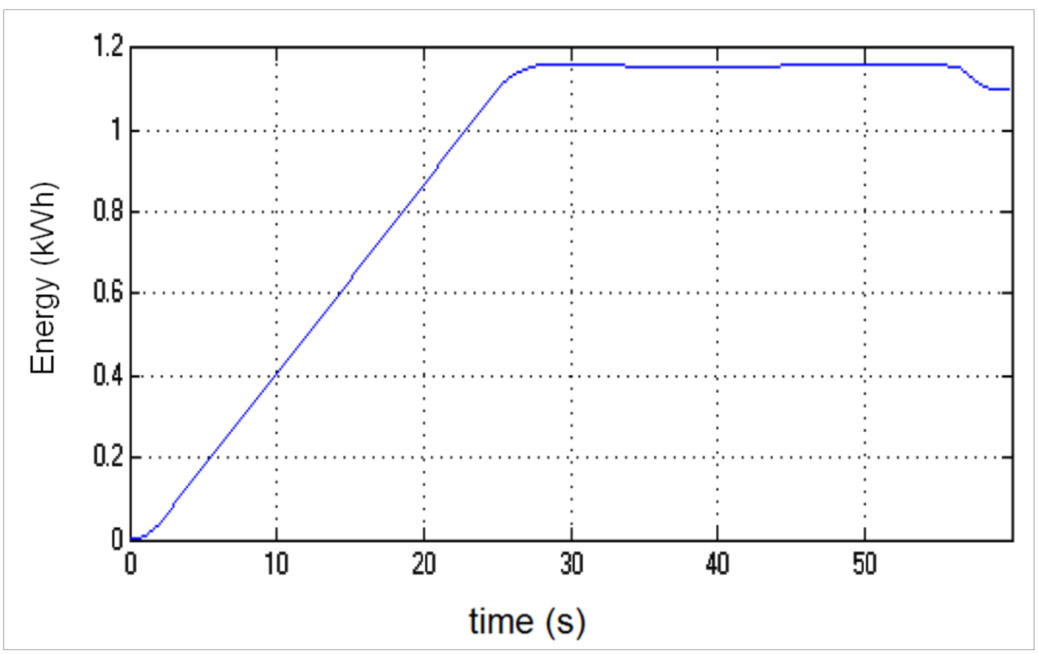

Fig. 2.61: Simulated energy grid for K=0, C=63F, H=0.6, H_1=1

From Fig. 2.62 to Fig. 2.63 are presented the grid power and grid energy for case 3 (K=0.5, C=63F, H=0.6, H_1=1.3).

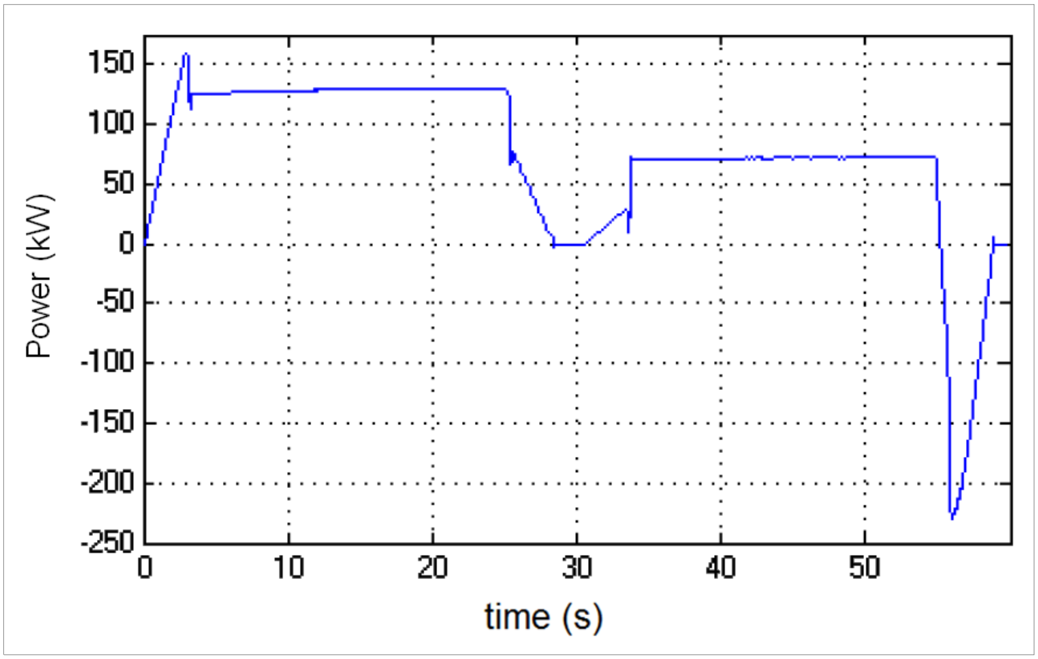

Fig. 2.62: Simulated power grid for K=0.5, C=63F, H=0.6, H_1=1.3

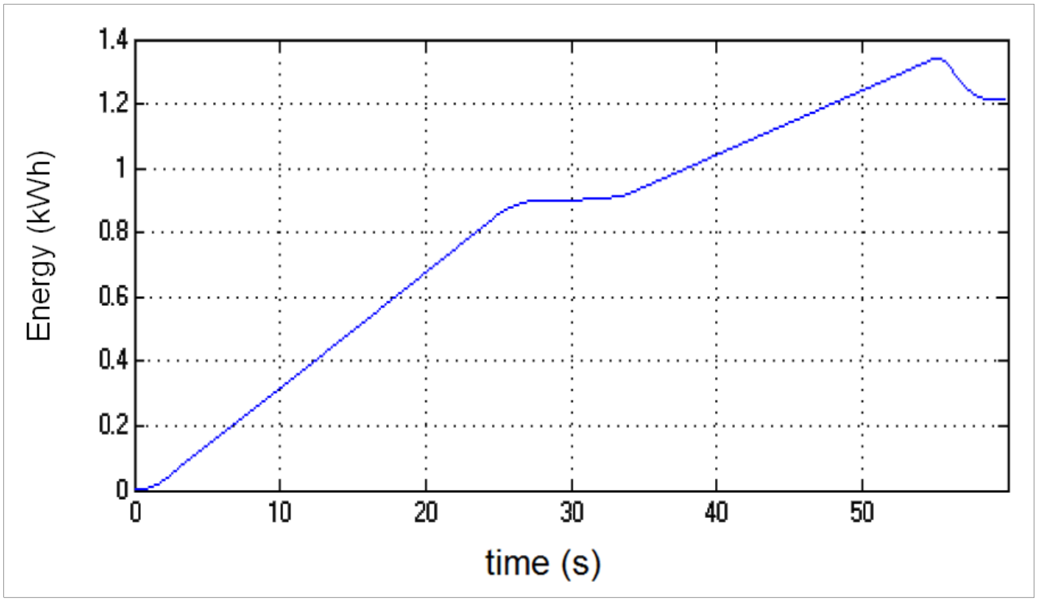

Fig. 2.63: Simulated energy grid for K=0.5, C=63F, H=0.6, H_1=1.3

From Fig. 2.64 to Fig. 2.65 are presented the grid power and grid energy for case 4 (K=1, C=63F, H=0.8, H_1=1.3).

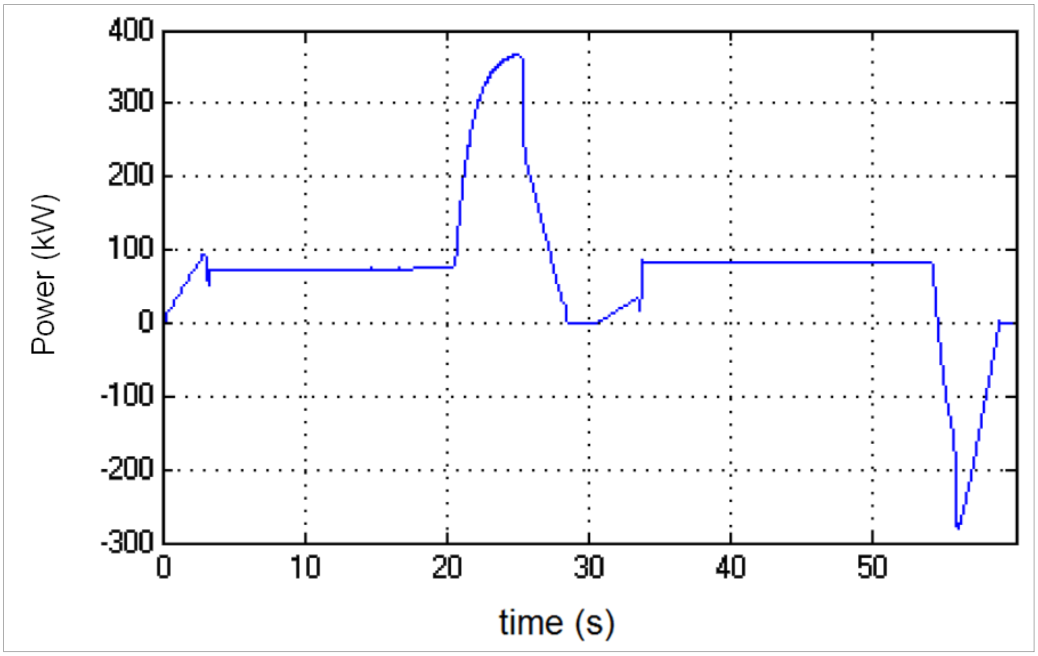

Fig. 2.64: Simulated power grid for K=1, C=63F, H=0.8, H_1=1.3

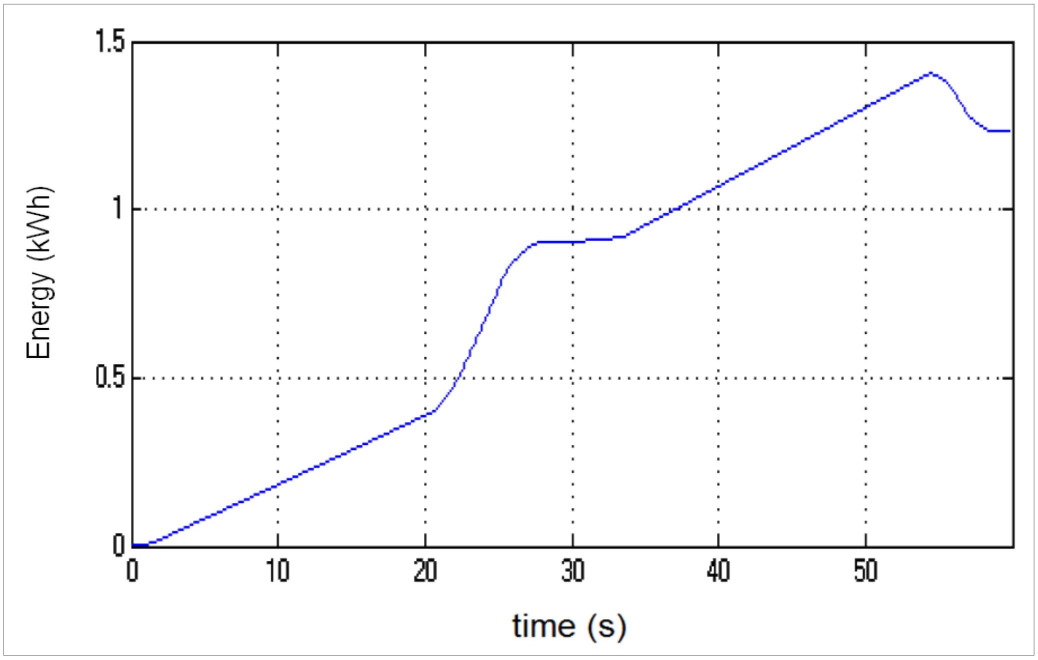

Fig. 2.65: Simulated energy grid for K=1, C=63F, H=0.8, H_1=1.3

From Fig. 2.66 to Fig. 2.67 are presented the grid power and grid energy for case 4 (K=1, C=75.78F, H=0.8, H_1=1.3).

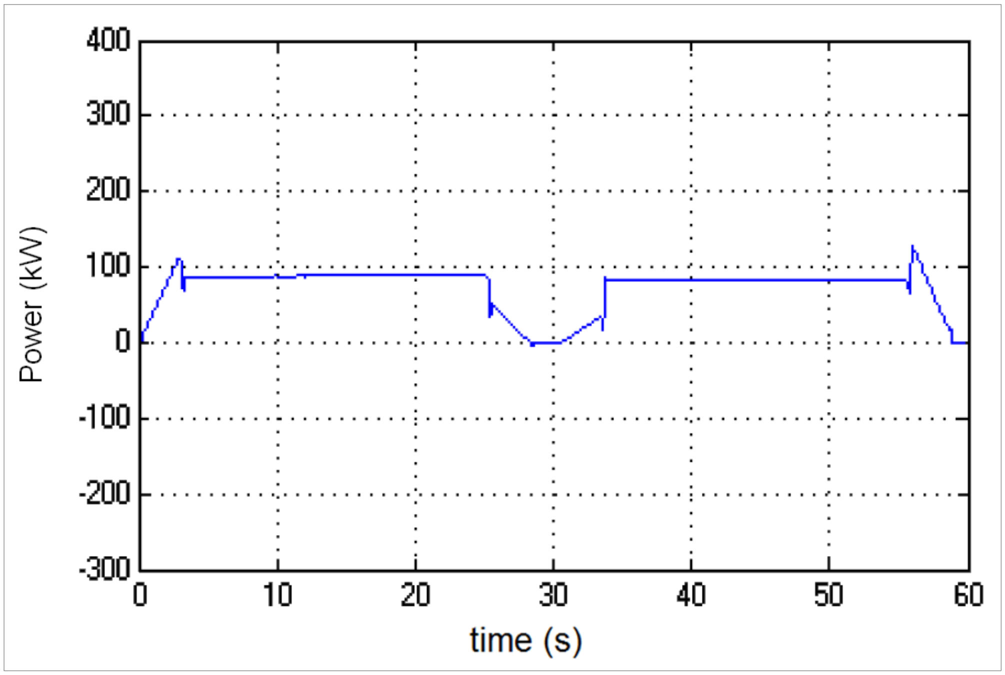

Fig. 2.66: Simulated power grid for K=1, C=75.78F, H=0.8, H_1=1.3

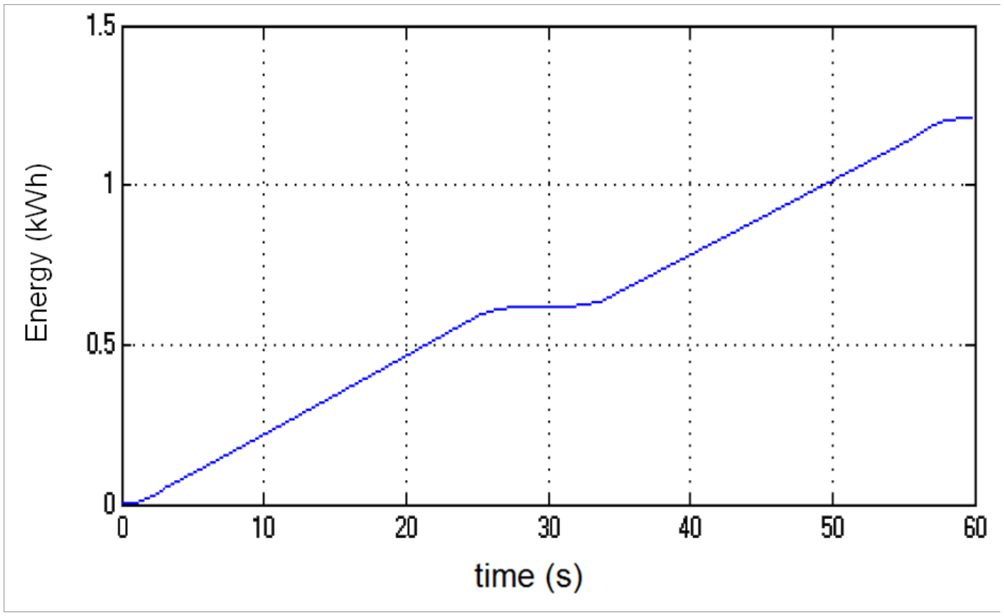

Fig. 2.67: Simulated energy grid for K=1, C=75.78F, H=0.8, H_1=1.3

It can be observed, in cases 3 and 4, that the I_{UC} current absorbed at regime during descending phase is greater than that absorbed in the case of K = 0. This is because for K > 0 the ultracapacitors draw power from the grid too. In this case, in the transient phase the current values are higher than the nominal values permitted by the UC modules.

In fact, when the maximum current delivered by the 4 strings is greater than 1000 A, the maximum current supplied from the single string is in the order of 250-300 A, much greater than the nominal value of 150 A.

However, since the period of time is limited and the subsequent phases of lifting and descending of the load are separate from the stage of translation, there is an accumulation cooling time and therefore these currents do not represent a danger to the ultracapacitors. It is, however, necessary to demonstrate this claim and only the thermal verification of the ultracapacitors with the calculation of the RMS output current (see below) will allow to considered as acceptable the indicated solution.

As given in the Maxwell document No. 1007239, supplier of the ultracapacitors, the following were calculated:

- RMS ultracapacitors current
- Duty cycle

Refering to the selected ultracapacitors module datasheet, in the following table are presented data that are used to make the previous verification.

Table 10: Ultracapacitors module specifications

Maximum Current (30")	1200 A
Thermal resistance (Rth)	0.032°C/W
Internal resistance	18 milliOhm
Maximum temperature	65 °C
Operating temperature	40 °C
Maximum delta T	25 °C
Delta T =	"I^2 x Rint x Rterm x duty cycle"
where: I = current (amperes)	
Resr = resistance (ohms)	0,018 Omh
Rth = thermal resistance (oC/W)	0,032 C/W

The verification results are presented in Fig. 2.68.

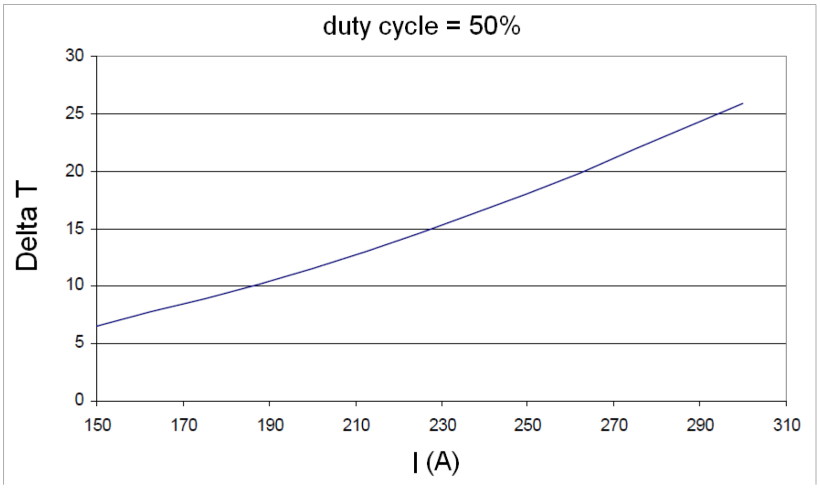

Fig. 2.68: Delta T vs I for duty cycle = 50%

As it can be seen from Fig. 2.68, the ultracapacitors may be used for currents up to 300A and duty cycle up to 50 %.

Another delicate point is in Fig. 2.64 in which it is noted that up to 20 sec. the value of the system power at regime is 70 kW. After the voltage across the ultracapacitors decreased to about 250V, the whole power is drawn from the grid, and thus the maximum power value is 370 kW for 8 sec.

It should be noted, however, that the power peaks have endure such a time that the thermal switch will not be affected while the magnetic switch for industrial use is calibrated for 7-8 times the rated current.

It should be noted, finally, that when the capacitors are charged, the residual energy can still be recovered if the rectifier is replaced with a converter that lets you work in two quadrants or must be properly dissipated, and for this reason it is assumed that all the energy that could be recovered is actually recovered (maximum energy value from the previous graphs).

2.14 Economic Evaluation of the simulation results

Thanks to the simulation model we know, at this point, the grid power involved and consumption per cycle for each of the 4 cases with recovery and know also the same values for the reference case, the one without electric storage (case 1). It can be then determined the payback time of the storage system for the different options available, Table 8, which is shown below for convenience:

	Parameters	***Description***
Case 1	K=0 C=63F, H=0 H_1=1	Reference case, no energy recovery
Case 2	K=0 C=63F H=0.6 H_1=1	Pgrid =0, i.e. . the grid supplies power only throughout the descending phase
Case 3	K=0.5 C=63F H=0.6 H1=1.3	The grid supplies power throughout the whole cycle
Case 4	K=1 C=63F, H=0.8 H_1=1.3	The grid supplies power throughout the whole cycle, power is constant and equal to the average requested power

Case 5	K=1 C=75.78F, H=0.8 H_1=1.3	The grid supplies power throughout the whole cycle, power is constant and equal to the average requested power. Supercapacitor capacity is increased.

Thes options are related essentially to three management strategies (cases 1, 2, 3) and two different values of the accumulation size (case 4, corresponding to the case 3 with increased accumulation size).

The convenience of the investment will depend from:

- the reduction of the energy bill, and therefore the unit cost of electricity in two cases (with and without accumulation system), the per hour usage time and the number of hours per year usage of the gantry crane and the consequent reduction in energy consumption;
- the duration of the investment, and therefore the duration of ulracapacitors;
- the cost of the interest on capital and an expected increase of the cost of energy.

The evaluation is done considering 25 work cycles / hour, and 4000 operating hours / year. It is also considered a plant life time of 15 years.

2.14.1 Cost of Investment

The cost of the storage system is a function not only of the volume of energy, but also of the type of cell adopted. The analysis of the cost of investment will take into account the rated voltage of the storage system and the type of ultracapacitor cell.

Fig. 2.69 [22] shows several curves, interpolated from real costs, in which is shown the specific cost/Wh of the stored energy in the ultracapacitors modules considering different types of cells and different voltages.

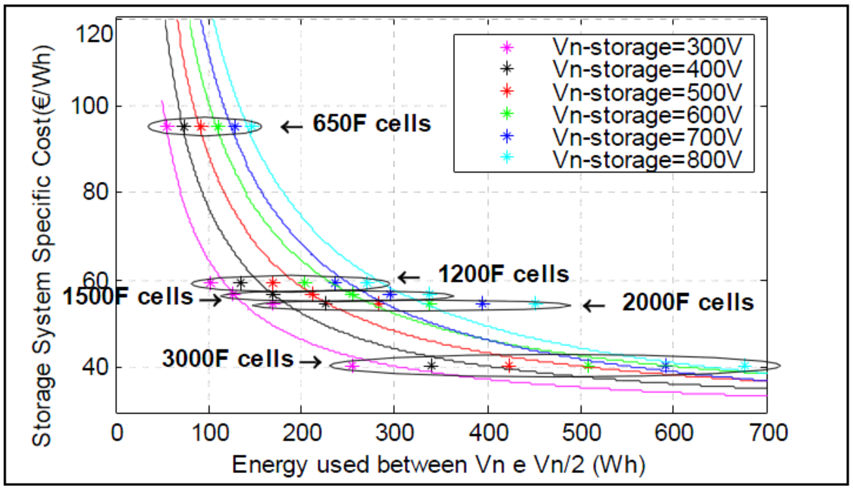

Fig. 2.69: Specific Cost/Wh for different types of cells and voltages.

The energy to be accumulated for K[1] = 0 is 5498kJ = 1.53kWh, which is outside the graph, but, referring to this value of energy, all curves represented tend asymptotically to a specific cost less than 40 €/Wh, for which the total cost of ultracapacitors would be about €60,000. This cost is less than the value obtained by considering the unit cost of the module BMOD0063 P125 equal to €5000, thus the total cost would be €80,000 (16 modules - Fig. 2.17).

At the cost of the ultracapacitors has to be added the cost of the power DC-DC converter (4 converters Fig. 2.17 – 4 ultracapacitor modules in series, 4 series in parallel), and is expressed by the following expression:

$$DC\_DC\_Cost\ [€] = 0.21*(8000 + 124\ (P\text{-}10))$$

where P is the nominal power of the single converter ($P = P_{UC\_total}/4$), that is P = 50kW for case 2 and case3; P=80kW for case 4 and case 5.

[1] K is the Grid Power ratio defined in paragraph 2.8.1

Thus, for P = 50kW we have a cost of €2700 per converter, for P = 70kW we have a cost of €3500 per converter.

2.14.2 Cost of the electric energy

The cost of electricity is determined using a binomial pricing; the cost of the electrical energy, in fact, takes into account the contractual power and that energy consumed. To this end, reference is made to the average prices of electricity in Italy, for the 1st trimester of 2012 to the end customers in medium voltage for other purposes (either for domestic use, nor for public lighting). This analysis, summarized in Table 11, has allowed to identify the following electric energy cost function :

$$Electricity\_Cost = 31.96P_C+0.1335W+865.27$$

where

- *Electricity_Cost* is the cost per year of the electric energy [€/year];
- P_C is the contractual power [kW], (for each case it is supposed to be the value of Table 9);
- W is the energy consumed in one year [kWh];

Table 11: MV consumer cost analysis

100÷500 kW MV consumer, 1st trimester 2012					
	fixed costs	**power costs**		**variable costs**	
Transmission (meas.)	€ 259,32			*transmission*	€ 5,21
distribution	€ 447,80	*distribution*	€ 31,96	*distribution*	€ 5,50
general charges	€ 158,15			*general charges*	€ 32,74
				supply and dispatching charges	€ 90,00
€ /year	**865,27**	€ /kW Year	**31,96**	€ /kWh	**0,1335**

2.14.3 Payback period

The following table summarizes, for the values of energy consumption from the grid previously calculated, costs, savings and payback time of the 4 investment solutions considered. The annual consumption was calculated using the *Electricity_cost* equation previously presented. Annual savings are calculated as the difference between the annual grid energy cost of the 1st case (2nd row – 3rd column) and the the annual grid energy cost of other cases (3rd column).

Table 12: Summerized costs and saving for the considered 4 cases

	Annual Consumption [kWh][2] (100.000 cycles)	**Annual Grid energy cost [€]**	**Annual savings [€]**	**Additional investment [€]**	**Payback time [years]**
Case 1	260.000	47.400	-----	-----	-----
Case 2	120.000	21.679	24.856	90.800,00	3,6
Case 3	130.000	22.215	24.320	90.800,00	3,7
Case 4	140.000	20.457	26.078	90.800,00	3,5
Case 5	125.000	19.406	27.129	121.500,00	4,5

For the additional investment cost calculation, the cost rlated to the 70kW DC-Dc converter was considered as it can operate in lower power (50kW) while a lower power DC-DC converter cannot operate in higher power.

With the existing costs of electricity and ultracapacitors, the best solution from the technical and economic point of view is the 4th case, the one that allows the maximum leveling of the grid energy .

[2] Refer to Table 9

In the following pictures are shown the cash flows during the 15 year period for the 4 considered cases. It can be observed that the payback times of the 4 cases are very close to each other.

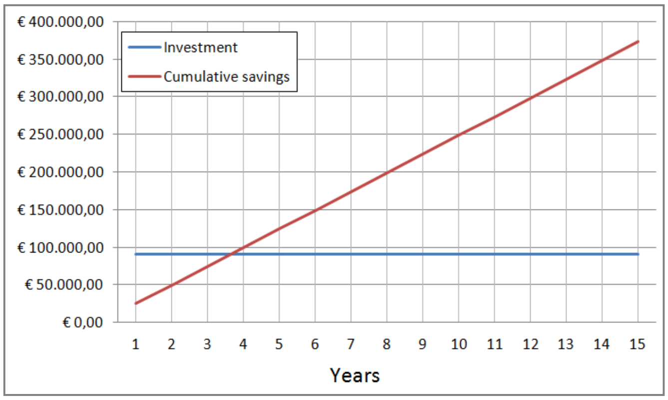

Fig. 2.70: Payback period – Case 2

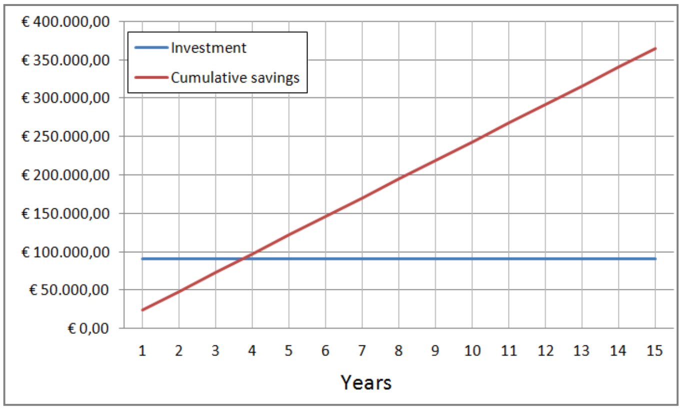

Fig. 2.71: Payback period – Case 3

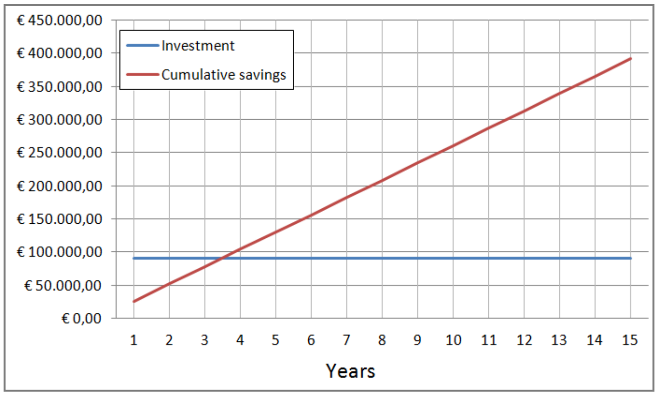

Fig. 2.72: Payback period – Case 4

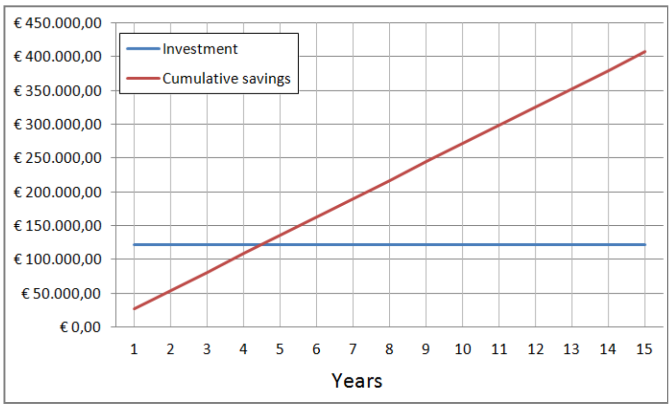

Fig. 2.73: Payback period – Case 5

The different solutions proposed, however, give results very close to each other, and all satisfying. Consequently, for the frequency of usage considered, it can be concluded that the implementation of the ultracapacitors in the lifting system is positive whatever management strategy is adopted.

The second consideration that can be drawn is that the return of investment is in any case assured in less than 5 years, thereby reducing the risks resulting from not having considered the possible cost of additional maintenance of a more complex system.

3. Active Front-End Converter

In this chapter the mathematical and simulation model of a Front End Converter with Active Filter capabilities is presented. The presented Front End acts as an Active power deliver to the local load and also as a power quality conditioner in order to compensate reactive power generated by neighboring drives. In order to perform this task, a control strategy is elaborated and presented. Simulation using Matlab Simulink platform are performed and presented.

The behavior of the Active Front End Converter in the presence of non-repetitive sags is presented. The presented Active Front End. Different conditions of non-repetitive sags are studied and simulation results are presented in this paper.

Moreover, it is presented the behavior of the Active Front End Converter in the presence of repetitive voltage notches in both single and double grid phases voltage notches.

3.1 Introduction

The development of technology over the years, especially the progress of power electronics applications, has brought about many technical conveniences and economical profits, but it has simultaneously created new challenges for power system operation studies. Power quality, in recent years, is receiving increasing attention by utility, customer, and consulting engineers. Line side harmonics and reactive power support still remain major concerns. With the proliferation of nonlinear power electronics load in a distribution network, utilities are trying to adopt newer methods to determine the true contribution of harmonics from a nonlinear load. Compliance with power utility requirements with respect to voltage fluctuation and harmonic injection at the Point of Common Coupling (PCC) is a necessity.

The growing use of non-liear loads and time-varying loads introduced distorsion of voltage and currents waveforms and increate the reactive power demand in AC networks. Harmonic and interharmonic distorsions are known to be source of several problems, such as increased power losses, excessive heating in rotating machinery, significant interference with communication circuits, flicker and audiable noise, incorrect operation of sensitive loads.

Diode/thyristor rectifiers are usually used as front-end for conventional utility grid interface. The advantages of this configuration include low cost, simplicity and high reliability. However, these rectifiers draw significant harmonic current from the utility grid. There have been three possible up-to-date solutions to reduce the harmonic pollution:

- Active filters that have shunt, series, or combined connection to the grid
- Active front-end converter topologies that are configured as thyristor rectifier with a boost PWM controlled converter.
- Conventional diode/thyristor rectifiers sets combined with newly installed PWM active front-end converters.

The first approach is to install an additional device, whose solely purpose is devoted to power quality enhancement whereas the other drives only focus on their outlet power to the loads. This method can be generally applied to various situations and the performance has been proven. However, it needs extra investment to purchase costly high power active devices. Furthermore, it must be managed and controlled in a precise and excessively reliable way.

The second approach assigns multiple functions on the front-end converters and distributes the power quality functions to all the units. Therefore, this approach can eventually provide effective and reliable power quality solutions. However, taking into account the vast number of conventional diode/thyristor front-end converters sets already in operation, the upgrade process may take a long time. In addition, the vast replacement of conventional diode/thyristor front-end converter is costly at the moment and may also interrupt the normal operation, which is reluctant for industry users to accept.

Therefore, it is taken into consideration the third approach. The motivation behind this approach is to bridge the gap between conventional diode/thyristor converters and newly installed active front-end converters and compromises a reasonable power quality solution with several active front-end units.

3.2 Active Front End operating principle

The term Active Front End Inverter refers to the power converter system consisting of the line-side converter with active switches such as IGBTs, the dc-link capacitor bank, and the load-side inverter. The line-side converter normally functions as a rectifier. But, during regeneration it can also be operated as an inverter, feeding power back to the line. The line-side converter is popularly referred to as a PWM rectifier in the literature. This is due to the fact that, with active switches, the rectifier can be switched using a suitable pulse width modulation technique.

The PWM rectifier basically operates as a boost chopper with ac voltage at the input, but dc voltage at the output. The intermediate dc-link voltage should be higher than the peak of the supply voltage. This is required to avoid saturation of the PWM controller due to insufficient dc link voltage, resulting in line side harmonics. The required dc-link voltage needs be maintained constant during rectifier as well as inverter operation of the line side converter. The ripple in dc-link voltage can be reduced using an appropriately sized capacitor bank. The active front-end inverter topology for a motor drive application is shown in Fig. 3.1.

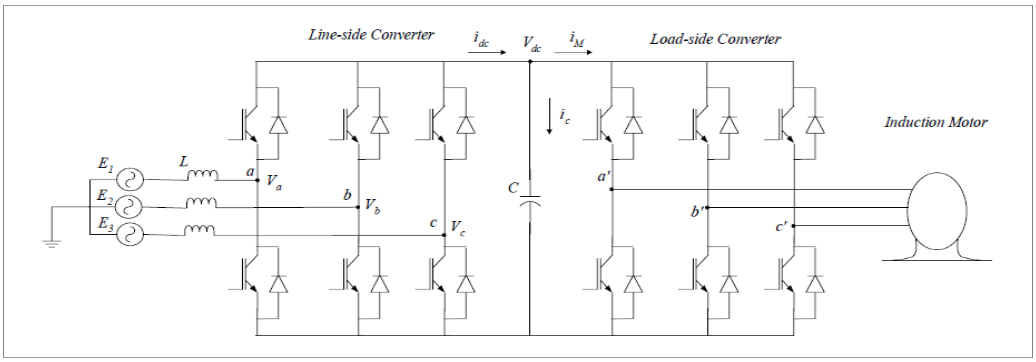

Fig. 3.1: Active front-end induction motor drive system

The topology shown in Fig. 3.1 has two three-phase, two-level PWM converters, one on the line side, and another on the load side. The configuration uses 12 controllable switches. The line-side converter is connected to the utility through inductor. The inductor is needed for boost operation of the line-side converter. A transformer on the supply side with appropriate secondary impedance also serves the same purpose.

For a constant dc-link voltage, the IGBTs in the line-side converter are switched to produce three-phase PWM voltages at a, b, and c input terminals. The line-side PWM voltages, generated in this way, control the line currents to the desired value. When DC-link voltage drops below the reference value, the feed-back diodes carry the capacitor charging currents, and bring the dc-link voltage back to reference value.

A per-phase equivalent circuit of the three-phase, line-side PWM converter is shown in Figure 1.2.

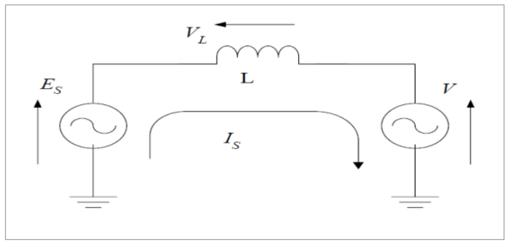

Fig. 3.2: Per-phase equivalent circuit

The source voltage E_S, and line inductance L represent the utility system. The three-phase voltages at the three input legs of the line side converter are represented by V. The voltage V can be viewed as a PWM voltage wave constructed from the dc link voltage V_d. The magnitude and phase of the fundamental component of V is controlled by the line-side converter. The voltage V_L, across inductor L, is $I_S\omega L$ where, ω is the angular frequency of supply voltage. Note that, the synchronous machine connected to an infinite bus can also be represented by the same per-phase equivalent circuit shown in Fig. 3.2. Similar to an overexcited or under-excited synchronous machine, the PWM converter can also draw line currents at leading, lagging or unity power factor.

As illustrated in Fig. 3.3, for unity power factor operation in rectifier mode of the line-side converter, the PWM voltage V needs to be larger than the supply voltage phasor E_S in magnitude and lags E_S by an angle δ. This makes E_S and line current I_S, to be co-phasal. The angle δ is called the power angle because it controls the power flow between the two sources.

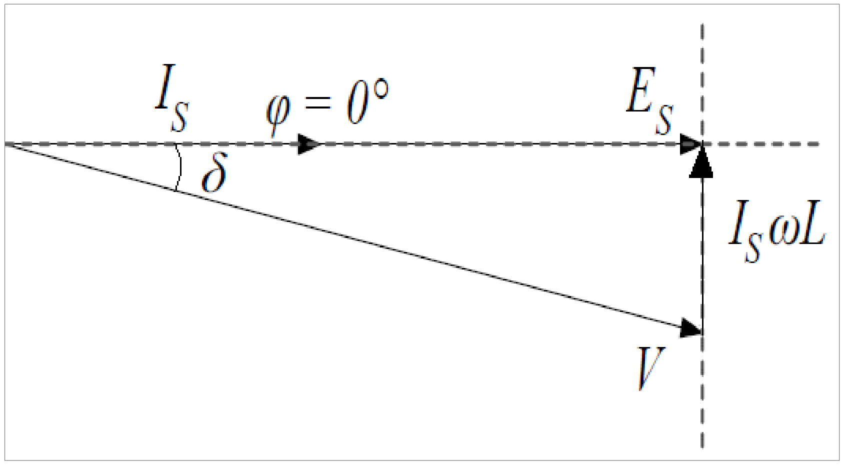

Fig. 3.3: PF=1 during motor mode

The regenerative mode of the line-side converter is shown in Fig. 3.4. The I_S phasor now reverses, causing reversal of $I_S\omega L$ phasor.

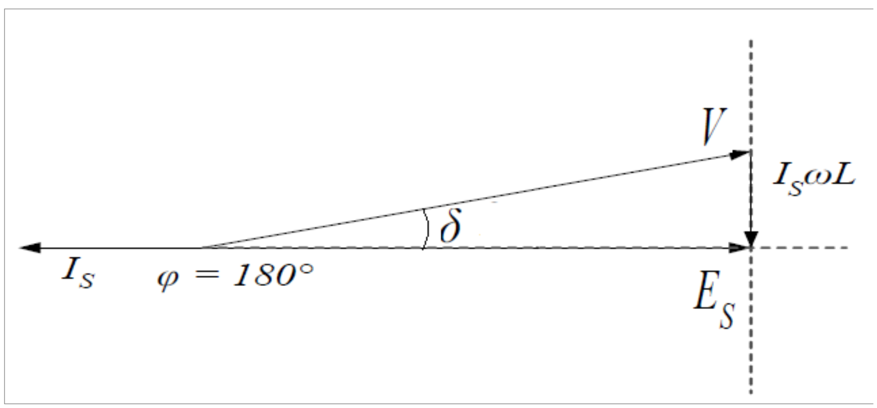

Fig. 3.4: PF=1 during regenerative mode

In order to satisfy the phasor diagram, the V phasor should lead phasor E_S by an angle δ. Thus the power angle δ also reverses.

Likewise, the leading power factor operation is illustrated in Fig. 3.5.

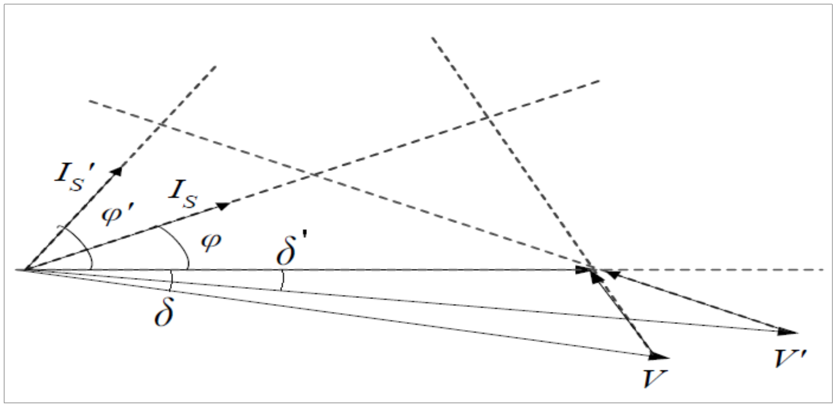

Fig. 3.5: Leading PF during motor mode

The active power P, and reactive power Q, are given by following expressions:

$$P = 3 \cdot E_S I_S \cos\varphi \qquad (1)$$

$$Q = 3 \cdot E_S I_S \sin\varphi \qquad (2)$$

where E_S and I_S are supply voltage and line current, while φ is the power factor angle.

From Fig. 3.4 we can write:

$$I_S \omega L \cos\varphi = V \sin\delta \qquad (3)$$

$$I_S \omega L \sin\varphi = V \cos\delta \qquad (4)$$

Therefore:

$$I_S \cos\varphi = \frac{V \sin\delta}{\omega L} \qquad (5)$$

$$I_S \sin\varphi = \frac{V \cos\delta}{\omega L} \qquad (6)$$

Substituting the values of $I_S \cos\phi$ and $I_S \sin\phi$ in Equation (1) and (2) respectively:

$$P = 3 \cdot E_S \frac{V \sin\delta}{\omega L} \tag{7}$$

$$Q = 3 \cdot E_S \frac{V \cos\delta - E_S}{\omega L} \tag{8}$$

The equations 1.1 through 1.6 indicate that the PWM voltage, *V*, and power angle, *δ*, can be controlled to control active and reactive power. It is also possible to maintain reactive power constant while varying active power. This is done by keeping phasors $V \cos\delta$ constant and varying phasor $V \sin\delta$.

3.3 Key Features of Active Front-End Inverters

The power electronics equipment is often viewed as a source of troublesome line-side interactions in the form of non-linear reactive currents and harmonics. However, with the advent of high power semiconductor devices capable of switching adequately fast, many new applications of power electronics equipment are being envisaged. One amongst them is Active front-end inverter, which can provide a solution to some power quality problems. The key features of this topology are discussed here.

- **Regenerative Capabilities –** In normal motoring mode of the drive, power flows from supply-side to the motor. The line-side converter operates as rectifier, whereas the load-side converter operates as an inverter. During regenerative braking mode, their respective roles are reversed. The system can continuously regenerate power if the machine is a generator, such as in wind generation system.

- **Unity Power Factor Operation** – With the line currents in phase with the line voltages, the unwanted reactive currents are eliminated. Since regeneration is also possible at unity power factor, the overall power quality is improved significantly. The converter will be able to supply the same active power but at reduced current ratings. Thus an increased cost of the converter on account of using active power switches can be justified for high power applications.
- **Reactive Power Compensation** – Alternatively, the kVA ratings saved due the unity power factor operation can be used to provide reactive power compensation to the utility system. The double-sided power converter thus acts as static VAR compensator while driving a variable speed motor load. This scheme can be an attractive alternative to the overexcited synchronous motor used as a VAR compensator.
- **As an Interface between Distributed Energy Source and Utility –** The lineside PWM converters are applicable whenever a DC bus is to be connected to the AC grid. Usually this is the case for distributed energy sources such as fuel cells, microturbines, or variable speed wind energy plants employing a dc-link.

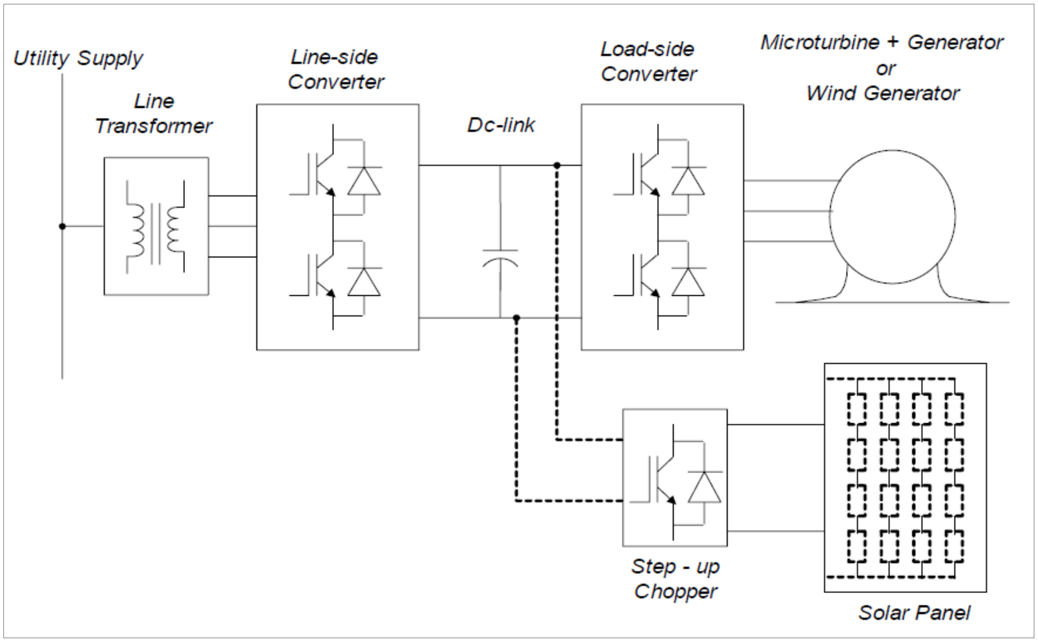

Fig. 3.6: Distributed energy source and utility interface

Figure 1.4 shows schematic representation of distributed energy sources connected to the utility grid. The line-side PWM converter facilitates the flow of power from distributed sources to the Utility at fixed frequency, and at desired power factor.

3.3.1 Comparison between Traditional Drives and Active Front-End Drives

The presence of non-linear loads in a power system has been significantly increased, and because of their ability to control electric power precisely and efficiently, the widespread use of power electronics converters is indispensable. Secondly, utilities are increasing concern about the non-linear currents in power system, resulting into stricter harmonic and power quality standards. This situation calls for alternative solutions in the form of various compensation techniques.

For large variable speed drives such as those used in mining excavators, the huge influx of non-linear currents, seriously affect the power quality at the point of common coupling. To ensure power grid compatibility, a reactive compensator such as a capacitor bank or a STATCOM device is required for such installations. Alternatively, an induction motor drive with an active front-end can be used. It can achieve powerful dynamic performance, while providing exceptional compatibility with the line in terms of power factor and total harmonic distortion. Fig. 3.7 shows the two schemes.

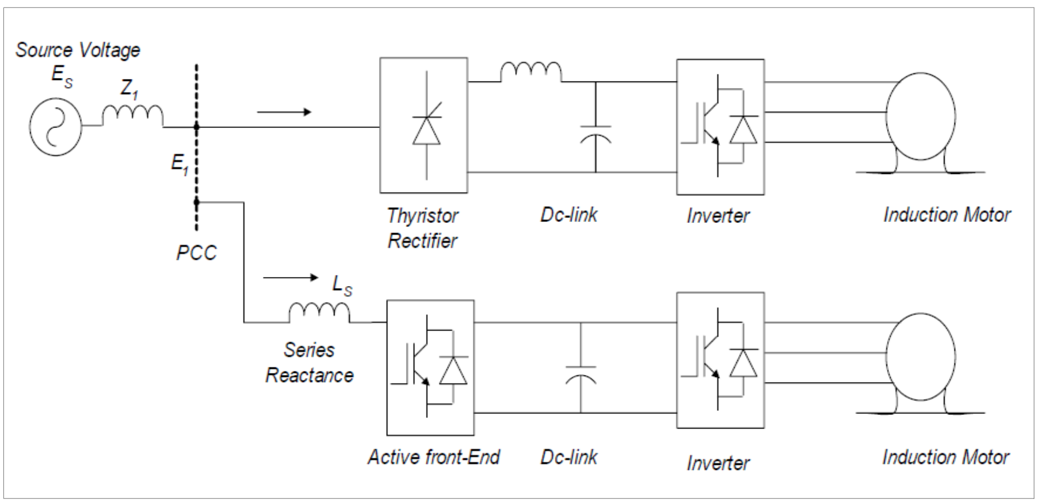

Fig. 3.7: Comparison between phase-controlled and active front-end rectifiers

As can be seen in Fig. 3.7 a rectifier consists of a standard phase-controlled thyristor. The drive typically operates near its full load at all the time. The line-side rectifier controls need to provide a stable dc-link voltage under all line and load conditions or drive performance may suffer.

Maintaining a stable dc-link voltage in the presence of wide power swings is difficult for phase-controlled thyristors because of the poor power factor to the line. Thus, when the distribution system voltage is weak, the voltage available for rectification is also reduced resulting in poor time response. The poor power factor and limited time response of phase-controlled rectifiers require a large amount of capacitance in the DC-link to minimize the voltage fluctuations seen by the inverter.

The use of high power IGBTs in active front-end inverter (AFE) topology as shown in Fig. 3.7 eliminates the shortcomings of traditional rectifier front ends. The active front end boosts the line voltage to a dc-link voltage higher than normally produced with a diode bridge. It takes an advantage of the network's inherent reactance to increase dc-link voltage greater than the peak of the line-to-line supply voltage. The line reactance is a disadvantage in a phase-controlled rectifier resulting in voltage notching.

The system can be designed to operate with sufficient control margins so that the desired dc-link voltage can be maintained, even in the presence of large dips in the incoming line voltage. The current flow between the line and the active rectifier is directly dependent on the voltage difference between line voltage and PWM voltage generated by the active rectifier. This voltage difference is applied across the line reactance. Adjusting the magnitude and phase of this voltage gives the active rectifier continuous control over the current amplitude and phase in all four quadrants of operation.

The controller regulates the dc-link voltage by maintaining the balance of active power supplied by the rectifier and the active power required by the inverter/load. At the same time, the controller can independently control flow of reactive power allowing unity power factor at the primary of the transformer or at any other given point in the network, like the point of common coupling that feeds the rectifier. This helps in improving the voltage regulations and overall efficiency.

However, there is a limit on the amount of power that can be transferred to or from the grid. The voltage ratio between the line voltage peak and dc-link voltage imposes this limit. Additionally, the current rating of active front-end rectifier imposes constraints on both the active and reactive power to be transferred to and from the power grid.

3.4 System configuration

Consider a simplified power system shown in Fig. 3.8.

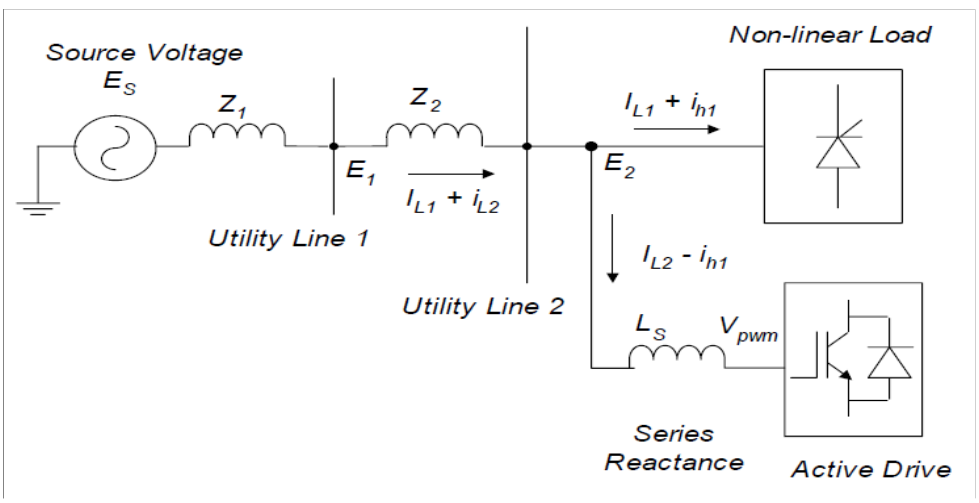

Fig. 3.8: A simplified power system

It is assumed that the system voltage E_S is purely sinusoidal. E_1 and E_2 are the intermediate line voltages which are not sinusoidal, but are distorted at varying degrees. V_{pwm} is the voltage generated by the active front-end converter, while Z_1 and Z_2 are transmission line impedances. L_S is the series reactance of an active drive used for boost operation.

The non-linear load, shown in figure, draws currents with active and non-active components. If the non-active currents are not compensated, it will result in source voltage distortion. The role of an active front-end converter, in this situation, is to supply the non-active currents needed to keep total harmonic distortion (THD) at the desired level. At the same time, the converter must draw real current to feed its own load which is induction motor.

The fundamental real current drawn by the active drive depends on the application. In applications like mine hoists, the drive draws the real power from utility to feed the continuously varying mine load. In other applications such as, an induction motor connected to an external energy source like a wind powered generator or a microturbine, the inverter may feed net real power back into the network.

3.5 Compensation Characteristics of an Active Drive

As illustrated in Fig. 3.8, the active front-end converter represents a shunt connected synchronous voltage source (STATCOM). The active drive can be viewed as a shunt compensator with an energy storage element in the form of a dc-link capacitor. Due to energy storage capability, the active drive has several beneficial features, which are used to maintain desired power grid compatibility.

These features are listed below.

- The maximum attainable compensating current of an active drive is limited only by the current ratings of the active switches and by the chosen ratio of peak line voltage to dc-link voltage. The active drive can maintain the maximum VAR compensation and the desired dc-link voltage, even in the presence of large dips in the incoming line voltage.

- The active front-end converter can be operated over its full current range even at the low line voltage levels. Sometime line voltages as low as 20% of the rated can also be tolerated.
- Operation over full current range help increase the stability margin in case of a fault, and thus improves overall transient stability.
- The response time of an active front-end converter for compensation purposes can be as fast as a fraction of a half cycle (~ 10ms). For thyristor controlled reactors, the dynamic response can be as slow as 5 to 6 cycles.
- The decoupled control strategy allows the compensator to exchange reactive as well as real power to and from the ac system. The two power exchanges are mutually exclusive.
- Due to real power exchange capability, the compensator can be used for power oscillation damping.

3.6 Steady-State Control

The steady state characteristics as well as differential equations describing the dynamics of the front-end rectifier can be obtained independent of an inverter and motor load. This is because the DC-link voltage can be viewed as a voltage source, if V_{dc} is maintained constant for the full operating range. The inverter is thus connected to the voltage source, whose terminal voltage V_{dc}, remains unaffected by any normal inverter motor operation.

Furthermore, as shown in Fig. 3.9, the rectifier can also be viewed as connected to the voltage source V_{dc}. Thus, the rectifier is able to control magnitude and phase of PWM voltages V_{abc} irrespective of line voltages E_{123}.

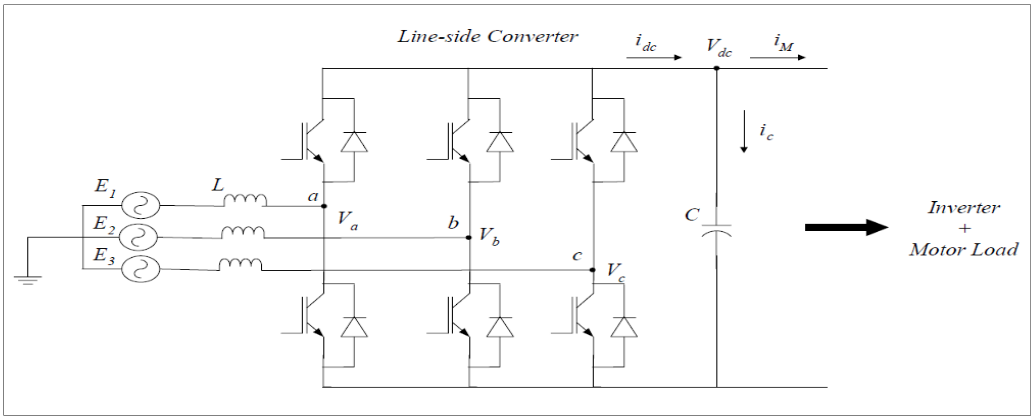

Fig. 3.9: A voltage source rectifier

The system is an exact replica of the inverter-motor system. The PWM voltages, V_{abc}, are now excitation voltages similar to the motor terminal voltages. The source voltages E_{123} can be compared to the motor counter emf voltages. Whereas, line inductance is similar to the motor leakage reactance.

During steady state, the system operation can be described using the phasor diagram shown in Fig. 3.10.

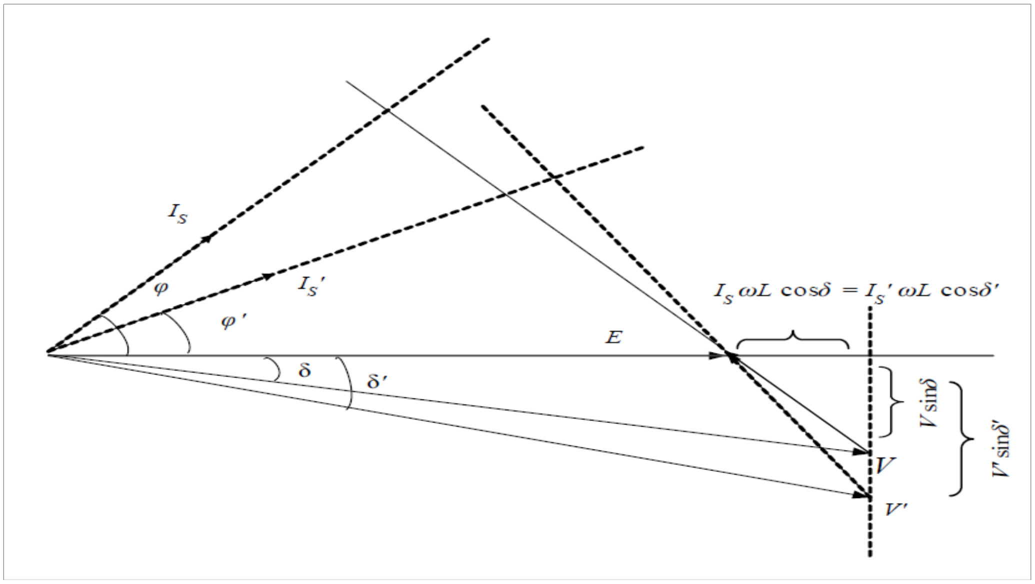

Fig. 3.10: Steady-state control of PWM rectifier

As explained earlier, the real and reactive powers are represented by:

$$P = 3E_S \frac{V \sin \delta}{\omega L}$$

$$Q = 3E_S \frac{V \cos \delta}{\omega L}$$

These equations suggest that an active rectifier can generate a desired, fixed valued reactive power while supplying the variable real power demanded by the motor.

As shown in Fig. 3.10, this can be done by keeping $V\cos\delta$ constant and varying $V\sin\delta$. Thus by controlling the magnitude and phase rectifier voltage V, the steady state control of active and reactive power is possible. However, the equations fail to explain simultaneous control over real and reactive power, which is required for a dynamic operation of an active drive.

Secondly, an important prerequisite for an active drive operation is a constant DC-link voltage, V_{dc}. A variable dc-link will introduce undesirable fluctuations in the magnitude and phase of PWM voltages generated by the rectifier. It will cause the active and reactive currents drawn by the rectifier to vary from the desired values. This will further introduce additional noise in the dc-link voltage, since these line currents charge and discharge the dc capacitor. To solve this non-linearity and at the same time achieve fast dynamic response, an effective control scheme is needed.

The voltage source rectifier connected to the utility can be effectively controlled using the field oriented approach, same as used for controlling the voltage source inverter feeding an induction motor. The rotating reference frame *d-q* theory is first used to obtain a dynamic *d-q* model of a line side converter. The dynamic *d-q* model is then used to implement field oriented control. The *d-q* theory is introduced in the next section.

3.7 The *d-q* theory

A system of three-phase, sinusoidal, time-varying voltages can be represented by an equivalent two-phase system. Consider a balanced, three-phase, Y-connected voltages, *E1*, *E2*, *E3*, which are 120 electrical degrees apart, as shown in Fig. 3.11.

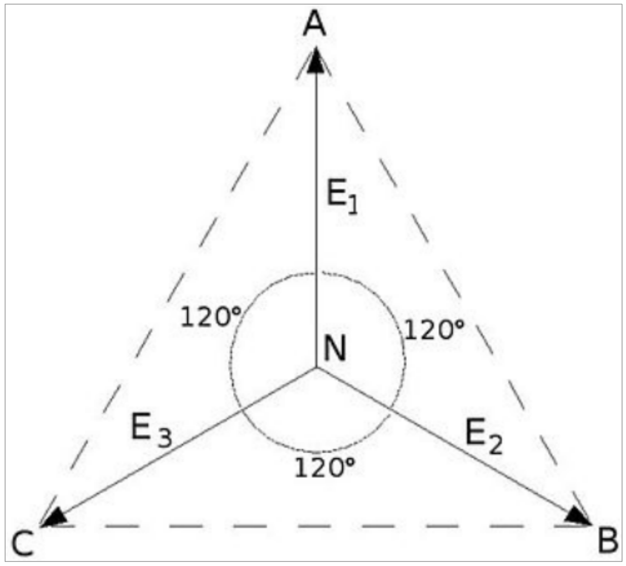

Fig. 3.11: Balanced, 3-phase, Y-connected system

Consider a stationary, two- axis coordinate system, where the q-axis is aligned with *E1*, and *d*-axis is orthogonal to the *q*-axis, as in Fig. 3.12.

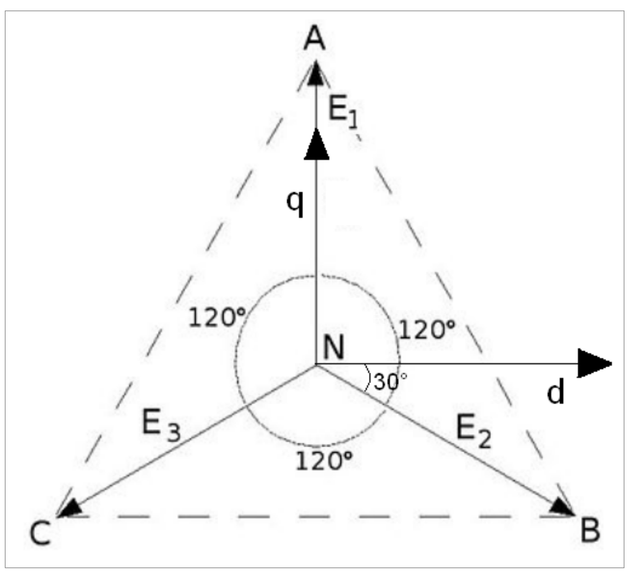

Fig. 3.12: 3-phase system superponed to a 2-phase d-q system

The three-phase voltages have component on both the *q* and *d* axes. The *q* and *d axes* components can be expressed as:

$$E_{qs} = E_1 - E_2 \cos 60 - E_3 \cos 60 = E_1 - \frac{E_2}{2} - \frac{E_3}{2} \tag{9}$$

$$E_{qs} = 0 + E_2 \cos 30 - E_3 \cos 30 = E_2 \sqrt{\frac{3}{2}} - E_3 \sqrt{\frac{3}{2}} \tag{10}$$

In matrix form:

$$\begin{bmatrix} E_{qs} \\ E_{ds} \\ E_{0s} \end{bmatrix} = \begin{bmatrix} 1 & -\frac{1}{2} & -\frac{1}{2} \\ 0 & \frac{\sqrt{3}}{2} & -\frac{\sqrt{3}}{2} \\ \frac{1}{\sqrt{2}} & \frac{1}{\sqrt{2}} & \frac{1}{\sqrt{2}} \end{bmatrix} \begin{bmatrix} E_1 \\ E_2 \\ E_3 \end{bmatrix} \tag{11}$$

However, in order that the two coordinate systems are equivalent, the instantaneous power in both the coordinate systems should be equal, thus:

$$P_{dq} = P_{123} \tag{12}$$

where P_{123} is power in three-phase circuit, and P_{dq} is power in equivalent two-phase system. To meet this requirement, the transformation matrix needs to be multiplied by a factor of $2/3$.

The new transformation matrix, C_1, is:

$$C_1 = \sqrt{\frac{2}{3}} \cdot \begin{bmatrix} 1 & -\frac{1}{2} & -\frac{1}{2} \\ 0 & \frac{\sqrt{3}}{2} & -\frac{\sqrt{3}}{2} \\ \frac{1}{\sqrt{2}} & \frac{1}{\sqrt{2}} & \frac{1}{\sqrt{2}} \end{bmatrix} \quad (13)$$

$$C_1^{-1} = \sqrt{\frac{3}{2}} \cdot \begin{bmatrix} \frac{2}{3} & 0 & \frac{\sqrt{2}}{3} \\ -\frac{1}{3} & \frac{1}{\sqrt{3}} & \frac{\sqrt{2}}{3} \\ -\frac{1}{3} & \frac{1}{\sqrt{3}} & \frac{\sqrt{2}}{3} \end{bmatrix} \quad (14)$$

The matrix system **(11)** is rewritten as:

$$\begin{bmatrix} E_{qs} \\ E_{ds} \\ E_{0s} \end{bmatrix} = \sqrt{\frac{2}{3}} \begin{bmatrix} 1 & -\frac{1}{2} & -\frac{1}{2} \\ 0 & \frac{\sqrt{3}}{2} & -\frac{\sqrt{3}}{2} \\ \frac{1}{\sqrt{2}} & \frac{1}{\sqrt{2}} & \frac{1}{\sqrt{2}} \end{bmatrix} \begin{bmatrix} E_1 \\ E_2 \\ E_3 \end{bmatrix} \quad (15)$$

Note that parameters E_{qs}, E_{ds} in two-phase stationary reference frame are still time-varying. Because most of the electric circuits are associated with inductances, the time varying parameters such as sinusoidal currents and voltages tends to make the system model complex, and system response is often sluggish.

R. H. Park proposed in 1920 to transform these variables to a fictitious reference frame rotating at some angular speed. If this speed of rotation is the same as the angular frequency of time-varying parameters, then all the parameters in this reference frame become time invariant or dc quantities. Because the effect of inductances associated with varying currents and voltages is removed, the system model is relatively simple and system response can be sufficiently fast.

In Fig. 3.13 and Fig. 3.14 is illustrated Park's transformation.

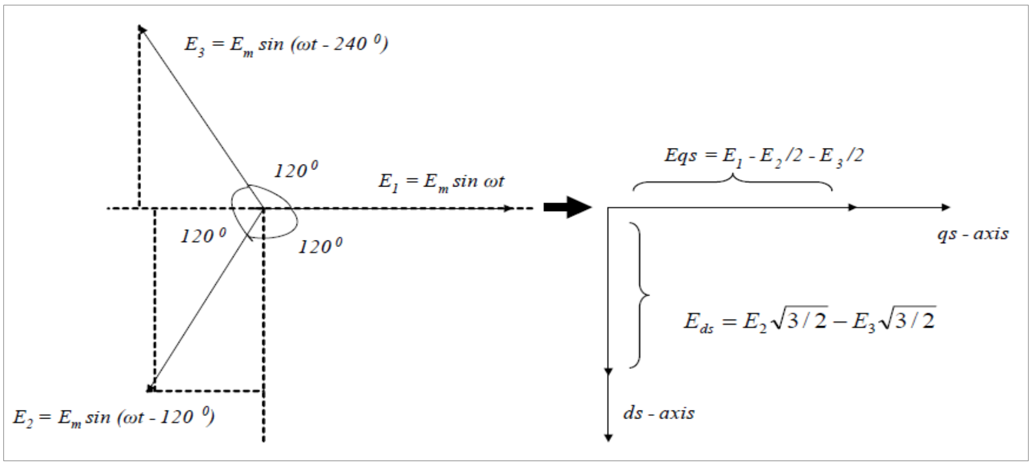

Fig. 3.13: Three-phase to two-phase transformation

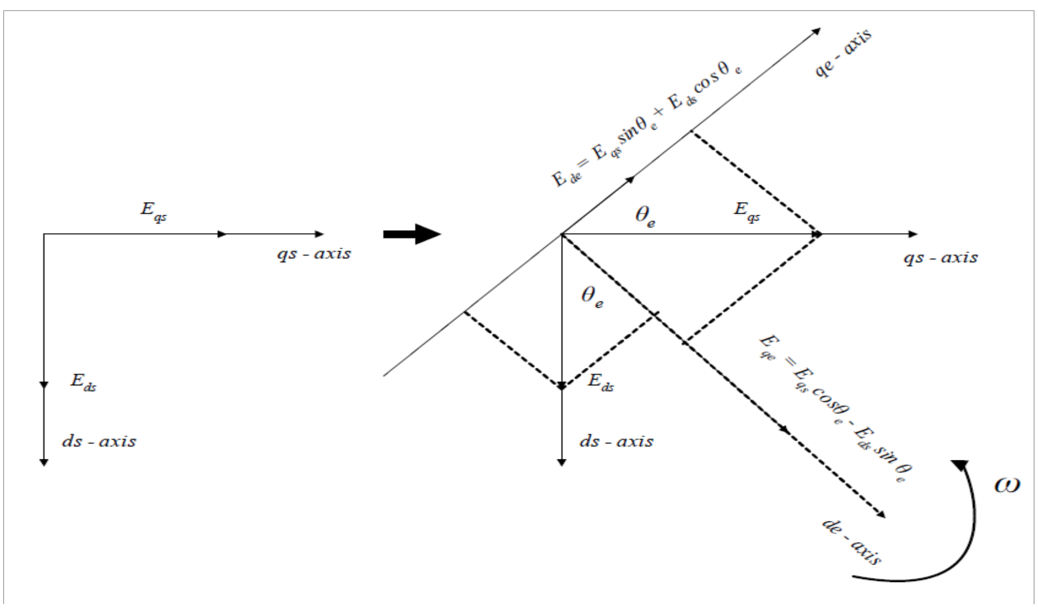

Fig. 3.14: Stationary to rotary reference frame, Park's transformation

The orthogonal axes *de* and *qe* are rotating at an angular speed of ω_e. The θ_e is the angular displacement such that:

$$\omega_e = \frac{d\theta_e}{dt} \tag{16}$$

The new variables in *de*-*qe* reference frame are:

$$\begin{bmatrix} E_{qe} \\ E_{de} \end{bmatrix} = \begin{bmatrix} \cos\theta_e & -\sin\theta_e \\ \sin\theta_e & \cos\theta_e \end{bmatrix} \begin{bmatrix} E_{qs} \\ E_{ds} \end{bmatrix} \tag{17}$$

The Park's transformation matrix is referred to as C_2:

$$C_2 = \begin{bmatrix} \cos\theta_e & -\sin\theta_e \\ \sin\theta_e & \cos\theta_e \end{bmatrix} \tag{18}$$

$$C_2^{-1} = \begin{bmatrix} \cos\theta_e & \sin\theta_e \\ -\sin\theta_e & \cos\theta_e \end{bmatrix} \tag{19}$$

Note that, both the matrices $C1$ and $C2$ are orthogonal matrices such that:

$$\begin{aligned} C_1^T C_1 &= C_1 C_1^T = I \\ C_2^T C_2 &= C_2 C_2^T = I \end{aligned} \tag{20}$$

where I represents an identity matrix.

3.8 Deriving the d-q model

Fig. 3.15 shows source voltages E_1, E_2, E_3 as line-to-neutral voltages for each of the three phases.

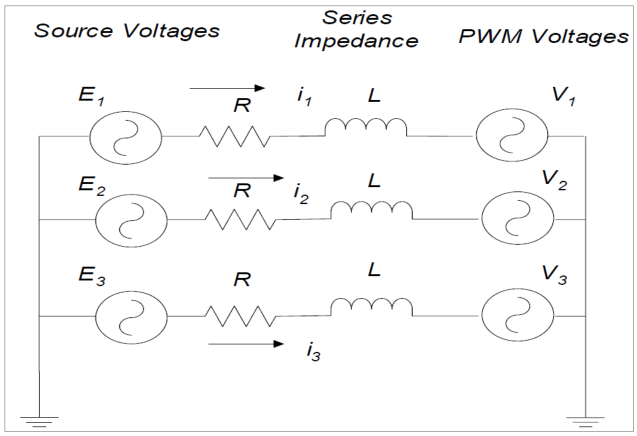

Fig. 3.15: Circuit representation of system mathematical model

The phase voltages E_1, E_2, E_3 and line currents i_1, i_2, and i_3 are given by:

$$\begin{aligned} E_1 &= E_m \sin \omega t; \\ E_2 &= E_m \sin(\omega t - 120); \\ E_3 &= E_m \sin(\omega t - 240); \end{aligned} \tag{21}$$

$$\begin{aligned} i_1 &= i_m \sin(\omega t + \varphi); \\ i_2 &= i_m \sin(\omega t - 120 + \varphi); \\ i_3 &= i_m \sin(\omega t - 240 + \varphi); \end{aligned} \tag{22}$$

The currents lead the source voltages by angle ϕ . E_m is the maximum line-to-neutral voltage, while i_m is the peak line current.

Referring to Fig. 3.15 the dynamic equations for each phase can be written as:

$$
\begin{aligned}
E_1 &= L\frac{di_1}{dt} + Ri_1 + V_1 \\
E_2 &= L\frac{di_2}{dt} + Ri_2 + V_2 \\
E_3 &= L\frac{di_3}{dt} + Ri_3 + V_3
\end{aligned}
\tag{23}
$$

In matrix form, Equation (23) can be written as:

$$
\begin{bmatrix} E_1 \\ E_2 \\ E_3 \end{bmatrix} = L\frac{d}{dt}\begin{bmatrix} i_1 \\ i_2 \\ i_3 \end{bmatrix} + R\begin{bmatrix} i_1 \\ i_2 \\ i_3 \end{bmatrix} + \begin{bmatrix} V_1 \\ V_2 \\ V_3 \end{bmatrix} \tag{24}
$$

Using transformation matrix C_1, we can write:

$$
\begin{bmatrix} i_{qs} \\ i_{ds} \\ i_{0s} \end{bmatrix} = C_1\begin{bmatrix} i_1 \\ i_2 \\ i_3 \end{bmatrix}, \quad \begin{bmatrix} E_{qs} \\ E_{ds} \\ E_{0s} \end{bmatrix} = C_1\begin{bmatrix} E_1 \\ E_2 \\ E_3 \end{bmatrix}, \quad \begin{bmatrix} V_{qs} \\ V_{ds} \\ V_{0s} \end{bmatrix} = \mathrm{C}_1\begin{bmatrix} V_1 \\ V_2 \\ V_3 \end{bmatrix} \tag{25}
$$

Pre-multiplying Equation (24) by C_1, is obtained:

$$
C_1\begin{bmatrix} E_1 \\ E_2 \\ E_3 \end{bmatrix} = L\frac{d}{dt}\left(C_1\begin{bmatrix} i_1 \\ i_2 \\ i_3 \end{bmatrix}\right) + RC_1\begin{bmatrix} i_1 \\ i_2 \\ i_3 \end{bmatrix} + C_1\begin{bmatrix} V_1 \\ V_2 \\ V_3 \end{bmatrix} \tag{26}
$$

Since $C1$ is a constant, it can be taken inside the derivative term:

$$\begin{bmatrix} E_{qs} \\ E_{ds} \end{bmatrix} = L\frac{d}{dt}\begin{bmatrix} i_{qs} \\ i_{ds} \end{bmatrix} + R\begin{bmatrix} i_{qs} \\ i_{ds} \end{bmatrix} + \begin{bmatrix} V_{qs} \\ V_{ds} \end{bmatrix} \qquad (27)$$

Equation (27) represents dynamic model in stationary reference frame. Using second transformation matrix, C_2, we can write:

$$\begin{bmatrix} i_{qe} \\ i_{de} \end{bmatrix} = C_2\begin{bmatrix} i_{qs} \\ i_{ds} \end{bmatrix}, \qquad \begin{bmatrix} i_{qs} \\ i_{ds} \end{bmatrix} = C_2^{-1}\begin{bmatrix} i_{qe} \\ i_{de} \end{bmatrix} \qquad (28)$$

Multiplying Equation (27) with C_2 and using equation (28), we can write:

$$C_2\begin{bmatrix} E_{qs} \\ E_{ds} \end{bmatrix} = LC_2\frac{d}{dt}\left(C_2^{-1}\begin{bmatrix} i_{qe} \\ i_{de} \end{bmatrix}\right) + RC_2\begin{bmatrix} i_{qs} \\ i_{ds} \end{bmatrix} + C_2\begin{bmatrix} V_{qs} \\ V_{ds} \end{bmatrix} \qquad (29)$$

Substituting eq. (29) in eq. (17) and known that terms, in the *qe-de* refering, are time-invariant:

$$\begin{bmatrix} E_{qe} \\ E_{de} \end{bmatrix} = LC_2\left(\frac{d}{dt}C_2^{-1}\right)\begin{bmatrix} i_{qe} \\ i_{de} \end{bmatrix} + LC_2C_2^{-1}\frac{d}{dt}\begin{bmatrix} i_{qs} \\ i_{ds} \end{bmatrix} + R\begin{bmatrix} i_{qe} \\ i_{de} \end{bmatrix} + \begin{bmatrix} V_{qe} \\ V_{de} \end{bmatrix} \qquad (30)$$

Substituting the Park transformation matrix, C_2:

$$\begin{bmatrix} E_{qe} \\ E_{de} \end{bmatrix} = L\begin{bmatrix} \cos\theta_e & -\sin\theta_e \\ \sin\theta_e & \cos\theta_e \end{bmatrix}\left(\frac{d}{dt}\begin{bmatrix} \cos\theta_e & \sin\theta_e \\ -\sin\theta_e & \cos\theta_e \end{bmatrix}\right)\begin{bmatrix} i_{qe} \\ i_{de} \end{bmatrix} + LI\frac{d}{dt}\begin{bmatrix} i_{qe} \\ i_{de} \end{bmatrix} + R\begin{bmatrix} i_{qe} \\ i_{de} \end{bmatrix} + \begin{bmatrix} V_{qe} \\ V_{de} \end{bmatrix} \qquad (31)$$

Differentiating with respect to time:

$$\begin{bmatrix} E_{qe} \\ E_{de} \end{bmatrix} = L \begin{bmatrix} \cos\theta_e & -\sin\theta_e \\ \sin\theta_e & \cos\theta_e \end{bmatrix} \left(\begin{bmatrix} -\omega\sin\theta_e & \omega\cos\theta_e \\ -\omega\cos\theta_e & -\omega\sin\theta_e \end{bmatrix} \right) \begin{bmatrix} i_{qe} \\ i_{de} \end{bmatrix} + L\frac{d}{dt}\begin{bmatrix} i_{qe} \\ i_{de} \end{bmatrix} + R\begin{bmatrix} i_{qe} \\ i_{de} \end{bmatrix} + \begin{bmatrix} V_{qe} \\ V_{de} \end{bmatrix} \quad (32)$$

Hence:

$$\begin{bmatrix} E_{qe} \\ E_{de} \end{bmatrix} = \omega L \begin{bmatrix} 0 & 1 \\ -1 & 0 \end{bmatrix} \begin{bmatrix} i_{qe} \\ i_{de} \end{bmatrix} + L\frac{d}{dt}\begin{bmatrix} i_{qe} \\ i_{de} \end{bmatrix} + R\begin{bmatrix} i_{qe} \\ i_{de} \end{bmatrix} + \begin{bmatrix} V_{qe} \\ V_{de} \end{bmatrix} \quad (33)$$

where $\omega = \frac{d\theta_e}{dt}$. Expanding eq. (33):

$$E_{qe} = L\frac{di_{qe}}{dt} + \omega L i_{de} + Ri_{qe} + V_{qe} \quad (34)$$

$$E_{de} = L\frac{di_{de}}{dt} + \omega L i_{qe} + Ri_{de} + V_{de} \quad (35)$$

Equations (34) and (35) represent the dynamic *d-q* model of an active front end inverter in a reference frame rotating at an angular speed of ω . In this model ω , i_{qe}, i_{de}, E_{qe}, and E_{de} are state variables while V_{qe} and V_{de} are the inputs.

Note that although the i_{qe} and *ide* components of line currents are orthogonal to each other, they are not perfectly decoupled. The dynamics of i_{qe} and i_{de} interfere with each other. Based on this dynamic model an effective method of control, one in which the two current components are decoupled is necessary.

3.9 Selecting the Rotating Coordinate System

A better insight into the dynamic behavior of the system is obtained by choosing a rotating system of coordinates, where the steady state oscillations disappear. For the dynamic model described in eq. (34) and (35), the pulse-width-modulated rectifier voltages serve as actuating voltages, while the line voltages assume the role similar to that of rotor induced voltages in induction motor . The PWM voltages control the line current so that desired power factor with respect to the line voltages can be achieved. A suitable choice of coordinate system in this case is the one defined by the line voltages.

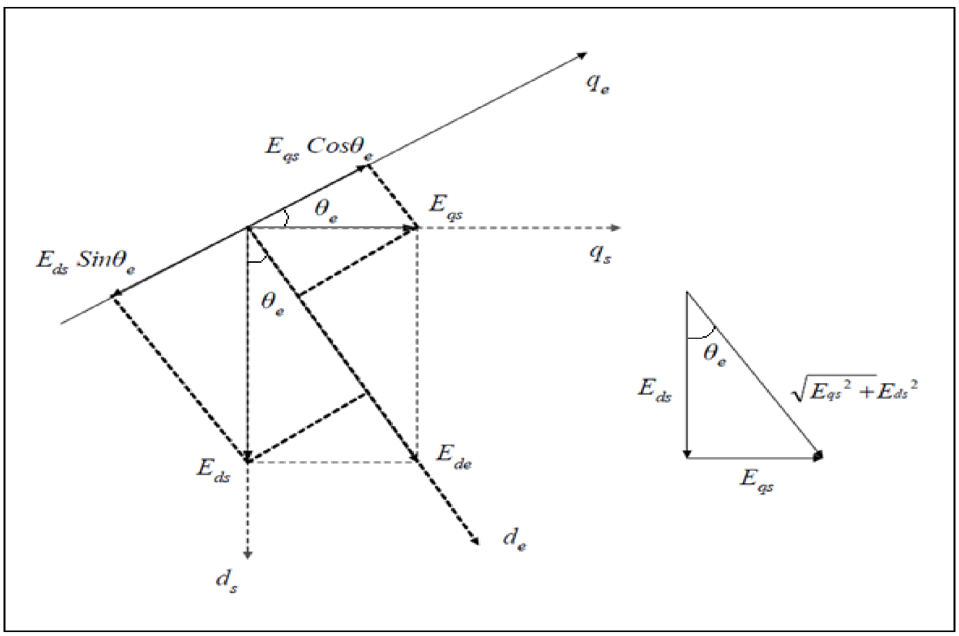

Fig. 3.16: Tracking θ_e

A moving coordinate frame formed by the sinusoidal line voltages is shown in Fig. 3.16. The two-phase voltages are represented by:

$$E_{qe} = E_{qs}\cos\theta_e - E_{ds}\sin\theta_e \tag{35}$$

$$E_{de} = E_{qs}\sin\theta_e + E_{ds}\cos\theta_e$$

E_{qe} and E_{de} are the projections of the E_{qs} and E_{ds} components on q and d axis respectively.

The angular speed of rotation of the moving coordinates, ω, is given by:

$$\omega = \frac{d\theta_e}{dt}$$

As illustrated in Fig. 3.16, select ω_e such that, $E_{qe} = 0$. The E_{qs} and E_{ds} components of source voltage thus form a right angle triangle so as to give,

$$\tan\theta_e = \frac{E_{qs}}{E_{ds}}$$

This choice helps to track θe by expressing θe in terms of Eqs and Eds as below,

$$\cos\theta_e = \frac{E_{ds}}{\sqrt{E_{qs}^2 + E_{ds}^2}}$$

$$\sin\theta_e = \frac{E_{qs}}{\sqrt{E_{qs}^2 + E_{ds}^2}}$$

sin θe. and *cos θe*. are used to rotate parameters at an angular speed of $\omega = \frac{d\theta_e}{dt}$.

Since θ_e is the angular displacement of the source voltages, the above approach ensures correct tracking of supply frequency even if it is varying and not constant.

3.10 Power Definitions in d-q Coordinate System

Using the system dynamic model established in previous sections, the control of line currents is carried out in a moving reference frame so that the feedback signals are dc quantities. This suggests that the current and/or power reference commands also need to be defined in a rotating reference frame. For this purpose the instantaneous active and reactive power in moving coordinate frame are defined below.

Referring to the generalized instantaneous power theory, the instantaneous active power P in three-phase coordinates is defined by:

$$P = E_1 i_1 + E_2 i_2 + E_3 i_3 \tag{36}$$

where E_1, E_2, E_3 are the source phase-to-neutral voltages, and i_1, i_2, i_3 are the line currents.

In matrix form we can write:

$$P = \begin{bmatrix} E_1 & E_2 & E_3 \end{bmatrix} \begin{bmatrix} i_1 \\ i_2 \\ i_3 \end{bmatrix} \tag{37}$$

Converting the parameters to two-phase moving coordinates using transformation matrices C_1 and C_2:

$$P = \left(C_1^{-1} C_2^{-1} \begin{bmatrix} E_{qe} \\ E_{de} \end{bmatrix} \right)^T \left(C_1^{-1} C_2^{-1} \begin{bmatrix} i_{qe} \\ i_{de} \end{bmatrix} \right)^T \Rightarrow$$

$$P = \begin{bmatrix} E_{qe} \\ E_{de} \end{bmatrix}^T \left(C_2^{-1} \right)^T \left(C_1^{-1} \right)^T C_1^{-1} C_2^{-1} \begin{bmatrix} i_{qe} \\ i_{de} \end{bmatrix} \qquad (38)$$

Since C_1 and C_2 are orthogonal, we can write:

$$\left(C_1^{-1} \right)^T C_1^{-1} = I, \qquad \left(C_2^{-1} \right)^T C_2^{-1} = I$$

and, thus, we can write:

$$P = \begin{bmatrix} E_{qe} & E_{de} \end{bmatrix} \begin{bmatrix} i_{qe} \\ i_{de} \end{bmatrix} = E_{qe} i_{qe} + E_{de} i_{de} \qquad (39)$$

As explained in previous section, E_{qe} is maintained equal to *0* at all the times, resulting in:

$$P = E_{de} \cdot i_{de} \qquad (40)$$

In the same manner, according to the generalized instantaneous power theory, the reactive power in three-phase coordinates is given by:

$$Q = E_{123} \times i_{123} = \begin{bmatrix} Q_1 \\ Q_2 \\ Q_3 \end{bmatrix} = \begin{bmatrix} \begin{vmatrix} E_2 & E_3 \\ i_2 & i_3 \end{vmatrix} \\ \begin{vmatrix} E_3 & E_1 \\ i_3 & i_1 \end{vmatrix} \\ \begin{vmatrix} E_1 & E_2 \\ i_1 & i_2 \end{vmatrix} \end{bmatrix}$$

$$Q_{123} = \left(C_1^{-1} E_{dqs}\right) \times \left(C_1^{-1} i_{dqs}\right) = C_1^{-1}\left(E_{dqs} \times i_{dqs}\right)$$

$$Q_{dqs} = \left(E_{dqs} \times i_{dqs}\right) = E_{qs} i_{ds} - E_{ds} i_{qs}$$

This is an expression for reactive power in two-phase stationary frame for a balanced three phase system. In *d-q* moving coordinates, the expression is given by:

$$Q_{dqe} = E_{qe} i_{de} - E_{de} i_{qe} \qquad (41)$$

Recall that E_{qe} is always maintained to zero value, so:

$$Q_{dqe} = -E_{de} i_{qe} \qquad (42)$$

Eq. (42) shows that for a positive i_{qe}, Q_{dqe} is negative, implying that the active rectifier is feeding the reactive power back to the source. Alternatively for a negative i_{qe}, the Q_{dqe} is positive, resulting in net inflow of reactive power from source to the load.

3.11 Dynamic Equations for an Active Front-End Converter

For the purpose of fast response, the control is carried out in the *d-q* reference frame. This type of control is referred to as *'field-oriented'* control. The starting point of the control is the system of non-linear differential equations which characterizes its behavior. As derived previously, the dynamics of an active front-end converter are given by a system of differential equations stated below.

$$L\frac{di_{qe}}{dt} = E_{qe} - \omega L i_{de} - R i_{qe} - V_{qe} \tag{43}$$

$$L\frac{di_{de}}{dt} = E_{de} + \omega L i_{qe} - R i_{de} - V_{de} \tag{44}$$

The differential equation governing DC-link voltage also needs to be added to the above set of system equations to completely define system dynamics.

$$C\frac{dV_{DC}}{dt} = i_{DC} - i_M \tag{45}$$

where, i_{dc} is the total dc-link current supplied by the rectifier, while i_M is the load-side dc current which is the result of induction motor operation. The i_{dc} and i_M currents are shown in Fig. 3.17. Fig. 3.18 and Fig. 3.19 show ac and dc side equivalent circuits respectively.

The dc current, i_M, can be viewed as a noise in dc-link voltage V_{DC}. A positive i_M (motoring-mode) will discharge the dc-link, while a negative i_M (regeneration-mode) will charge the dc-link to a higher potential.

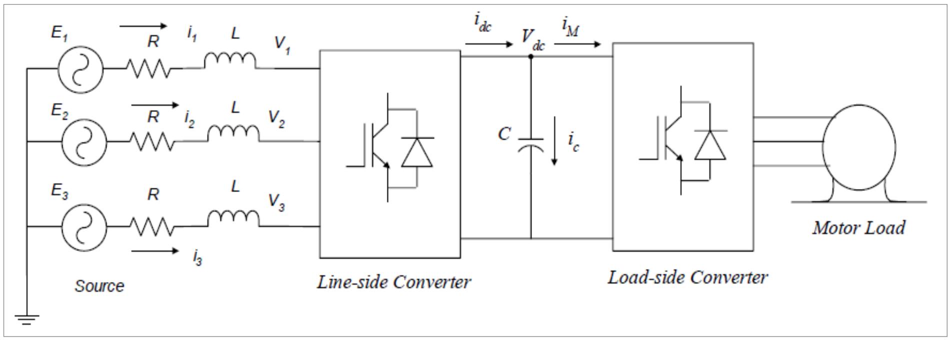

Fig. 3.17: DC-link dynamics controlled by line-side converter

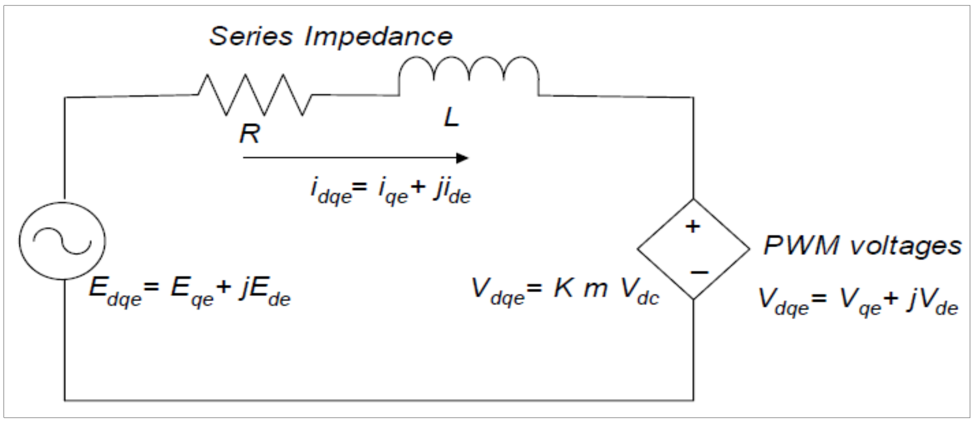

Fig. 3.18: AC-side per-phase equivalent circuit

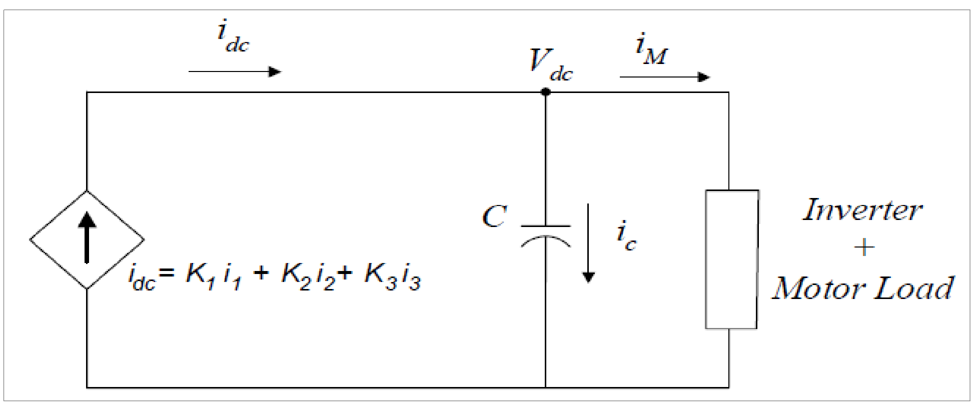

Fig. 3.19: DC-side equivalent circuit of an active drive

If the dc-link current i_{DC} supplied by the line side converter equals to i_M, then we have:

$$C\frac{dV_{DC}}{dt}=0.$$

In other words, dc-link voltage remains constant.

In Eq. (43), the terms E_{qe} and E_{de} are computed from source voltages, E_1, E_2, and E_3. Since line voltages are known, the angular frequency, ω, can be easily estimated. The PWM voltages V_{qe} and V_{de} are the two inputs to the system which are generated using the sine-triangle PWM controller. L_S and R represent series impedance.

Fig. 3.18 illustrates ac-side per-phase equivalent circuit representation of Eq. (43). V_{dqe} appears as a controlled voltage-source which is a function of a modulation index and dc-link voltage V_{DC}. On the other hand, **Fig. 3.19** shows dc-side equivalent circuit representation of Eq. 4.2. The dc-link current i_{DC} appears as a current source, which controls the capacitor voltage while supplying the current required by the motor load.

3.12 Control of the Active Drive

The system to be controlled is basically multiple-input-multiple-output (MIMO) type system. The PWM voltage commands, V_{qe} and V_{de}, are the two inputs to the system. The resultant i_{qe}, and i_{de} currents are the output of the system.

These two output currents are utilized for two different purposes. The i_{qe} component is assigned to produce the desired reactive power (Q=-$E_{de}i_{qe}$). Thus, i_{qe} is considered as a reactive compensation command.

Further, the real component of line currents is required to maintain constant voltage across dc-link capacitor, and also to drive a physical load connected to the motor. Thus, i_{de} is assigned to supply the desired real power ($P=E_{de}i_{qe}$) to the system.

The control problem is to choose V_{qe} and V_{de} in such a way as to force i_{qe} and i_{de} to track the respective reactive and real power reference trajectories.

3.12.1 Feed-Back Control

The suitable control strategy for the above mentioned non-linear system is the one which effectively eliminates the coupling between the two current components. This is done by forcing the system into current-command mode using high gain feedback. Firstly, the current reference commands need to be generated.

To ensure constant DC-link voltage, the PI control loop is applied to the dc-link voltage error, resulting in the current reference command, i_{de}*. The dc current, i_M, fed to the load through an inverter is added to i_{de}* to form a new current reference command as:

$$i_{de}* = K_{dI}'\int\left(V_{DC\_ref} - V_{DC}\right)dt + K_{dP}'\left(V_{DC\_ref} - V_{DC}\right) + i_M \qquad (46)$$

Secondly, the reactive power compensation algorithm will generate a second current reference command i_{qe}*. The PI controllers shown in Fig. 3.20 are then applied directly to the error between current reference and actual values, as shown below:

$$V_{de}* = K_{dI}\int \left(i_{de}* - i_{de}\right)dt + K_{dP}\left(i_{de}* - i_{de}\right) \tag{47}$$

$$V_{qe}* = K_{qI}\int \left(i_{qe}* - i_{qe}\right)dt + K_{qP}\left(i_{qe}* - i_{qe}\right) \tag{48}$$

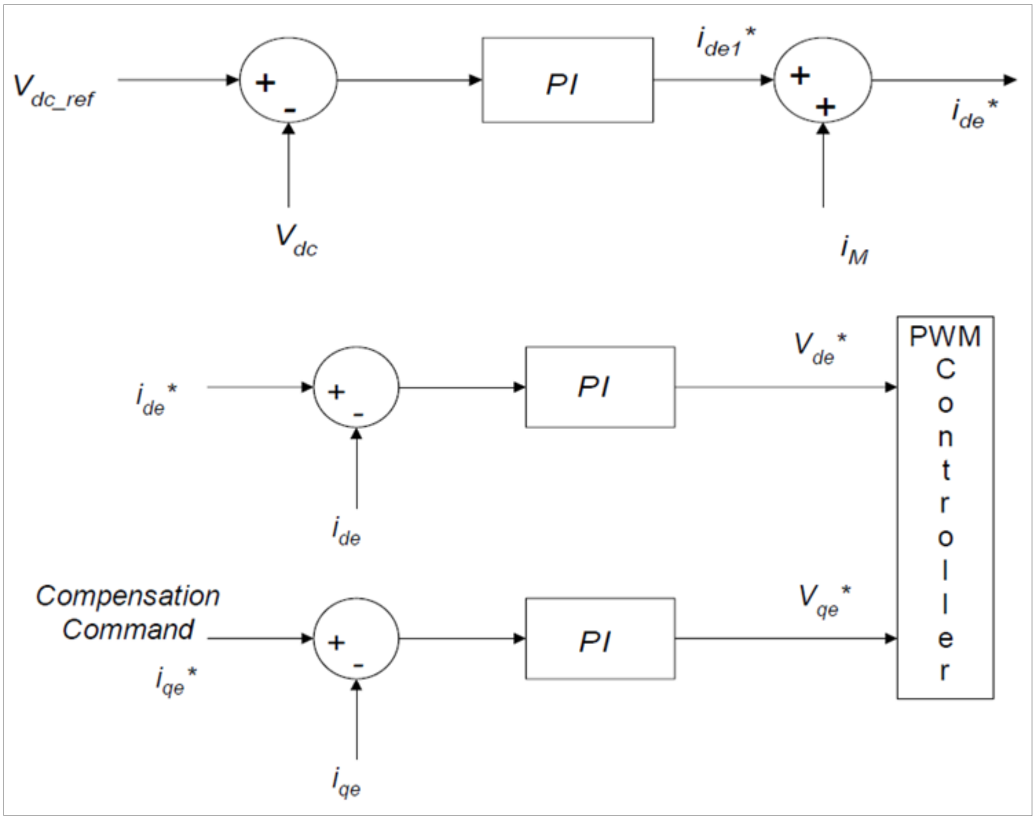

Fig. 3.20: High-gain feedback controller for line-side converter

By appropriately choosing the gains of the PI controllers, i_{qe} and i_{de} can be made to track i_{qe}* and i_{qe}* respectively. Consequently the new references, V_{de}* and V_{de}* for the PWM controller are generated. The PWM controller, if not saturated, will produce a switching pattern such that desired active and reactive power can be provided.

3.12.2 Estimating Angular Frequency of Source Voltages

The three-phase source voltages, separated by 120 electrical degrees, rotate at an angular speed of ω radians per second. Since the control is carried out in moving coordinates, all the variables must be converted to the moving coordinate system, rotating at an exact same angular speed of ω rad/ sec.

The source voltage frequency usually remains unchanged during normal operation of the power system. However, even a small variation in ω will cause error in all the parameters that are transformed into the rotating coordinate system. This will result in erroneous feedback and consequently affect the performance of the system. For this reason, the supply frequency needs to be tracked and continuously estimated in real time.

Recall, for a given supply frequency, we choose *d*-*q* axes such that E_{qe} component always remains zero. Now if the supply frequency changes, E_{qe} will no longer be zero. The error in E_{qe} can be minimized by a PI controller to track ω in real-time as:

$$\omega = K_I \int \left(0 - E_{qe}\right) dt + K_P (0 - E_{qe}) \tag{49}$$

The new angular displacement θ_e, is then given by:

$$\theta_e = \int \omega \cdot dt \tag{50}$$

By choosing appropriate gains for the PI controller the variations in supply frequency can be tracked accurately. This is illustrated in Fig. 3.21.

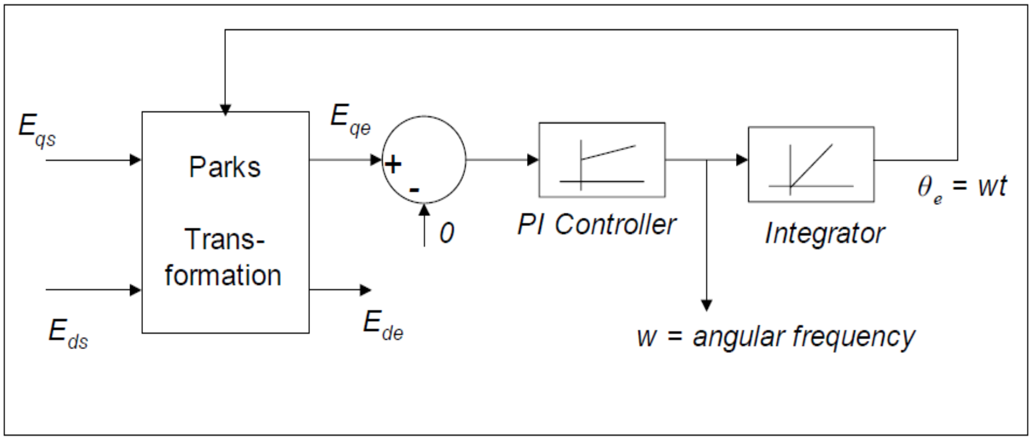

Fig. 3.21: Supply voltage frequency estimation

3.12.3 Input-Output Linearization Control

For a relatively constant V_{DC}, the field oriented high-gain feedback control scheme, explained in the previous section, removes the coupling effect. In other words, the current equations are decoupled, and the equations are linear as long as dc-link voltage is constant. Recall the system dynamic equations:

$$
\begin{aligned}
L\frac{di_{qe}}{dt} &= E_{qe} - \omega L i_{de} - R i_{qe} - V_{qe} \\
L\frac{di_{de}}{dt} &= E_{de} + \omega L i_{qe} - R i_{de} - V_{de} \qquad (51) \\
C\frac{dV_{DC}}{dt} &= i_{DC} - i_M
\end{aligned}
$$

The PWM voltages *Vqe* and *Vde* can be represented in terms of modulation index and dc-link voltage as:

$$V_{qe} = G \cdot M_{qe} \cdot V_{DC} \qquad (52)$$

$$\mathrm{V}_{de} = G \cdot M_{qe} \cdot V_{DC} \qquad (53)$$

Where G is the PWM controller gain and M_{qe} and M_{de} are modulating vectors in d-q coordinates. For large variations in dc-link voltage; however, the equations are no longer linear. This situation arises when the motor load changes suddenly or during high acceleration and decelerations (regeneration) of motor shaft.

During DC-link variations, the i_{de} current reference varies as a function of V_{DC}. The dynamics of i_{de} then interfere with the dynamics of i_{qe}, resulting into unsatisfactory performance. This coupling of currents can be effectively eliminated by considering an input-output linearization controller.

In dynamic eq. (51), V_{qe} and V_{de} are the inputs, controlled in such a way as to generate desired currents. Now define new variables V_{qe}' and V_{de}' such that:

$$V_{qe}' = V_{qe} - E_{qe} + \omega L i_{de} + R i_{qe} \qquad (54)$$

$$V_{de}' = V_{de} - E_{de} - \omega L i_{qe} + R i_{de} \qquad (55)$$

So that the new system dynamic equations become:

$$L \frac{di_{qe}}{dt} = -V_{qe}' \qquad (56)$$

$$L \frac{di_{de}}{dt} = -V_{de}' \qquad (57)$$

In equations (56)-(57), the dynamics of i_{de} and i_{qe} are decoupled. The high gain feedback controller is then applied to these currents to generate new voltage commands.

The final voltage commands however, should account for the substitution made in equations 54 and 55. Thus new voltage references are given by:

$$V_{qe}* = V_{qe}'* + E_{qe} - \omega L i_{de} - R i_{qe} \tag{58}$$

$$V_{de}* = V_{de}'* + E_{de} + \omega L i_{qe} - R i_{de} \tag{59}$$

3.12.4 Feed-Forward Compensation

The linearization controller explained in the previous section decouples the two current controllers effectively, and allows the system operation during variable dc-link. However, the system still suffers from slow response.

Refer to the Fig. 3.17 again, and consider following sequence of events. If the motor load changes suddenly, dc current i_M will rise sharply, resulting in a dip in DC-link voltage. The linearization controller now tries to restore the dc-link voltage back to its reference value. If the rate of rise of dc current i_M is faster than rate of restoration of DC-link voltage, the V_{dc} will continue to decrease until it reaches zero potential. Alternatively, the rate of rise of i_M can be restricted to avoid considerable decrease in DC-link voltage. In other words the system time response would be slow.

A better dynamic response is achieved by employing feed-forward compensation. The power required to generate the desired electromagnetic torque is measured in the dc-link using dc voltage and current sensors. This power needs to be supplied from the source. Thus, the feed-forward compensation current i_{d_f} can be obtained from:

$$i_{d\_f} = K_1 \frac{V_{DC} i_{DC}}{E_{DE}} \qquad (60)$$

where, E_{de} is source voltage and K_1 is proportional gain in feed-forward loop. K_1 is allowed to vary to maintain the stability in the current loop, and it is also dependent on line voltage fluctuations.

Fig. 3.22 illustrates feed-forward compensation with input-output linearization controller.

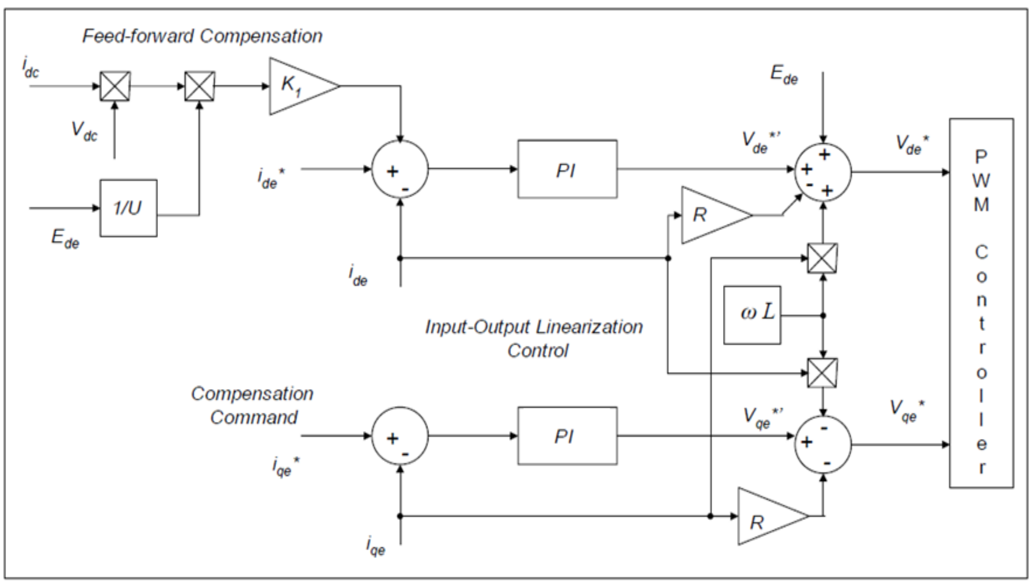

Fig. 3.22: Feed-forward compensation for input-output linearization controller

3.12.5 Complete Control Scheme for Active Front-End Converter

Based on above discussions the complete control scheme for control of active front-end converter is implemented using two ac voltage sensors, three line current sensors, one dc current sensor, and one dc voltage sensor.

Fig. 3.23 illustrates the control of front-end converter.

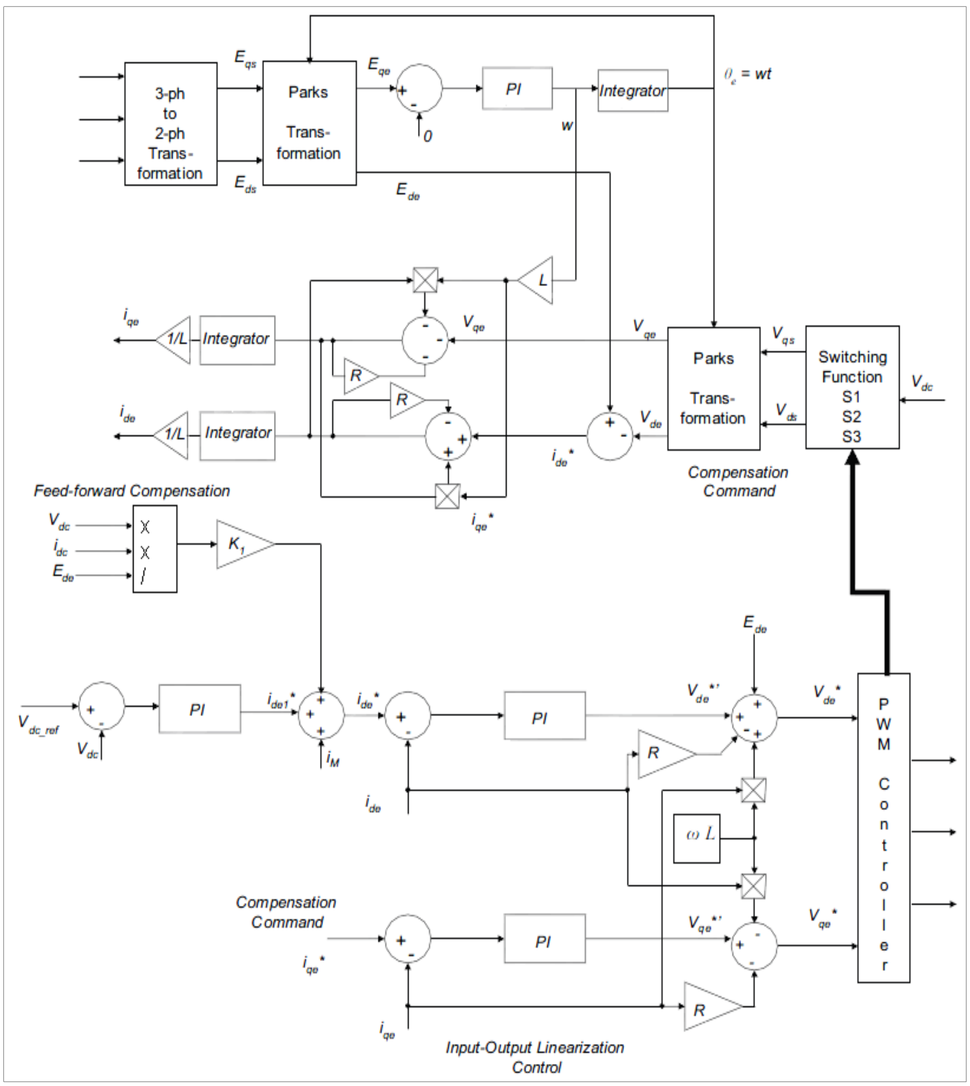

Fig. 3.23: Complete control scheme for front-end converter

The two ac voltage sensors are connected to the source voltage. From these line sensors, the three source voltages (phase-neutral) are available for use. These voltages are further transformed into equivalent two-phase moving coordinates E_{qe} and E_{de}. The *de*-*qe* axes are aligned such that the E_{qe} component of the source voltages always remains at zero value.

The next step is to generate current references. The i_{de} reference is formed as a function of dc-link voltage variations and feed-forward compensation. The dc current i_M, is measured by the dc current sensor placed on load-side of the capacitor. The i_{qe} reference current is generated from the reactive power compensation command. In current-command control mode, the actual currents i_{qe} and i_{de} are forced to follow the reference commands using high-gain feedback and input-output linearization controller.

The new input for the system, V_{qe} and V_{de}, are fed to PWM controller to provide required switching pulses using either sine-triangle or space-vector PWM algorithm. The instantaneous values of currents i_{qe} and i_{de}, can be measured using three current sensors. Alternatively, they are estimated using the system dynamic model shown in eq. (51). In the model, L, ω, E_{qe} and E_{de} are all known; V_{qe} and V_{de} are unknown. The instantaneous values of PWM voltages are estimated from the switching signals to IGBT devices, and the dc-link voltage as shown below:

$$V_{qs} = \frac{V_{DC}}{4}\left(2S_1 - S_2 - S_3\right) \tag{61}$$

$$V_{ds} = \frac{V_{DC}}{4}\sqrt{3}\left(S_2 - S_3\right) \tag{62}$$

where S_1, S_2, S_3 are integer variables which cannot assume any values other than +1 and -1.

When the IGBT in the upper half of the first leg of the rectifier-bridge is switched on, $+V_{dc}$ is connected to the phase-1 of the supply. Thus, S_1 assumes value equal to 1. When this IGBT is switched off, $-V_{dc}$ is connected to the phase-1 of the supply. Thus, S_1 assumes value equal to -1. In the same manner S_2 and S_3 assume value equal to either 1 or -1. This approach measures instantaneous values of PWM voltages without needing to employ three current sensors.

3.13 Simulation Model

The dynamic simulation model is builded using the Matlab Simulink platform.

In Fig. 3.24 is presented a sketch of the simulation model that applies the control scheme shown in Fig. 3.23.

As it can be seen , the Active Front End Converter is Interfaced with the grid via a 380V/50kVA trasformer, as the one that is used to interfaced the non linear loads connected at the PCC point.

The Active Front End Converter in parallel with three phase loads which are connected with the grid via breakers in different instant of time. This is to vary the condition of load connected in the PCC point of the system.

The switching frequency of the Active Front End converter is 5 kHz, meanwhile the Back End converter used to drive the Active Front End own load has a switching frequency of 5 kHz, meanwhile the DC-link Voltage is 600V.

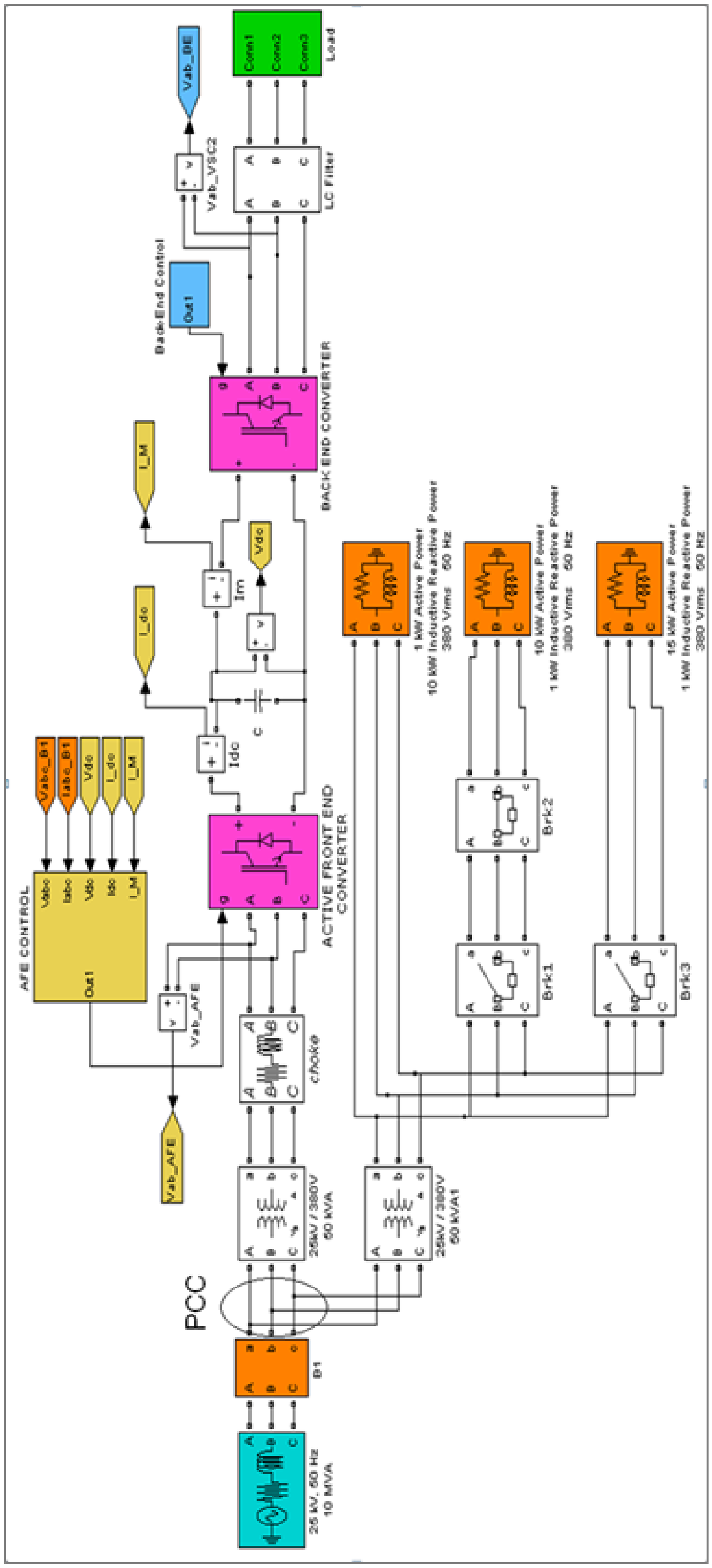

Fig. 3.24: Simulation model of the AFE

3.14 Simulation Results

In the following sections simulation results are shown. First simulation results under normal condition mode are presented. Afterwards, simulations in presence of voltage sags and voltage notches are presented.

3.14.1 Normal Condition mode

In normal condition mode, the AFE has to manage, in adition to its own load, the non linear load changes in the PCC point. These changes modify the phase displacement between voltage and current of the same phase of the grid, bringing to a non unity power factor condition. The Active Front End manages to bring the Power Factor back to unity.

The simulation parameters are presented in Table 13.

Table 13: Normal Condition mode simulation parameters

DC link Capacitor	2.5 mF
L	2 mH
R	0.015 Ω
AFE PWM modulator frequency	5 kHz
Back End PWM modulator frequency	5 kHz
DC-Link Voltage	600 V

In Fig. 3.25 are presented the simulation results for the E_{abc} at PCC point, i_{abc} at PCC point, $V_{dc\text{-}Link}$ and modulation index m in an interval of time of 0.5 sec..

For the first 100ms the AFE has to drive his own resistive-inductive (RC) load and has also to perform power factor correction due to the presence of the RC load connected at the PCC point. After the first 12ms we can see that the grid currents are in phase with the grid voltages , the value of the DC-Link has stabilized to 600 V with ripple 0.5V, the grid active current I_{de} flows through the RC load connected at the PCC point and the AFE, the reactive current I_{qe} stabilized around zero (unity power factor condition) and the modulation index m stabilized around 0.75.

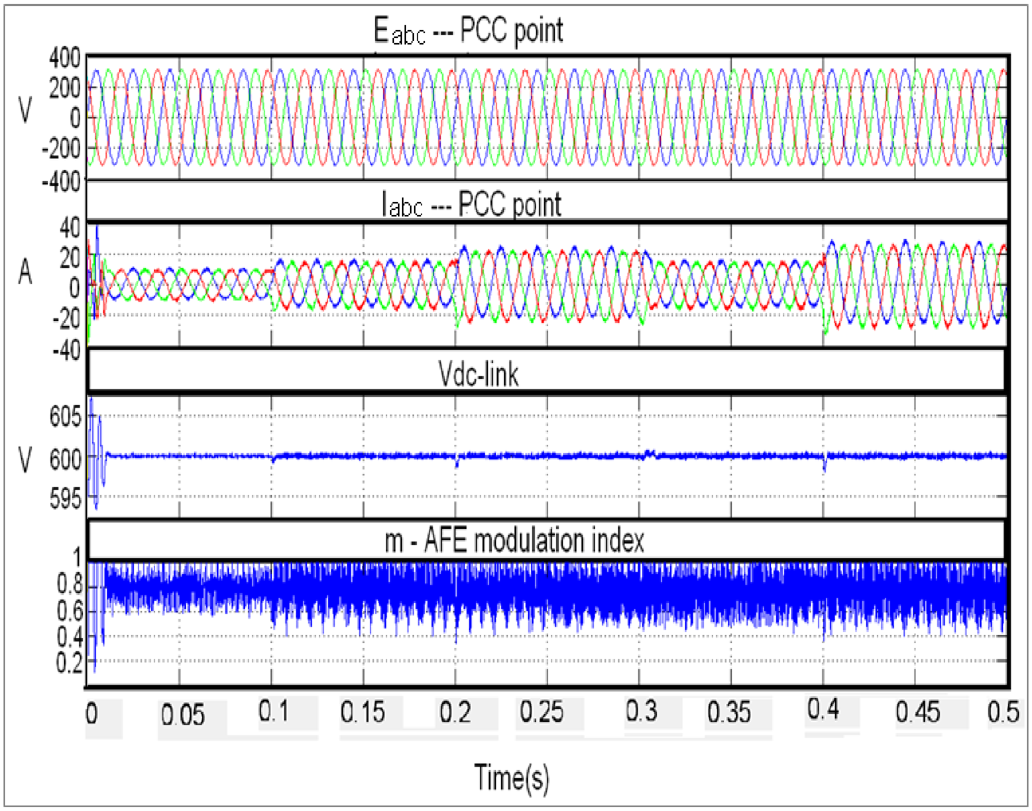

Fig. 3.25: AFE Normal Mode simulation results

In Fig. 3.26 is shown the I_{qe} and I_{de} flow at the PCC point, meanwhile, in Fig. 3.27 is shown the DC-link voltage over time.

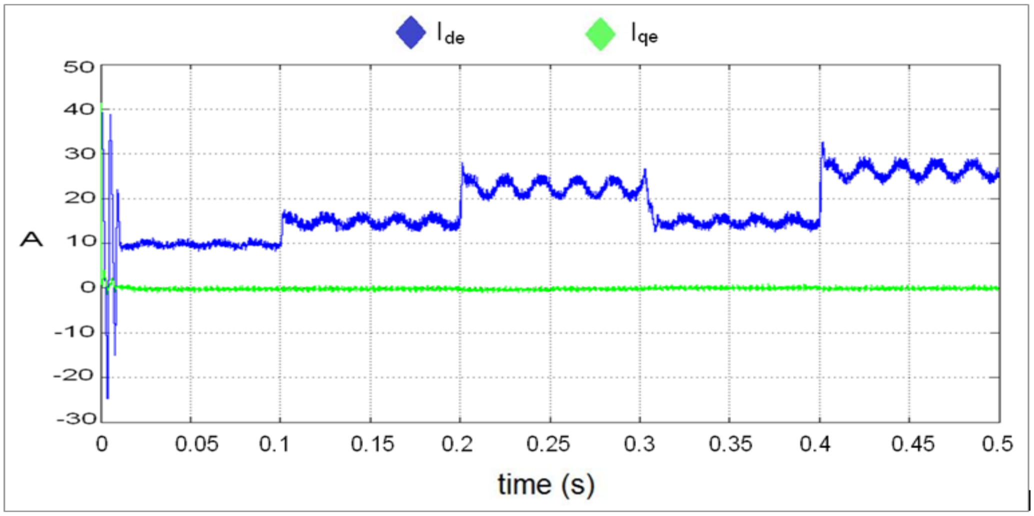

Fig. 3.26: Grid i_{qe} and i_{de}

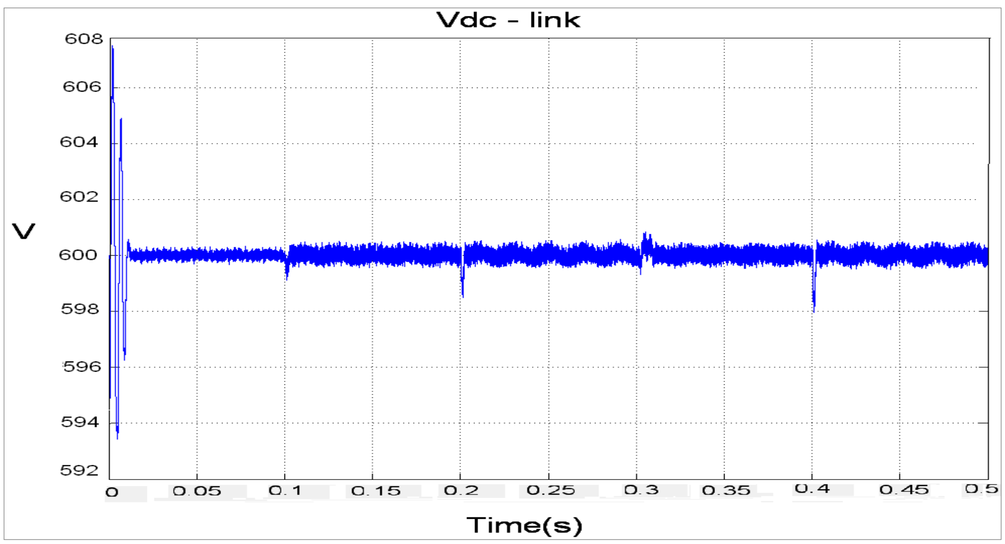

Fig. 3.27: DC-link voltage over time

At 0.1s, The AFE load changes and so does the overall I_{de} current. The V_{dc} drops to 599V and then settles back to 600V (1V ripple). At 0.2s, 0.3s and 0.4s step changes occur to the RC load connected in parallel with the AFE. As you can see, in these instants, after a small amount of settling time, the dc-link stabilizes to 600V and the phase shift between E_{123} and i_{123} returns to zero. Note that for the whole time the AFE tries to maintain the i_{qe} to zero to obtain Unity Power Factor in all mentioned working conditions.

In Fig. 3.28 is shown the E_1 and i_1 on the same graph. $E_1$was scaled by a 0.1 factor for better visualization. Note that, after each load step change, the AFE bring the phase displacement to 0.

In Fig. 3.29 is presented a zoom of the Fig. 3.28 to better appreciate the step load change at 0.2s and the successive modification of the phase displacement between E_a and i_a.

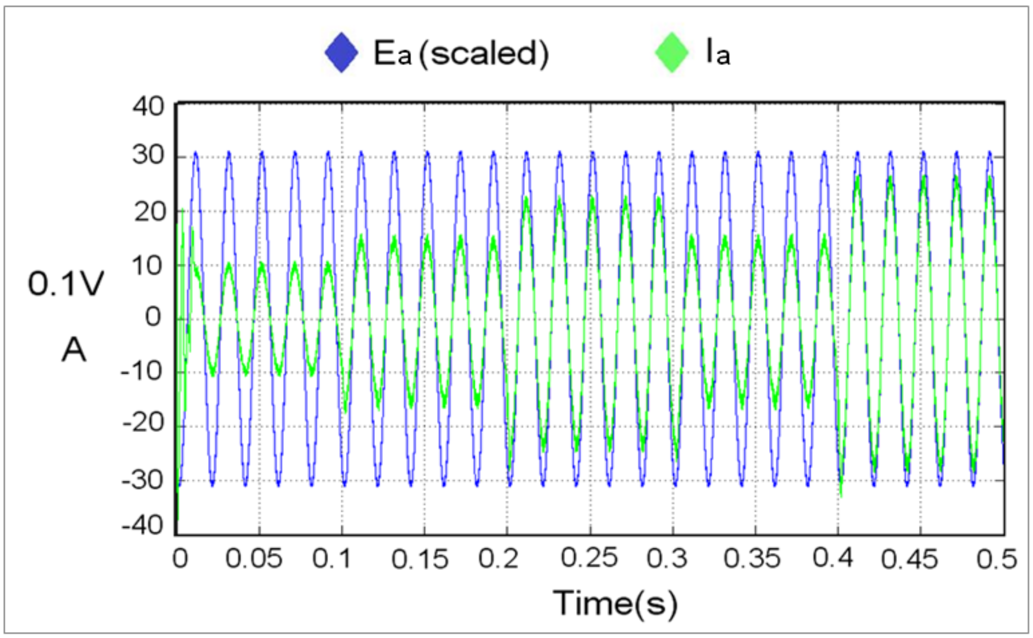

Fig. 3.28: Phase displacement between E_1 voltage and I_1 current of phase 1

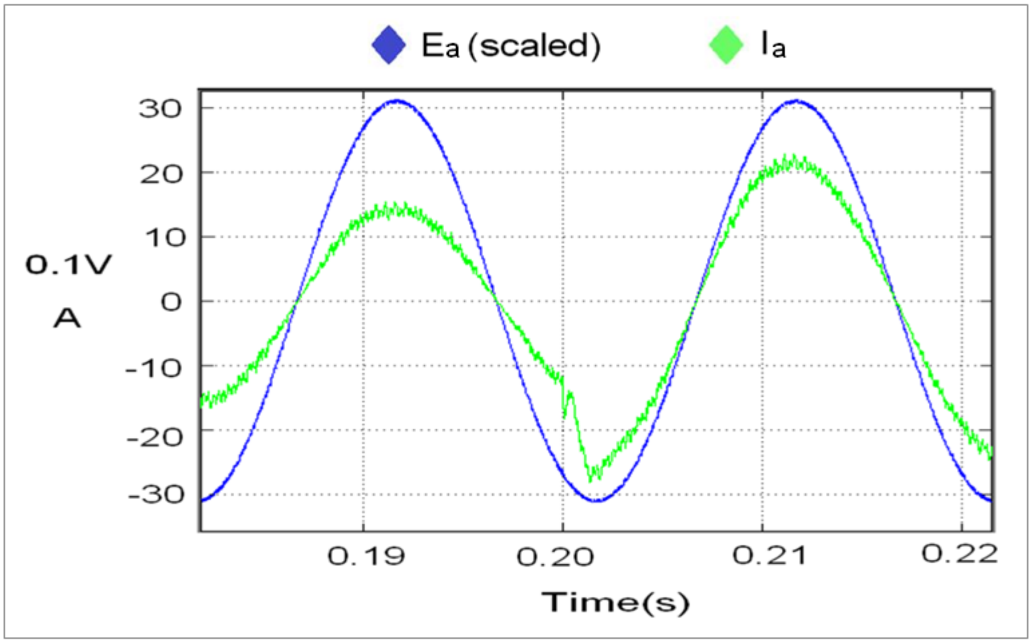

Fig. 3.29: Phase displacement between E1 and I1 at 0.2s instant load step change

As it can be seen, the simulated model gives a good reppresentation of the behavior of the Active Front End Converter performing simultaneously power delivering to the own load and Reactive Power compensation tasek during different load conditions, in normal mode conditions.

3.14.2 AFE in presence of voltge sags

There are several types of voltage fluctuations that can cause problems, including surges and spikes, sags, harmonic distortions, and momentary disruptions. (For definitions of these terms, see the "Power Quality Glossary" sidebar, next page.)

A voltage sag is not a complete interruption of power; it is a temporary drop below 90 percent of the nominal voltage level. Voltage sags are probably the most significant power quality problem facing industrial customers today, and they can be a significant problem for large commercial customers as well. There are two sources of voltage sags: external (on the utility's lines up to your facility) and internal (within your facility). Utilities continuously strive to provide the most reliable and consistent electric power possible.

Whether or not a voltage sag causes a problem will depend on the magnitude and duration of the sag and on the sensitivity of your equipment. Many types of electronic equipment are sensitive to voltage sags, including variable speed drive controls, motor starter contactors, robotics, programmable logic controllers, controller power supplies, and control relays. Much of this equipment is used in applications that are critical to an overall process, which can lead to very expensive downtime when voltage sags occur.

Here will be presented the behavior of the presented Active Front End converter in presence of non-repetitive voltage sags.

Different ways are used to mitigate the voltage sags, such as:

- **Flywheel**

  A flywheel and motor-generator (M/G) combination can protect critical processes against all voltage sags where the duration is shorter than the hold-up time of the flywheel.

- **Static UPS with minimal energy storage**

  These devices are primarily intended to maintain supply during supply interruptions by providing, for example, sufficient support to allow for an orderly shutdown of processes.

- **Dynamic Voltage Restorer (DVR)**

During a voltage sag, a dynamic voltage restorer (DVR) adds the missing voltage through a transformer, installed in series with the load.

- **Shunt connected synchronous machine**

  The capability of the synchronous machine to supply large reactive currents enables this system to lift the voltage by 60% for a few seconds.

- **Statcom**

  A static VAR compensator is a current injector connected in parallel (shunt) with the load (Figure 6). A statcom mitigates voltage sags by injecting reactive power into the system.

- **Transformless series injection**

  In the event of a voltage sag, the static switch of this series injection device is opened and the load is supplied by an inverter.

3.14.2.1 Single phase voltage sag

First we will analyze the case in which an isolated voltage sag occurs in one of the phases. The simulation parameters are the ones presented in Table 13.

The Voltage sag was simulated considering the fault resistance R_{on}=0.3Ω and the ground resistance R_g=0.3Ω. It was first considered the fault in the A Phase of the grid and then in both phase A and B.

In Fig. 3.30 are shown the simulation results for the E_{abc} at PCC point, i_{abc} at PCC point, V_{dc} and modulation index m in function of time.

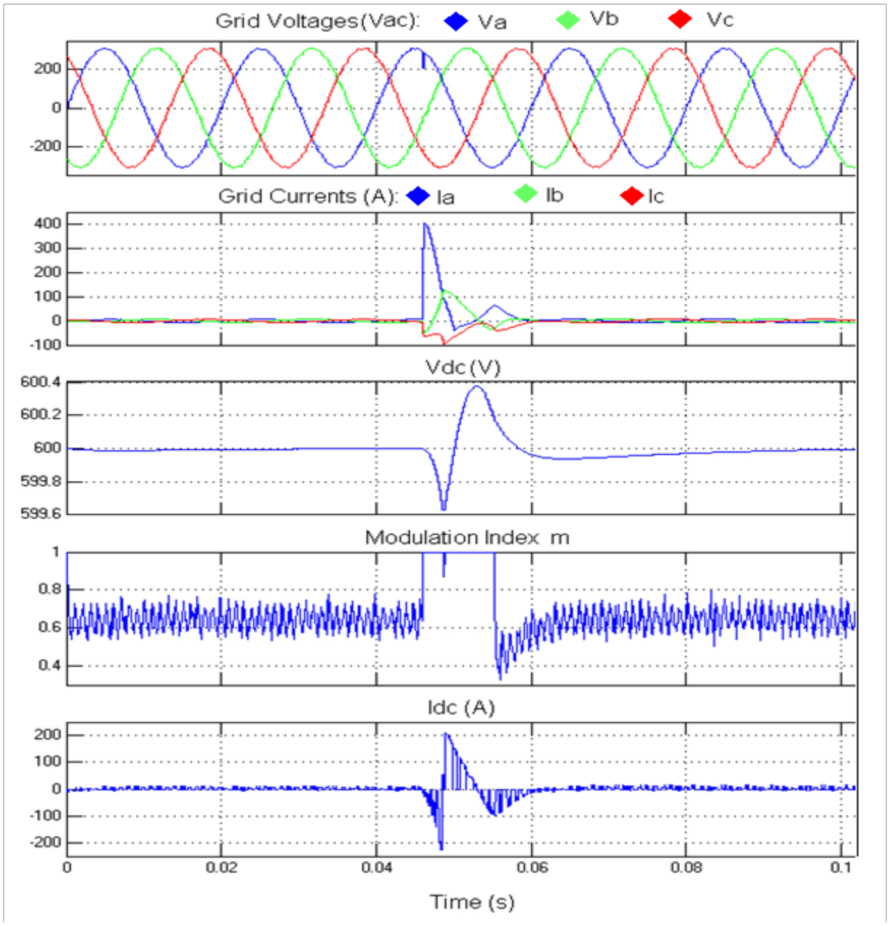

Fig. 3.30: Parameters simulation at PCC point Voltage Sag in Phase A at t=0.046s

It can be seen that in t=0.046s a voltage sag of the duration of 1ms occurs in phase A. It can be seen that in that exact instant the current of phase A increases and the V_{dc} decreases. The modulation index m changes as well, as the Active Front End tries to recover.

In Fig. 3.31 it can be seen better what happens in phase A in terms of voltage and current when the voltage sag occurs. From 0s to 0.046s it can be seen that the current and voltage of Phase A are in phase. At t = 0.046s a current spike occurs due to the voltage sag. After the voltage sag (t = 0.047s) the Active Front End tries to set to zero once again the phase between voltage and current (unity power factor).

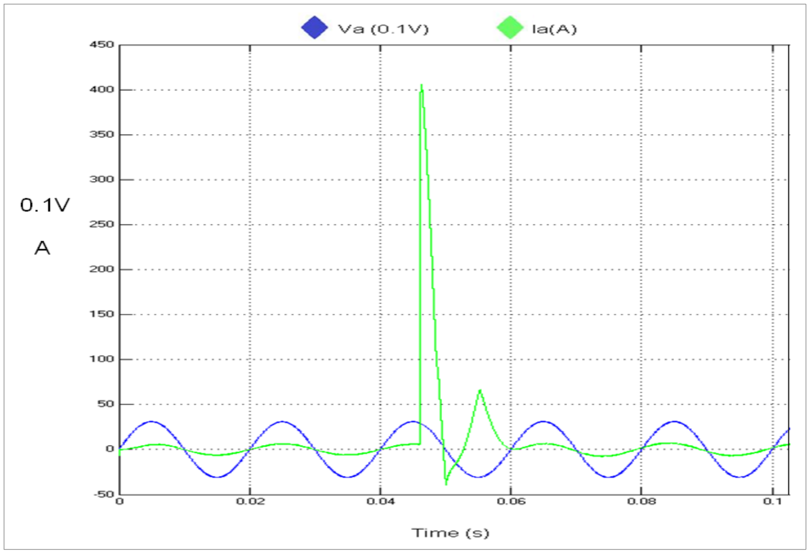

Fig. 3.31: Phase displacement between voltage and current in Phase A

In Fig. 3.32 is shown the Active Power (P) and the Reactive Power (Q).

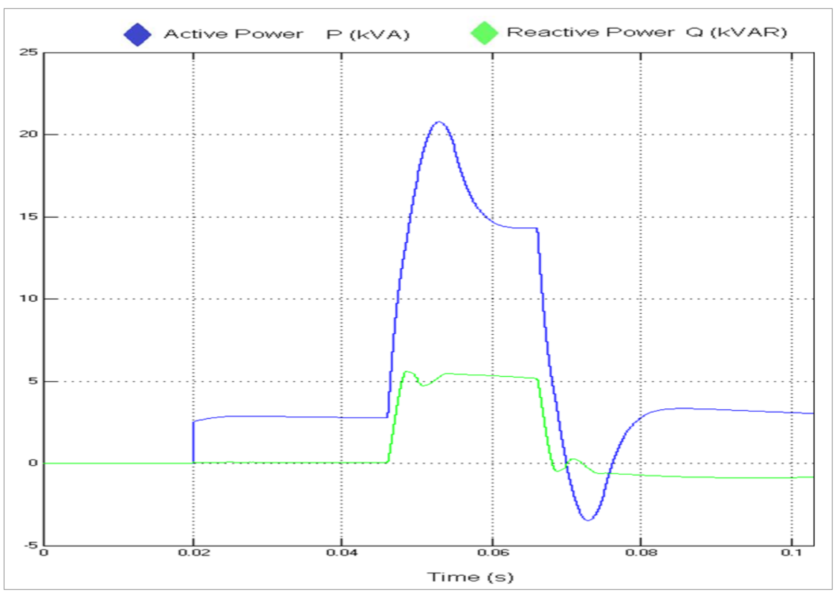

Fig. 3.32: Active Power and Reactive Power Flows, single Voltage Sag

When the Phase displacement between Voltage and Current of certain phase is equal to zero, the Reactive Power is equal to zero too. This can be seen in Fig.8 in the time interval 0:0.046 in which the Reactive Power is Q=0, meanwhile the Active Power is different from zero due to the load connect to the Active Front End. When the Voltage Sag occurs there is a positive Reactive Power flow due to the changed phase displacement and an increase of the Active Power demand due to the rapid decrease of the V_{dc}, as can be seen in Fig. 3.30. At t=0.047, after the restored voltage level in Phase A, the Active Front End Tries to reset the phase displacement to zero, and so the Reactive power tends to zero.

3.14.2.2 Double phase voltage Sags

In Fig. 3.33 are shown the simulation results for the E_{abc} at PCC point, i_{abc} at PCC point, V_{dc} and modulation index m in function of time for the case when in both phases A and B a voltage Sag occurs.

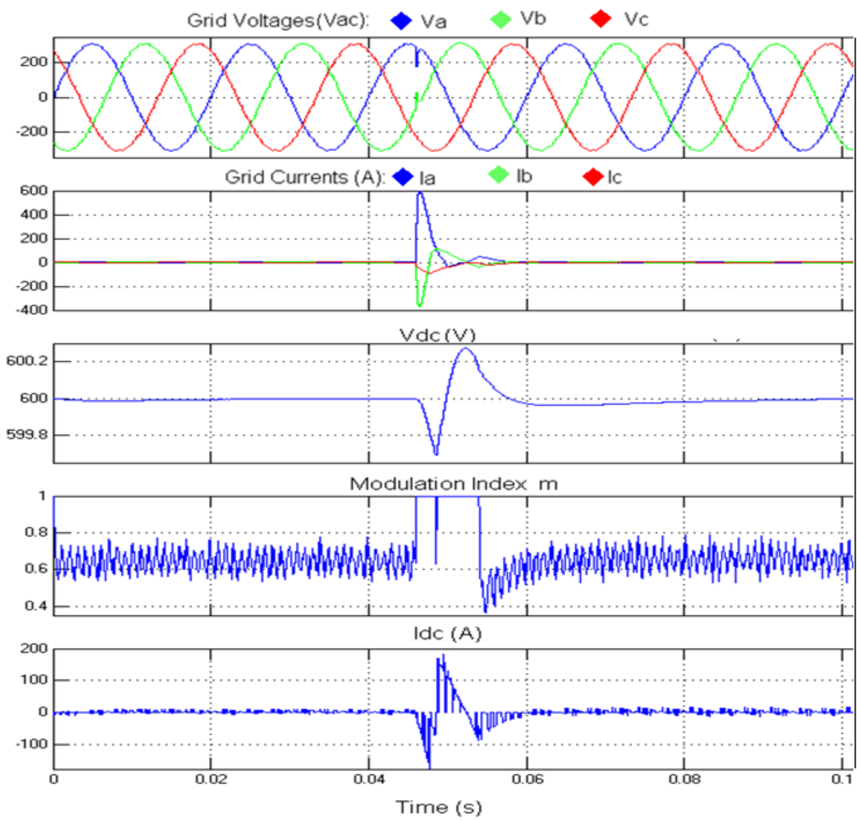

Fig. 3.33: Parameters simulation at PCC point Voltage Sag in Phase A and B at t=0.046s

It can be seen that in t=0.046s a voltage sag of the duration of 1ms occurs in phase A and phase B. It can be seen that in that exact instant the current of phase A increases, the current of phase B decreases due to the fact that in that instant the voltage in phase B has a negative value and the V_{dc} decreases. The modulation index m changes as well, as the Active Front End tries to recover.

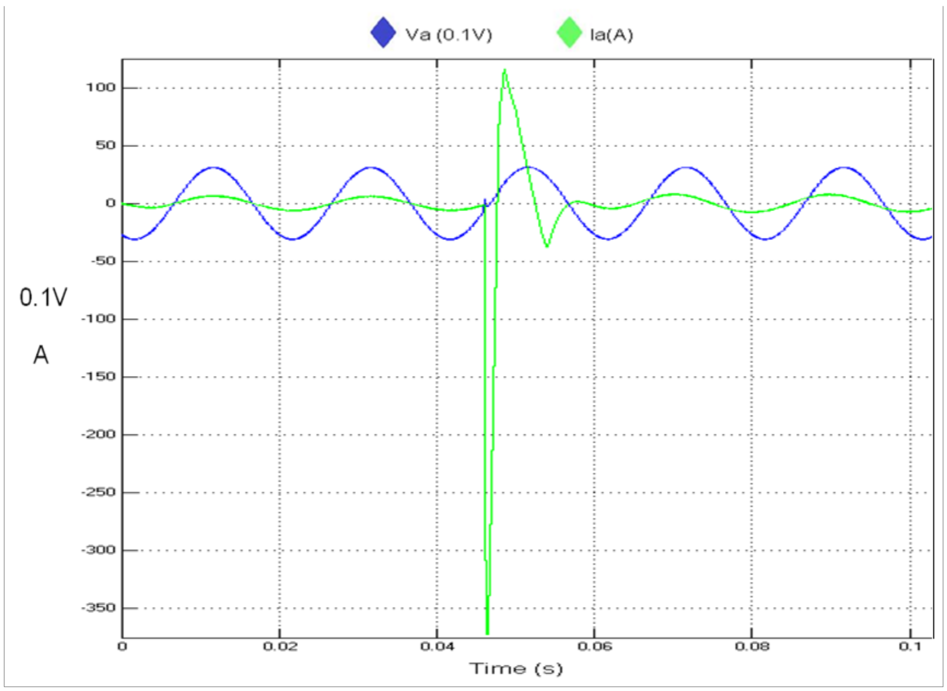

Fig. 3.34: Phase displacement between voltage and current in Phase B

In Fig. 3.34 is presented the phase displacement between voltage and current in Phase B in which we can see the rapid decrease of the Phase B current when the Voltage Sag occurs.

In Fig. 3.35 is presented the Power flow in the system during the double Voltage Sag.

As it can be seen, comparing to the first case (**Fig. 3.32**) the Active Power is almost the same, but the Reactive Power Peak is almost doubled (from 5.5kVAR to 12kVAR).

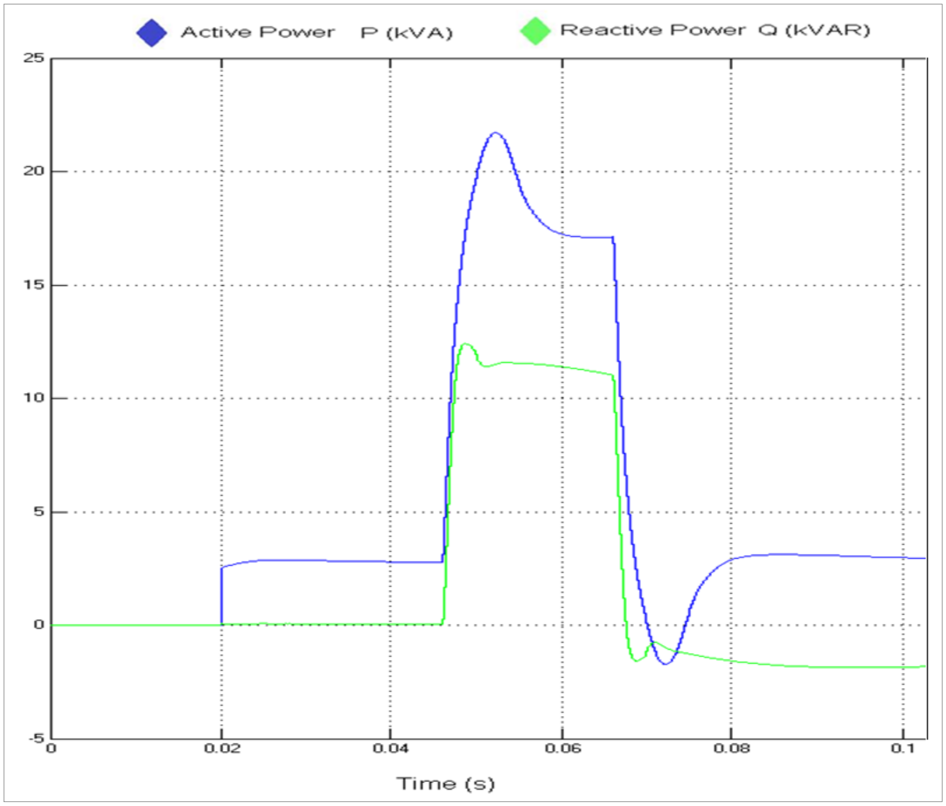

Fig. 3.35: Active Power and Reactive Power Flows, Double Voltage Sag

3.14.3 AFE in presence of voltge notches

Voltage Notching is described as a recurring power quality disturbance due to the normal operation of power electronic devices (i.e. rectifier), when current is commutated from one phase to another. Voltage Notching is described by IEEE as a recurring power quality disturbance due to the normal operation of power electronic devices (i.e. rectifier), when current is commutated from one phase to another.

Voltage Notching is primarily caused by three-phase rectifiers or converters that generate continuous DC current. As mentioned, the voltage notches happen when the current commutates from one phase to another. Subsequently, a momentary short circuit between two phases will occur during this period.

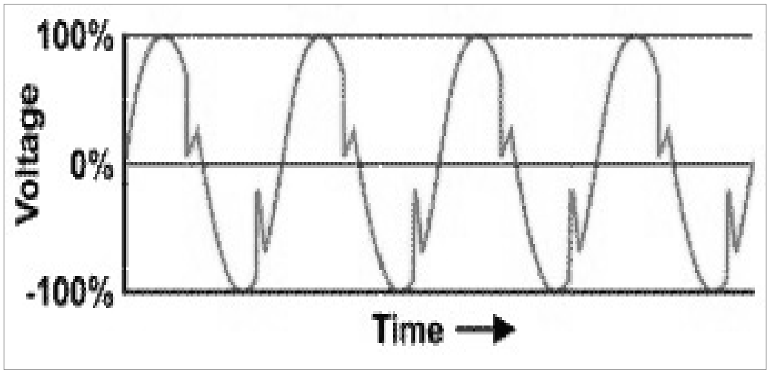

Fig. 3.36: Voltage Notches

Two case studies were considered. The first a case considered a train of voltage Notches occurring in Phase A and the second case considered the same voltage notches train occurring in both phase A and Phase B.

In Table 14 are presented the simulation parameters. The dynamic simulation model is built using the Matlab Simulink platform.

Table 14: Voltage notches simulation parameters

DC link Capacitor	2.5 mF
L	2 mH
R	0.015 Ω
AFE PWM modulator frequency	5 kHz
Back End PWM modulator frequency	5 kHz
DC-Link Voltage	600 V

3.14.3.1 Single phase voltage notches

The Voltage notches are simulated considering the fault resistance $R_{on}=0.4\Omega$ and the ground resistance $R_g = 0.3\Omega$. It was first considered the fault in the A Phase of the grid and then in both phase A and B. An interval of time of 86 ms was considered in which the voltage notches occurred.

In Fig. 3.37 are shown the simulation results for the E_{abc} at PCC point, i_{abc} at PCC point, V_{dc} and modulation index m in function of time.

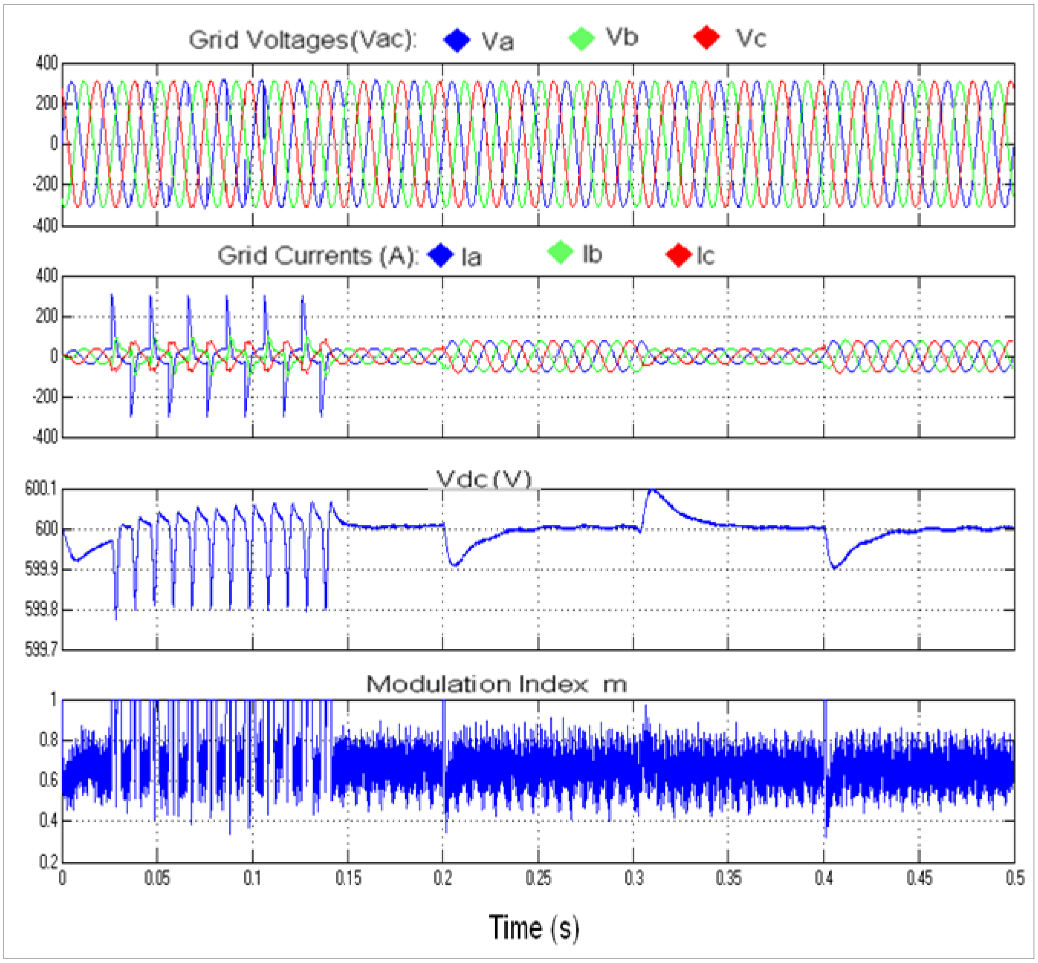

Fig. 3.37: Single phase Notches Parameters simulation at PCC point Voltage notches occurred in Phase A from t=0.046.s to t=0.1262

It can be seen that in the time interval [0.046 0.1262] a total of 12 voltage notches occurred in phase A, each with a duration of 0.2ms.

It can be seen that in that exact instant when the voltage notch occurs the current of phase A increases and the V_{dc} decreases. The modulation index m changes as well, as the Active Front End tries to recover and bring the Power Factor back unity.

In Fig. 3.38 it can be seen better what happens in phase A in terms of voltage and current when the voltage notches occur.

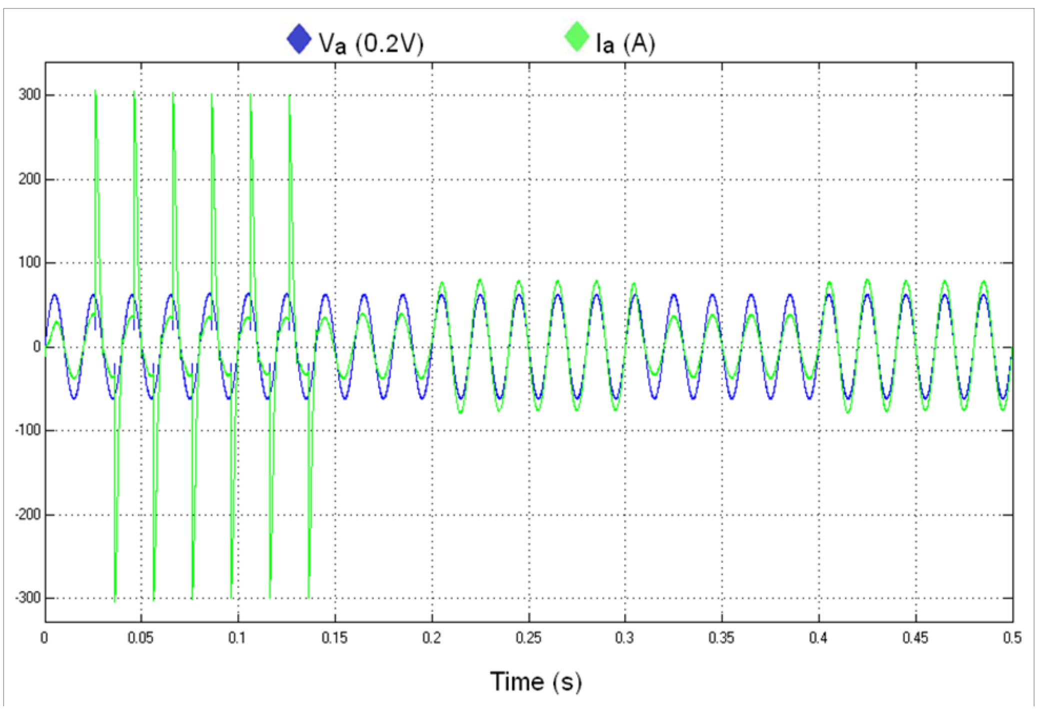

Fig. 3.38: Phase displacement between voltage and current in Phase A Single Phase Notches event.

From 0s to 0.046s it can be seen that the current and voltage of Phase A are in phase (unity Power Factor). From t = 0.046s to t = 0.1262s current spikes corresponding to the voltage notch instant occur. At t = 0.1262 (After the Voltage Notches event) the Active Front End Tries to set to zero once again the phase between voltage and current. As it can be seen, after each current spike the AFE tries to recover the unity Power Factor.

In Fig. 3.39 is shown the Active Power (P) and the Reactive Power (Q).

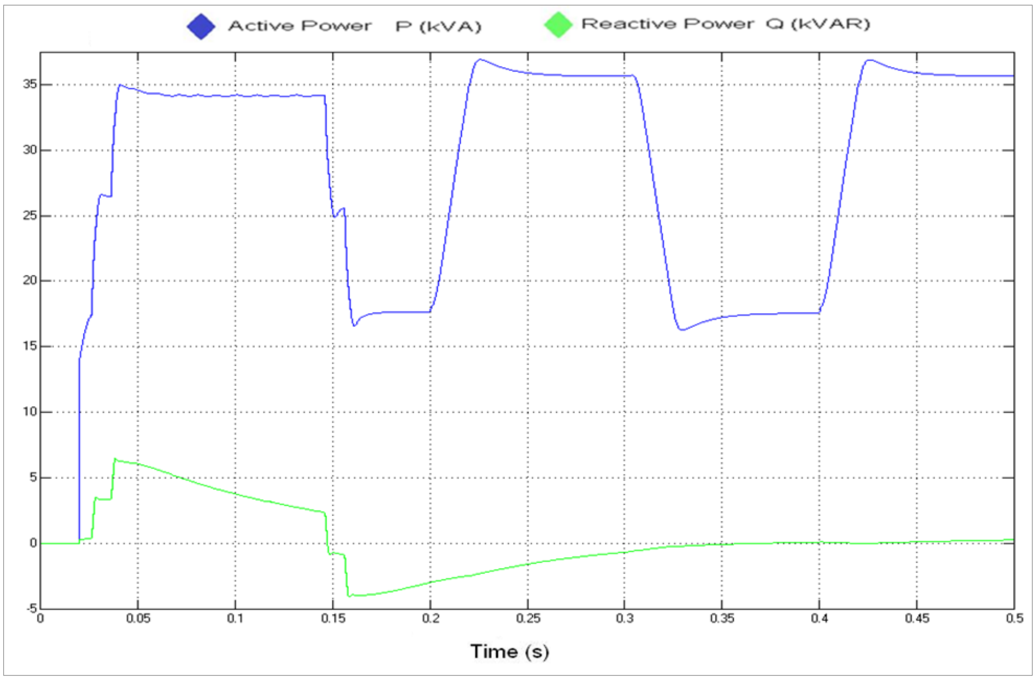

Fig. 3.39: Active Power and Reactive Power flows, single phase Voltage Notches event.

When the Phase displacement between Voltage and Current of certain phase is equal to zero, the Reactive Power is equal to Zero too. This can be seen in Fig. 3.38 in the time interval 0:0.046 in which the Reactive Power is Q=0, meanwhile the Active Power is different from zero due to the load connect to the Active Front End. The changes of the active power are due to the changes of the load conditions of the AFE.

When the Voltage Notches occur there is a positive Reactive Power flow due to the changed phase displacement and an increase of the

Active Power demand due to the rapid decrease of the V_{dc}, as can be seen in Fig. 3.39. At t=0.1262, after the restored voltage level in Phase A, the Active Front End tries to reset the phase displacement to zero, and so the Reactive power tends to zero.

In Fig. 3.40 are presented the active and reactive currents in the rotary reference frame, relative to the single phase voltage notches event.

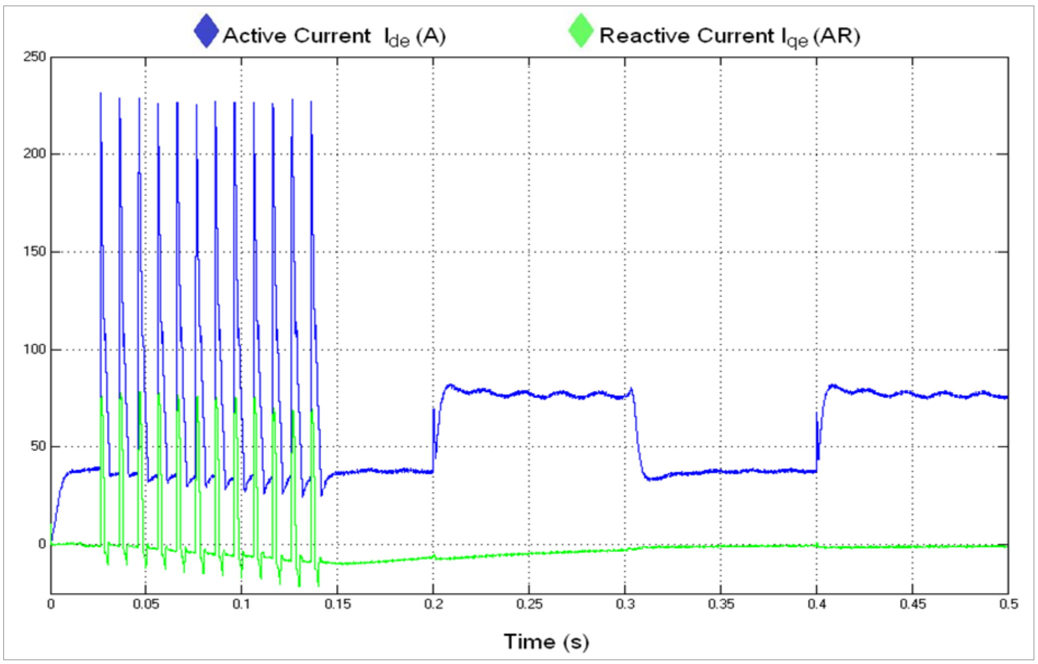

Fig. 3.40: Active and Reactive Currents in the rotary reference frame, single phase notches event.

As it can be seen in Fig. 3.40, after the Voltage Notches event, Iqe is negative, meaning that the phase current is anticipating the phase voltage (Fig. 3.38). Iqe then tend to zero, meaning that the phase displacement between voltage and current tends to zero too (unity Power factor).

3.14.3.2 Double phase voltage notches

In Fig. 3.41 are shown the simulation results for the E_{abc} at PCC point, i_{abc} at PCC point, V_{dc} and modulation index m in function of time.

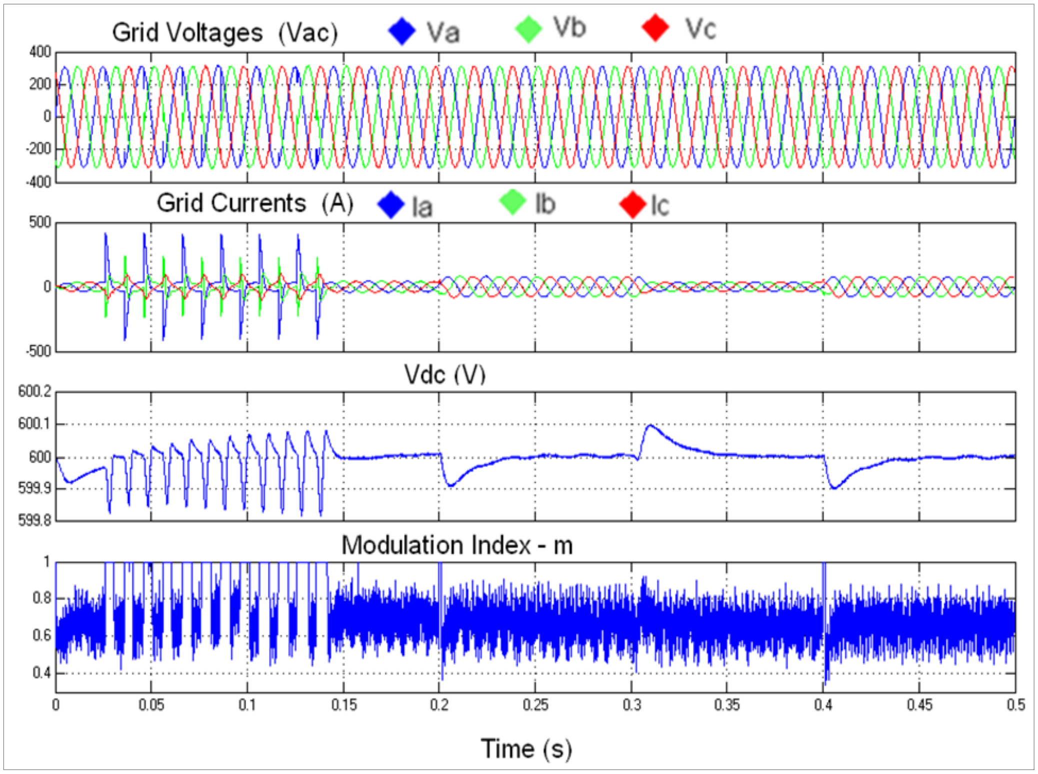

Fig. 3.41: Parameters simulation at PCC point for voltage notches in Phase A and Phase B at time interval [0.046s 0.1262s].

It can be seen that in time interval [0.046s 0.1262s] a Voltage notches event in both phase A and Phase B occurs. It can be seen that in that exact instant of the voltage Notches current spikes occur in both phase A and phase b (positive or negative current spike depending on the instant positive or negative value of the phase voltage) and the V_{dc} decreases. The modulation index m changes as well, as the Active Front End tries to recover the unity Power factor.

In Fig. 3.42 is presented the phase displacement between voltage and current in Phase B in which we can see the current spikes when the Voltage Notch occurs.

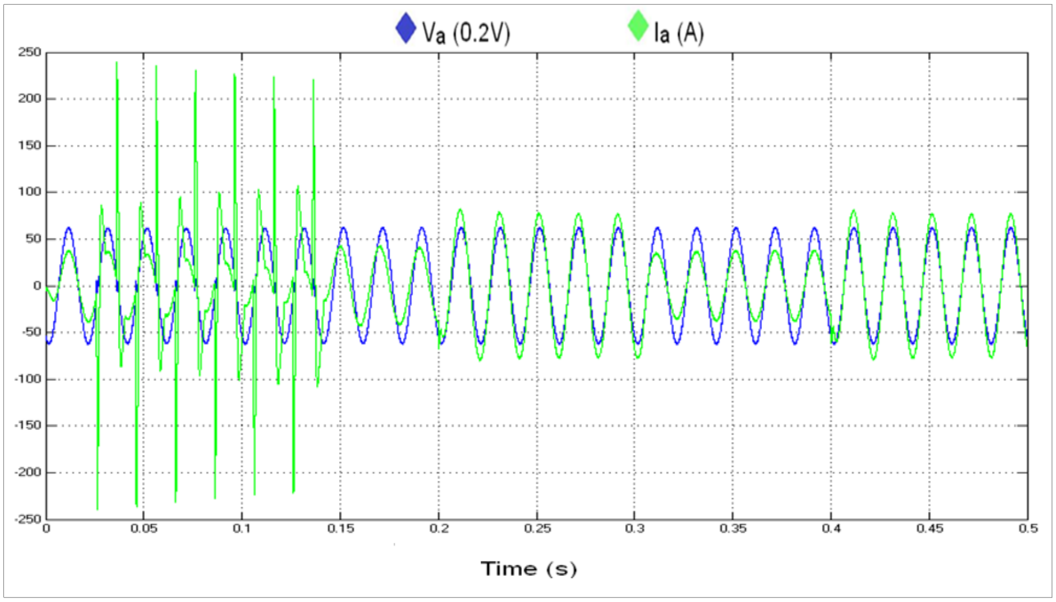

Fig. 3.42: Phase displacement between voltage and current in Phase B. Double phase Voltage Notches event.

In Fig. 3.43 is presented the Power flow in the system during the double phase Voltage Notches event.

As it can be seen, comparing to the first case (Fig. 3.39) the Active Power is almost the same, but the Reactive Power Peak is 2 times greater (from 7kVAR to 14kVAR).

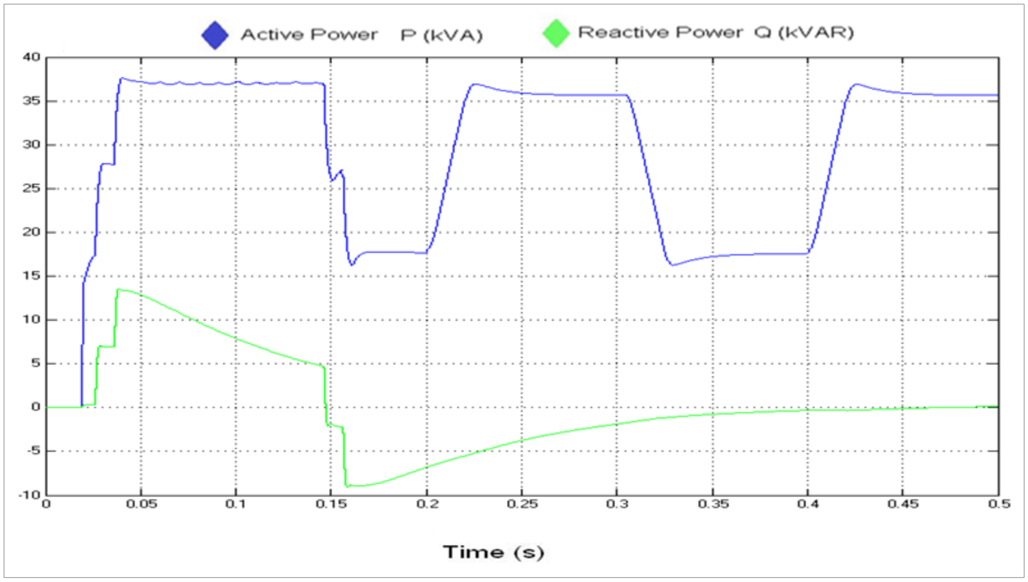

Fig. 3.43: Active and Reactive Power , Double phase Voltage Notches Event.

In Fig. 3.44 are presented the Active and reactive currents in the rotary reference frame.

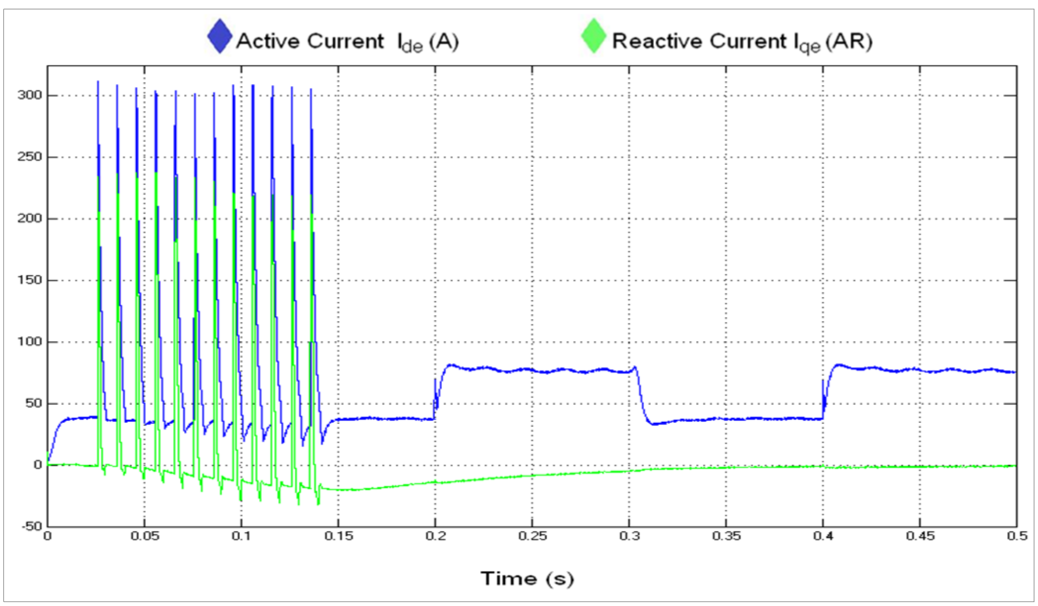

Fig. 3.44: Active Currents and Reactive Currents in the rotary reference frame. Double Phase Voltage Notches event.

It can be seen that after the Voltage Notches event, the AFE tends to bring the Power Factor to unity while it also drive its own load.

As it could be seen previously, after the Voltage notches occurrence, in both case, the presented Front End reset to zero the Phase Displacement between the voltages and currents of the grid assuring unitary Power Factor.

4. Appendix I - Direct Torque Control technique

For proper operation of a drive is motor torque control is necessary. In fact, in addition to cases in which the primary purpose is the regulation of speed (as in scalar control), it is always necessary to check the torque value in the innermost control loop.

Actually control in which torque and flux vector can be controlled separately with high dynamics are most used. In cases, however, in which the required dynamic is not very high, it is preferred to work with a faster control technique than the vectorial one. A technique in which the number of transducers is lower and the control algorithm is more simple.

Before analyzing the operation of this type of control it is shown below the operation of an inverter, regardless of the type of modulation. Was obtained the output voltage (Vs) by the vector composition of the tensions on the Park axis, direct axis and quadrature axis.

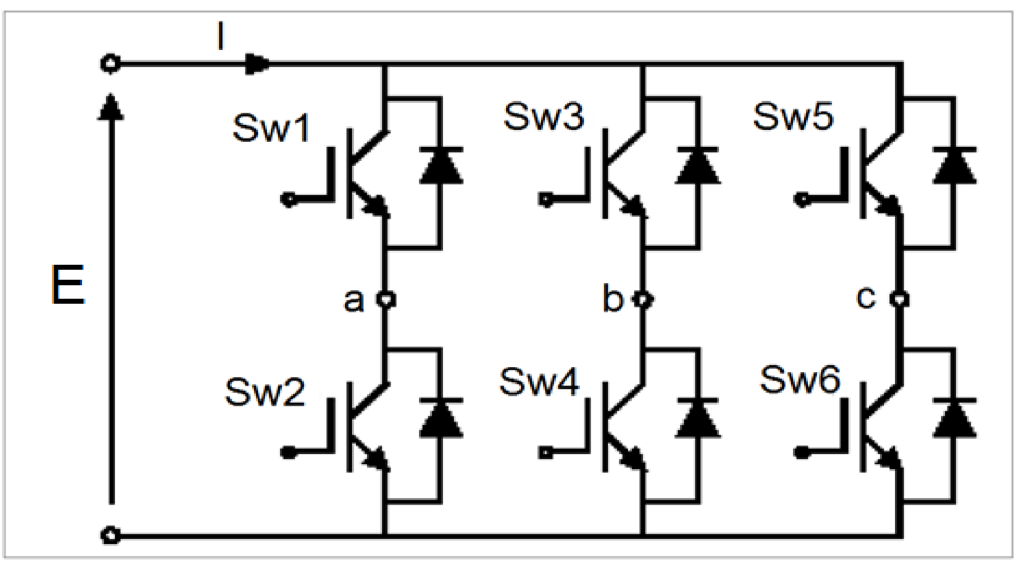

Fig. 4.1: Inverter

The inverter can be represented as in Figure 8 where E is input the voltage and Sw1-6 are the six switches. Taking into account that, for each branch, if a switch is ON the other belonging to the same branch must necessarily be OFF to prevent the short circuit. The possible configurations of the inverter are $2^3 = 8$, and thus 8 voltage vectors.

For each possible configuration of the switches the output voltages are represented in terms of the vector space according to the following equation:

$$\vec{V}_S^S = \sqrt{\frac{2}{3}}\left(V_a + V_b e^{J\frac{2}{3}\pi} + V_c e^{J\frac{4}{3}\pi}\right)$$

where V_a, V_b, Vc are the phase voltages. It represents the conduction states of the three branches of the inverter, Sa (t), Sb (t), Sc (t) according to the following table:

Table 15: Inverter switches configuration

Sw1	Sw2	Sw3	Sw4	Sw5	Sw6	Sa(t)	Sb(t)	Sc(t)	$\vec{V}_s^s$
OFF	ON	OFF	ON	OFF	ON	0	0	0	$\vec{V}_0^s$
ON	OFF	OFF	ON	OFF	ON	1	0	0	$\vec{V}_1^s$
ON	OFF	ON	OFF	OFF	ON	1	1	0	$\vec{V}_2^s$
OFF	ON	ON	OFF	OFF	ON	0	1	0	$\vec{V}_3^s$
OFF	ON	ON	OFF	ON	OFF	0	1	1	$\vec{V}_4^s$
OFF	ON	OFF	ON	ON	OFF	0	0	1	$\vec{V}_5^s$
ON	OFF	OFF	ON	ON	OFF	1	0	1	$\vec{V}_6^s$
ON	OFF	ON	OFF	ON	OFF	1	1	1	$\vec{V}_7^s$

Considering the resulting eight permissible configurations, we define concatenated the voltages by the following expressions:

$$V_{ab} = E\left[S_a(t) - S_b(t)\right]$$

$$V_{ab} = E\left[S_a(t) - S_b(t)\right]$$

$$V_{ca} = E\left[S_c(t) - S_a(t)\right]$$

In the absence of zero-sequence component and assuming the machine symmetrical:

$$V_a + V_b + V_c = 0 .$$

The phase voltages can be expressed in function of the concatenated voltages by the following expressions:

$$V_a = \frac{2V_{ab} + V_{bc}}{3}$$

$$V_b = \frac{V_{bc} - V_{ab}}{3}$$

.

$$V_c = \frac{-V_{ab} - 2V_{bc}}{3}$$

By substituting it is obtained:

$$V_a = E\frac{2S_a(t)-S_b(t)-S_c(t)}{3}$$

$$V_b = E\frac{2S_b(t)-S_a(t)-S_c(t)}{3}$$

$$V_c = E\frac{2S_c(t)-S_b(t)-S_a(t)}{3}.$$

Thus, from the previous expressions of the voltages in the space vector, it is obtained:

$$\vec{V}_S^S = \sqrt{\frac{2}{3}}\left[S_a(t) + S_b(t)e^{J\frac{2}{3}}\pi + S_c(t)e^{J\frac{4}{3}}\pi \right] \bullet E.$$

To make the model of the regeneration phase is necessary to calculate the instantaneous current value of the DC-link, which feeds the inverter.

As shown in Fig. 4.2, the IDC is the instantaneous value of the DC-link current, Iu, Iv and Iw are the instantaneous values of the currents of the three upper branches of the inverter and Ia, Ib and Ic are the currents flowing in the stator windings.

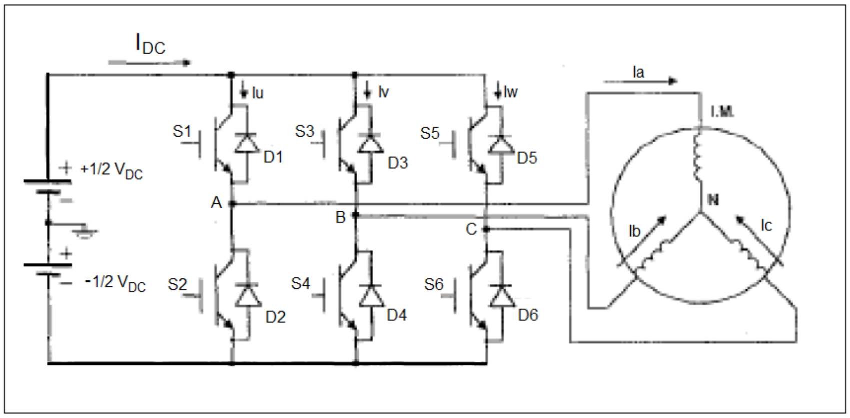

Fig. 4.2: inverter feeding an induction motor

Known the configuration of the switches ($S_a(t)$, $S_b(t)$ and $S_c(t)$) and the calculated stator current, from the mathematical model of the motor is possible to derive the I_{DC}. When $S_a(t) = 1$, point A is connected to the positive branch of the Dc-link and the current flows through S_1 if I_a is positive or through D1 if I_a is negative, therefore $I_u = I_a$. Instead, the current flows in the lower branch (through D2 or S2) when $S_a(t) = 0$, therefore $I_u = 0$. Repeating the same type of reasoning for the other three branches of the inverter, it can be written:

$$\begin{Bmatrix} I_u = I_a S_a \\ I_v = I_b S_b \\ I_w = I_c S_c \end{Bmatrix},$$

therefore:

$$I_{DC} = I_u + I_v + I_w = I_a S_a + I_b S_b + I_c S_c.$$

This expression is of course also valid in the recovery phase in which the power flow is reversed (Fig. 4.3).

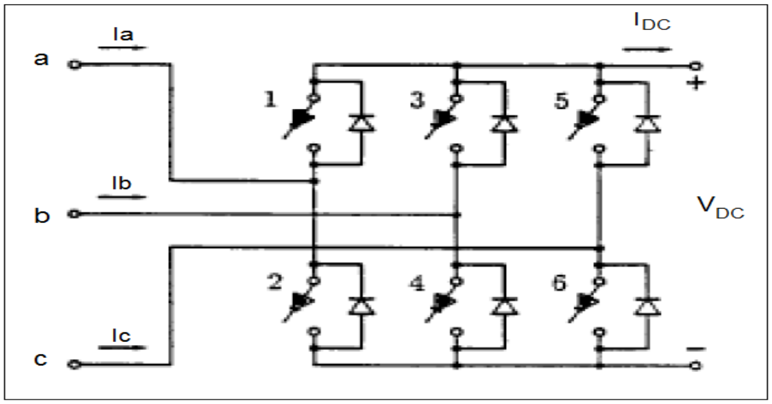

Fig. 4.3: Current flow during braking

Defined in the inverter, we now pass to the illustration the type of control carried out on the motor, and then the definition the strategy that allows to define the commutation instant of the switching components. Such a strategy is called "Direct Torque Control" (DTC) because the commutation instants of the inverter switches (schematized above) are directly defined to track the reference torque without using the control of the phase currents. The absence of a direct control over the phase currents allows to operate with hardware and software schemes greatly simplified.

From Ohm's law, for a stator phase we can deduce the variation of the stator flux resulting from the application for a period ΔT of a certain voltage configuration:

$$\Delta \phi_s = V_S \Delta T - R_S i_S \Delta T \ .$$

Therefore, considering the resistive drop due to the stator resistance, not negligible at low speed, the vector direction $\Delta\Phi_s$ (flux variation) is, therefore, that of the corresponding voltage vector applied and its module is proportional to the product of the voltage for the time of application.

Regarding the control of the stator flux, this can be controlled along the six directions of the voltage vector or held in place by applying a zero vector. To vary the module of the stator flux is, threfore, necessary to apply voltage vectors that have adequate radial components. Instead, to vary the torque and therefore the slip, the stator flux speed has to be varied compared to the rotor flux by applying voltage vectors that have appropriate tangential components (Fig. 4.4).

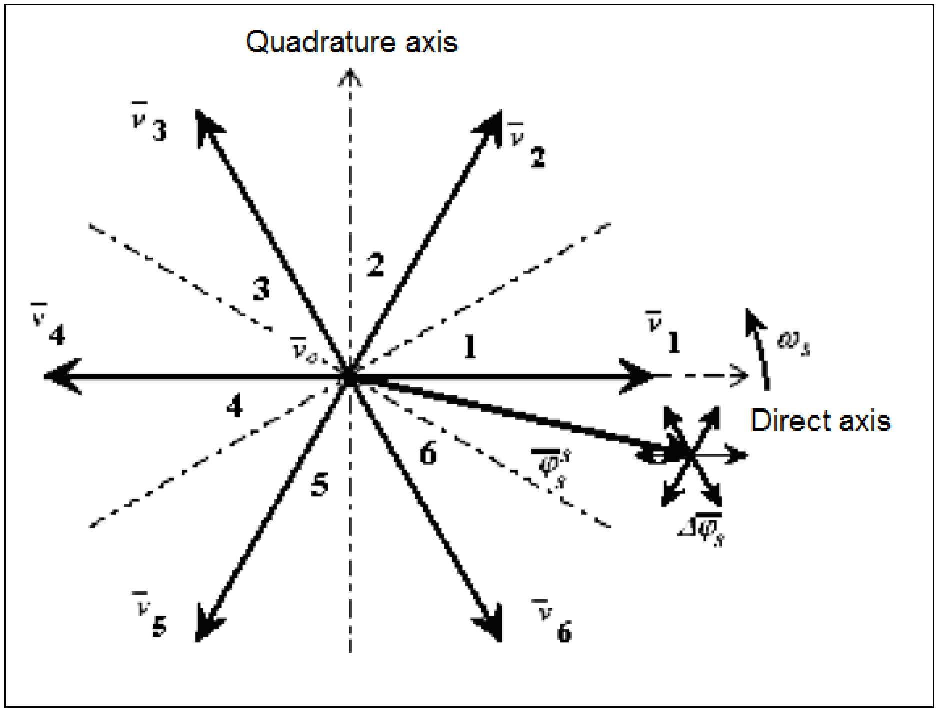

Fig. 4.4: Vector representation of the inverter voltages and the corresponding flux variation in a time interval ΔT.

The torque can be expressed as a function of the module of the rotor flux Φ_r and of the quadrature component, with respect to such flow, of the stator flux vector Φ_{qs}:

$$C = P\frac{L_m}{\sigma L_r L_s}\Phi_r \Phi_{qs} .$$

As the rotor flux is linked to the stator flux by a low pass type dynamic relationship, it can be observed that accelerating the stator flux, increases the component Φ_{qs} while the module of the rotor flux Φ_r does not vary appreciably, thus leading to an increase in torque.

Increasing the angular velocity of the stator flux with respect to the mechanical speed, the instant slip increases, and thus the torque, vice versa when the speed is reduced. Combining the equation of torque expressed with the rotor variables, is obtained:

$$C = P\omega_s \frac{\Phi_r^2}{R_r}.$$

The coefficient ω_s is the electrical pulsation of the rotor flux (in the rotor reference), or the instantaneous flow pulsation. Notice that the torque, keeping constant the module of the rotor flux, tracks the trend of pulsation flow.

From these considerations it is clear that to increase the value of the torque and therefore the instantaneous value of ω_s, it is necessary to apply to the machine a voltage vector that has a significant tangential component relative to the direction of rotation of the stator flux. So it is possible to control the torque and flux acting respectively on the radial and tangential component of the flux, through the choice of suitable voltage vectors between those allowed by the inverter control strategy.

In Table 16 are summarized the vectors in function of the applied sector (θ_s) and errors of torque ΔT and flux λ.

Table 16: Vectors applied in various sectors depending on the errors

λ	**ΔT**	**θ_s (1)**	**θ_s (2)**	**θ_s (3)**	**θ_s (4)**	**θ_s (5)**	**θ_s (6)**
1	1	V_2	V_3	V_4	V_5	V_6	V_1
1	-1	V_6	V_1	V_2	V_3	V_4	V_5
0	1	V_0	V_7	V_0	V_7	V_0	V_7
0	-1	V_0	V_7	V_0	V_7	V_0	V_7
-1	1	V_3	V_4	V_5	V_6	V_1	V_2
-1	-1	V_5	V_6	V_1	V_2	V_3	V_4

According to the above, it is easy to understand how the DTC behaves in the regenerative phase. Suppose that the stator flux vector is for example in sector 1, if the torque error is negative (ΔT = -1) and the flux error is zero (λ = 0), the zero vector has to be applied(V_0 or V_7). In this way, the rotation speed of ω_s flux is reduced compared to the machine flux and therefore a negative torque value is obtained (negative slip). If the flux error is a positive, the output vector of the inverters must have a positive radial component and negative tangential component so as to always reduce the speed of the flux comparing to the machine flux (V6). In Fig. 4.5 is shown the block diagram of the DTC control.

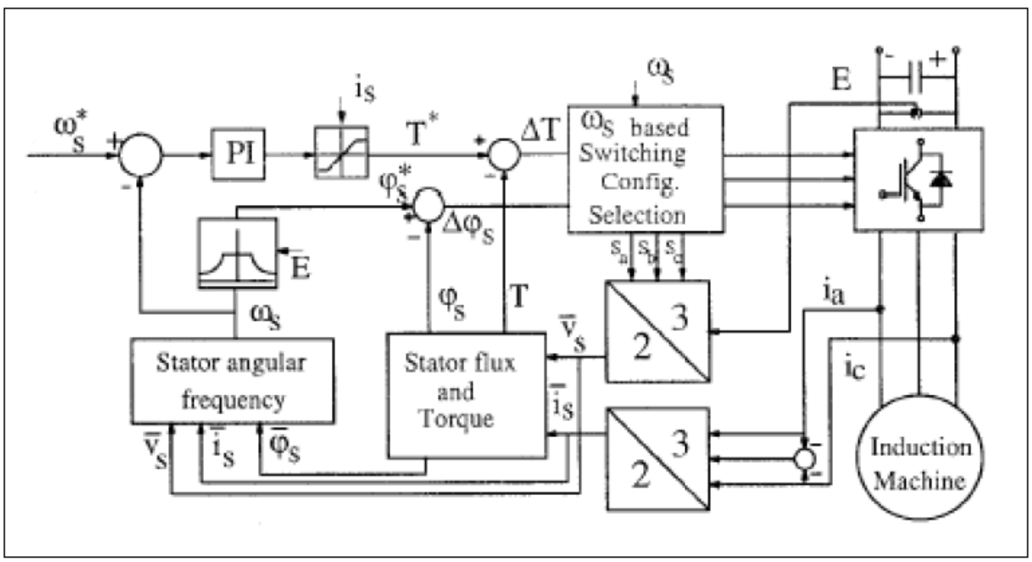

Fig. 4.5: Block diagram of DTC

Referring to Fig. 4.5, the reference values of electromagnetic torque T and stator flux φ_s are compared with the respective measured values to generate the torque error and the flux error.

The two generated errors are the inpu parameters of a pulse generator that controls the inverter in such a way as to apply to the motor voltage vectors to compensate such errors.

In the feedback loop, based on the state of conduction of the branches S_a, S_b, S_c, $\vec{V}_s^s$ is calculated and according to the measured currents, φ_s and T are calculated. The user acts on ω_s*, while the reference torque T* is obtained through a PI controller. This solution is appropriate since the regenerative braking is obtained simply with a negative torque command. In this way the behavior of the electric motor is similar to that of an internal combustion engine. In fact, when the vehicle is in motion and the accelerator is released, the output PI controller is a negative torque value.

5. Appendix II – EMC Measurements

This appendix provides theoretical and experimental discussions on conducted electromagnetic interference (EMI) emissions in the automotive applications. These issues are even more relevant (and the relative regulations more severe) as today's vehicles are equipped with a large number of sensitive electronic communication and control systems together with several switching power converters. As example it is shown the conducted emission of an electric vehicle in absence and in presence of filter.

5.1 Introduction

EMC (Electro Magnetic Compatibility) is today an important issue to deal with in every kind of environment and in every application making use of electric/electronic equipment.

Every electrical or electronic apparatus, system or installation has not to disturb the proper function of other near devices by emitting electromagnetic disturbance signals (emission); besides, every electrical or electronic apparatus, system or installation has to work properly in the presence of electromagnetic disturbance signals in the surrounding environment (immunity).

Automotive traction drives and related power electronics can cause broadband emissions which could impair the control systems normal modes of operation. Control electronics perform many safety and communication relevant functions so that its error-free operation is mandatory with respect to EMC.

Traditionally, Electromagnetic Compatibility and Safety have been regarded as two separate disciplines, but the increase in electronic and electric apparatus performing safety and control functions is leading to a re-think of this relationship. In fact, safety assurance requires a detailed analysis of all reasonably foreseeable risk, including that posed by exposure to electromagnetic fields.

Risk mitigation is required for all identified EMI risk that could have an adverse effect on safety. With the use of advanced and high speed devices in electronic and electrical apparatus, together with the requirement to comply with legislative requirements, EMC has grown to be an integral part of traditional engineering design and management, both crucial issues in reducing design and manufacture cost and ensuring compliance with EMC legislation. From this point of view the susceptibility performance criteria have to be defined based on the apparatus functionality and environment.

5.2 Apparatus Conformity Assestement

It is also reasonable that a contractor should have access to the existing EMC documentation through the operator responsible person, to ensure that the EMC specification for new equipment added is sufficient for many electrical sub-systems concerned with:

- the propulsion of the vehicle, including the traction converter, transformer or motors;
- the stopping of the vehicle - including the braking apparatus electronics;
- a whole variety of ancillary equipment ranging from auxiliary power, air conditioning, and door controls.

Each supplier's documentary evidence, that his equipment meets the specified EMC requirements will be included in the electric vehicle. It then remains only for the vehicle manufacturer to validate, from an EMC viewpoint, the installation and wiring techniques employed. This will be partly by reference to the management plan (which lays down the essential EMC working practices), partly by reference to the quality assurance procedures for the vehicle manufacturer's organization, and by whole vehicle EMC (emission) tests.

In conclusion the preparation of the Technical Documentation, for vehicle will be based on rigorous testing of sub-systems and, the validation of installation and design practices by a combination of:

- EMI RISK ANALYSIS: The vehicle environment is abundant with many sources or electromagnetic interference. Some of these sources are transitory dependent, and the magnitude of the interference may not be easily predictable. Critical equipment that is susceptible to external interference may be unpredictable and therefore potentially dangerous.
- RISK ACCEPTABILITY - It is clearly not satisfactory to have an EMI related hazards that could have catastrophic consequences and that could occur frequently; however it may be acceptable to have an EMI related hazard with negligible consequences that occur frequently. Environmental induced failures such as electromagnetic interference, temperature and vibration are treated as part of the failure integrity. Hazardous systematic failures due to electromagnetic interference can be assessed through enhanced EMC testing. All tests are completely defined by standard IEC 61000-4-4.
- EMC SAFETY REQUIREMENTS - The EMC requirements are treated as minimum requirements unless the product standard

specifically includes safety requirements. While the overall objective of the approval process is to demonstrate that the apparatus is safe for use in its intended electromagnetic environment - this assumes that the electromagnetic characteristic of the intended environment is known.

These essential requirements to comply with in this case of applications are described in the EMC European Directive 2004/108/CE. Among the normative references of this standard series, other standards are recalled:

- IEC 61800-3 Ed.2: Adjustable speed electrical power drive systems
- Part 3: EMC requirements and specific test.
- IEC 61851-21: Electric vehicle requirements for conductive connection to an a.c./d.c. supply. 2nd ed, 2010.

To the purpose of performing EMC testing and characterization of power electronic converters, electric drives and related control systems to be used in automotive driver's, the main reference standard is the EN 50121-3-2.

The frequency range considered for EMC testing of electrical and electronic apparatus intended for use on vehicle rolling stock is from d.c. to 400 GHz, even if, at present, testing is not defined for frequencies above 1 GHz. The application of tests shall depend on the particular apparatus, its configuration, its ports, its technology and its operating conditions.

5.3 EMC Testing

The test site for the emission EMC testing, both conducted and radiated, is a semi-anechoic chamber. It is a shielded room covered with ferrite absorber tiles and it is equipped with the main EMC testing instrumentation, as an EMI receiver, a broadband antenna, an RF generator with the relative power amplifier, LISNs (Line Impedance Stabilization Network), CDNs (Coupling Decoupling Network), electric, magnetic and current probes, test generator related to the electrostatic discharge and fast electromagnetic pulses test . Other facilities that can be used are several PCs equipped with modelling, simulation and design software as Matlab and Ansys.

5.4 Test Set-Up

In Fig. 5.1 is shown the current probe method test set-up scheme for conducted emission specified in CISPR-14 and CISPR-16. The EUT (Equipment Under Test) is supplied by a linear power supply via two LISN (Line Impedance Stabilization Network), one for each DC power line (line and ground).

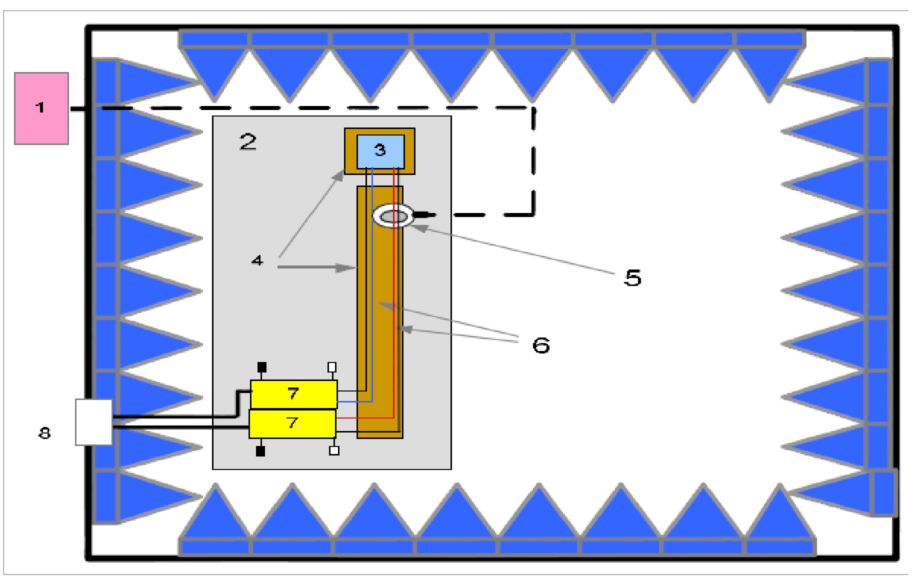

Fig. 5.1: Conducted emission testing set-up (current probe method) scheme (top view): 1 EMI receiver 2 ground plane, 3 EUT, 4 non-conductive supports, 5 current probe, 6 power lines, 7 LISN, 8 DC power supply.

In Fig. 5.2 is shown the test set-up according to CISPR-14 and CISPR-16 for the radiated emissions.

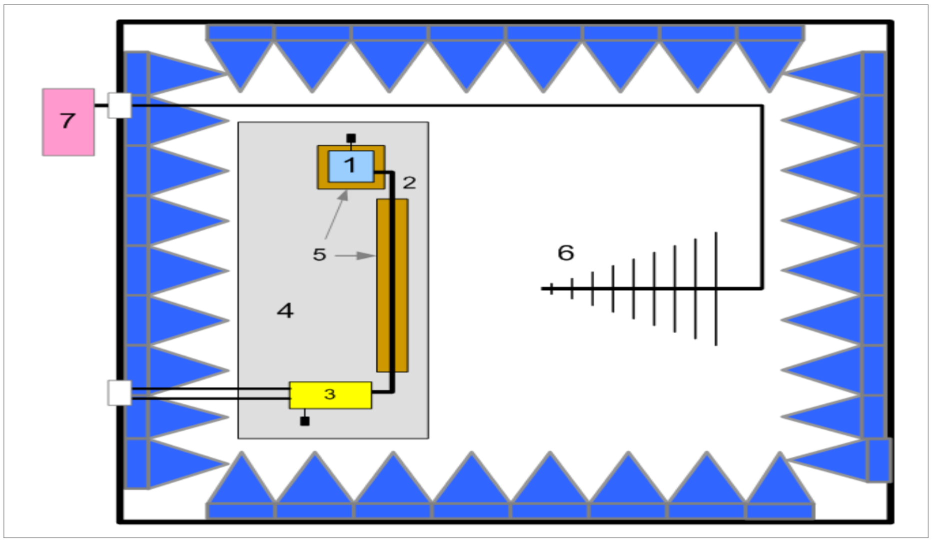

Fig. 5.2: Radiated emission testing set-up scheme (top view): 1 EUT, 2 cables, 3 LISN (Line Impedance Stabilization Network), 4 ground plane, 5 non-conductive supports, 6antenna, 7 EMI receiver.

In Fig. 5.3 is shown the architecture of the electric vehicle under test and in Table 17 its main specifications, meanwhile in Fig. 5.4 is shown a picture of the device under test.

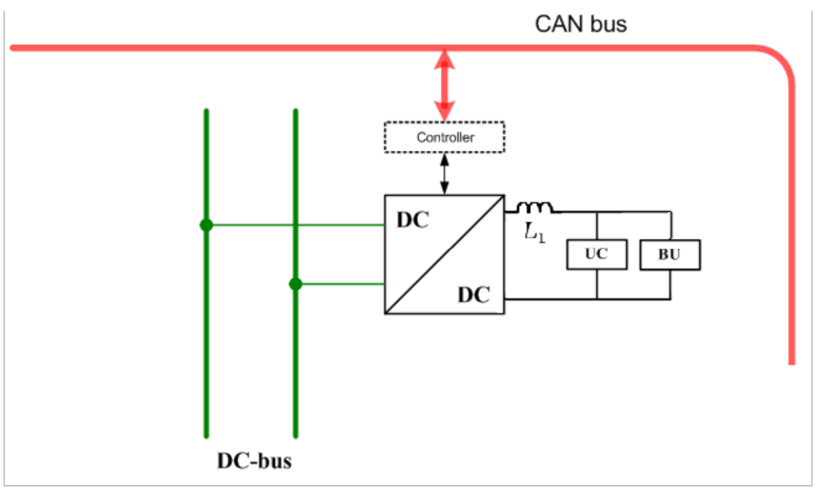

Fig. 5.3: architetture of the vehicle system

Fig. 5.4: Electric wheelchair

Table 17: Device under test specifications

Device specifications	Value
Overall Traction power (W)	205
Battery pack max current (A)	17.5
Rated Voltage (V)	24
Rated Voltage of Super Condensators (V)	25.6
Battery module	Pb
Max current of Super Condensators (A)	30

The conducted and radiated emission tests have been carried out in the frequency range between 150 kHz and 1GHz. This experimental activity has been accomplished in the semi-anechoic chamber, with ferrite tiles, located in the Laboratory of the University of Rome “Roma Tre”. In order to carry out the radiated measures below 1GHz, the pyramidal polystyrene has been replaced with ferrite tiles. In Fig. 5.5 is shown the anechoic chamber and in Fig. 5.6 the comparison between the characteristics frequency of the two paneling.

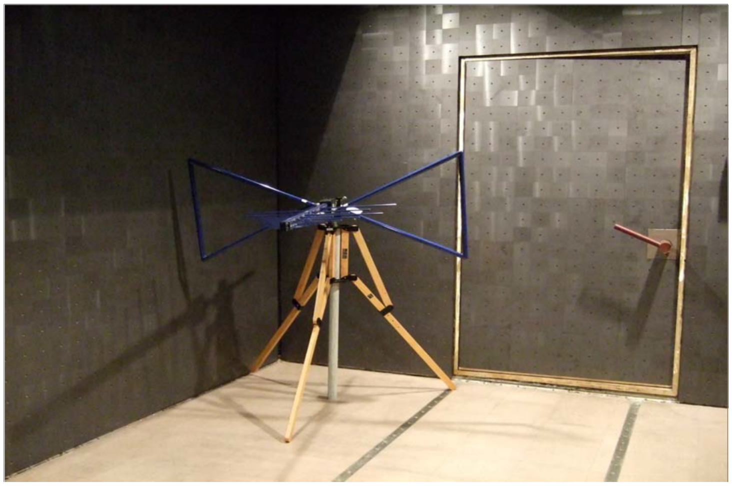

Fig. 5.5: Semi-anechoic chamber with ferrite tiles

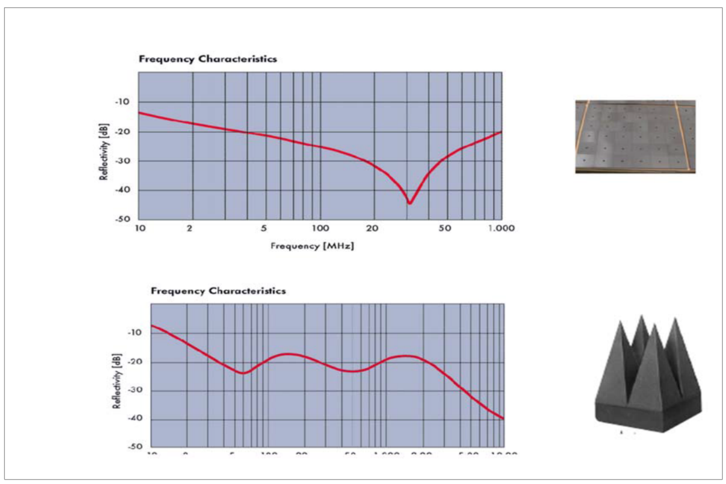

Fig. 5.6: Frequency characteristics of ferrite tiles and pyramidal polystyrene ferrite

5.5 Experimental results

Both conducted and radiated emissions measurements have been carried out in normal operational conditions of the electric vehicle, that is, with the drive wheels in movement.

In Fig. 5.7 is shown the conducted emission. No EMI filter is applied to the electric vehicle. The green line represents the conducted emission limits prescribed by IEC 61851-21 in the 150kHz – 30MHz frequency range. With no EMI filter the conducted emission fails the limits.

The most critical frequency range is 500kHz-5MHz (Fig. 5.8) in which the conducted emissions are above the prescribed limits in the whole frequency range. The concentration of the conducted disturbance emission in this frequency range is mainly caused by the switching power converter hardware.

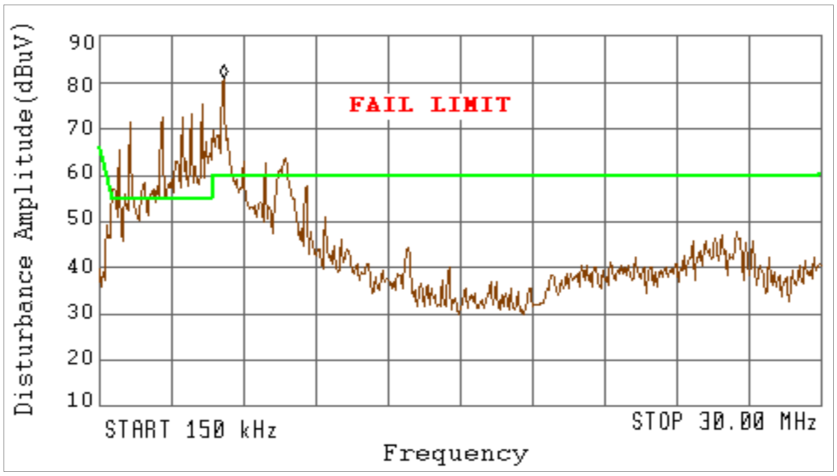

Fig. 5.7: Conducted emissions 150kHz-30MHz. No Emi filter

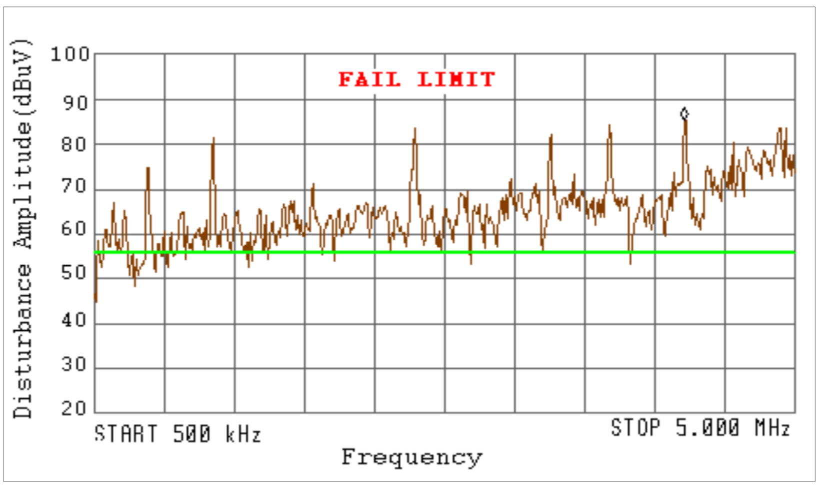

Fig. 5.8: Conducted emissions 500kHz-5MHz. No Emi filter

In Fig. 5.9 and Fig. 5.10 are shown the radiated emission of the electric vehicle carried out with a Bilog antenna in the 30MHz – 1GHz frequency range in horizontal and vertical polarization of the antenna. The IEC 61851-21 doesn't prescribe limits on radiated emission, so limits prescribed by CEI EN 61800-3 were considered.

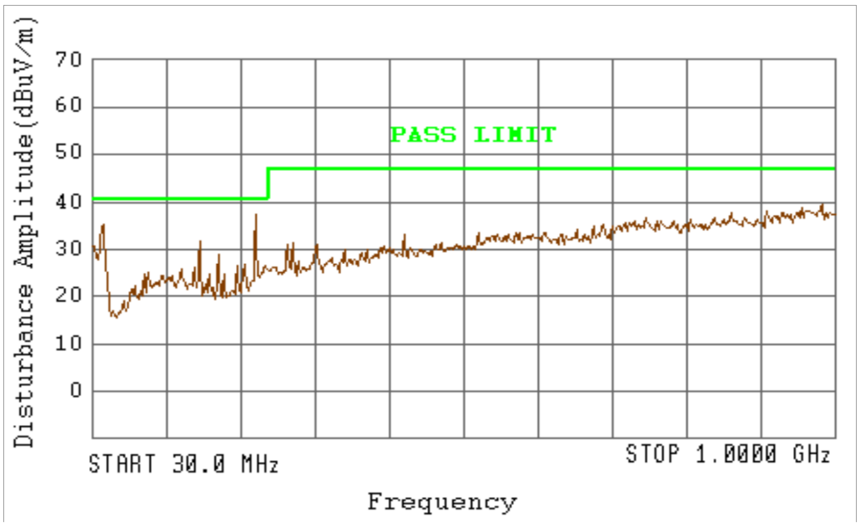

Fig. 5.9: Radiated Emissions, horizontal polarization

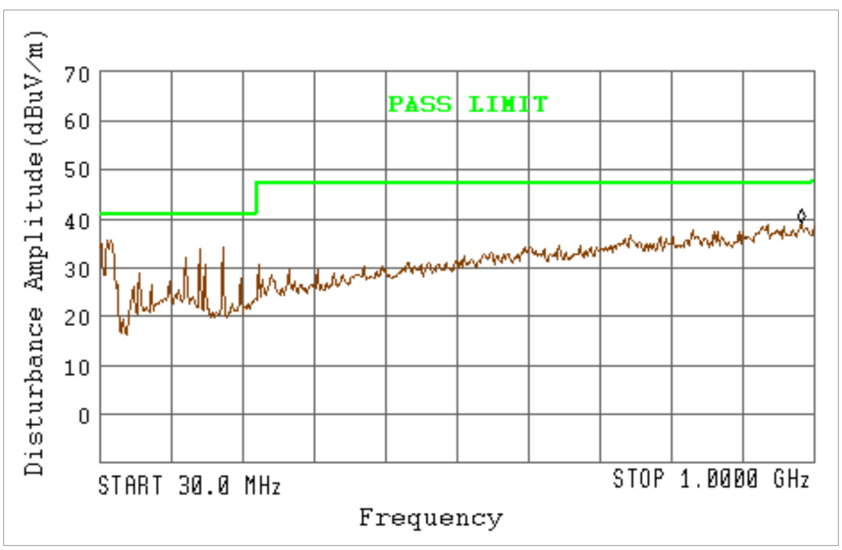

Fig. 5.10: Radiated Emissions, vertical polarization

The radiated emissions resulted under the limit. So an EMI filter was used for the attenuation of the conducted emissions only.

In Fig. 5.11 is presented the general scheme of the EMI Filter. For the selection of the components, a common mode inductor L_c = 0.3mH, ceramic capacitors C_y=C_x=10nF have been chosen. The leakage inductance of the realized common mode inductor can be used as a differential mode inductor (L_d in the EMI filter Fig. 5.11) instead of a dedicated inductor. Considering that the leakage inductance of the common mode inductor is about 56uH, it can be considered L_d = 56uH, so no further differential mode inductor is inserted, inserting only the differential mode capacitors C_x. In this way a good EMI performance can be archived with no considerable increase in EMI filter size (total size is mainly due to inductors).

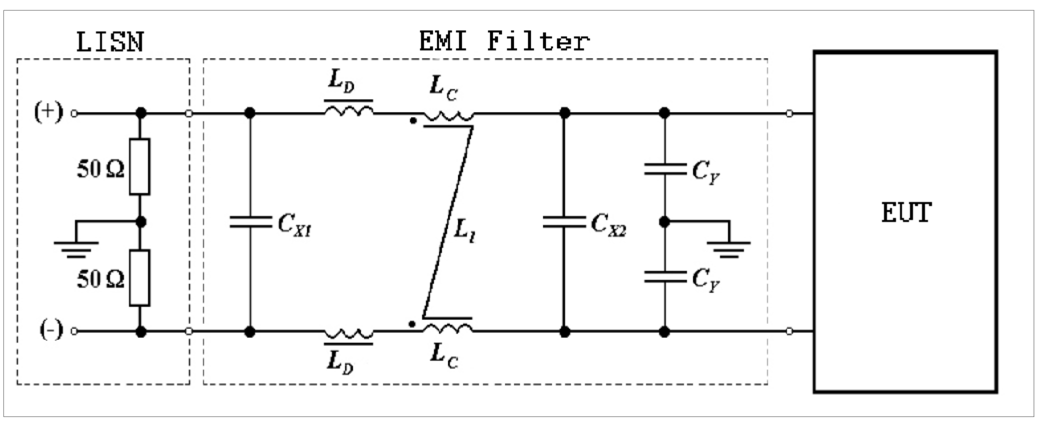

Fig. 5.11: EMI filter

In Fig. 5.12 is presented the Bode plot of the designed EMI filter. It has a cut-off frequency of 106 kHz. So all the frequencies in the range 150 kHz – 30MHz are attenuated.

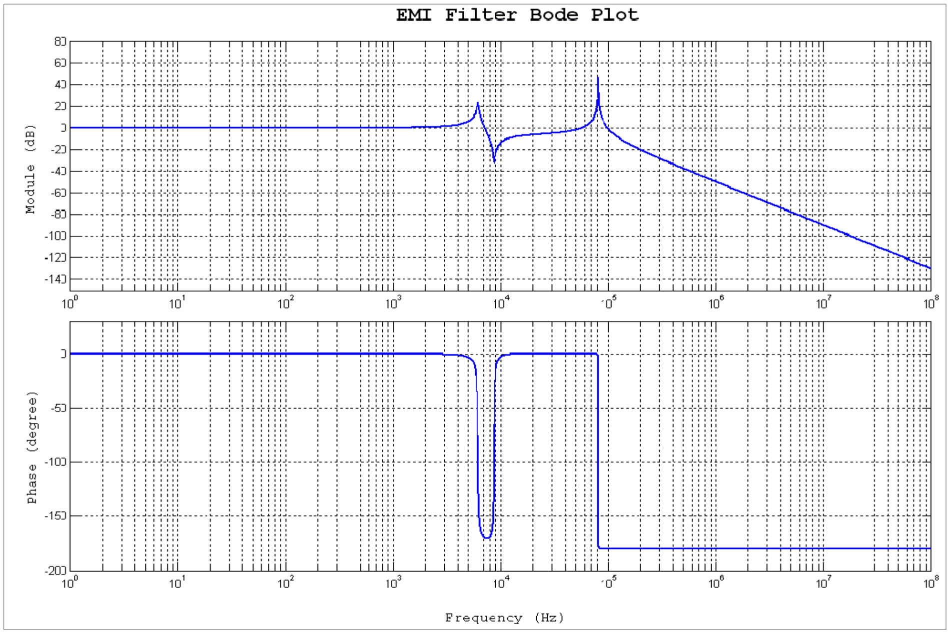

Fig. 5.12: EMI filter Bode plot

With the designed EMI filter applied the overall conducted emissions are attenuated enough to satisfy the limits prescribed by the IEC 61851-21 with an acceptable safe margin, as it can be seen in fig. 12. The most critical frequency range seems to be 500 kHz-5MHz (fig.13) in which the conducted emission are below the limits.

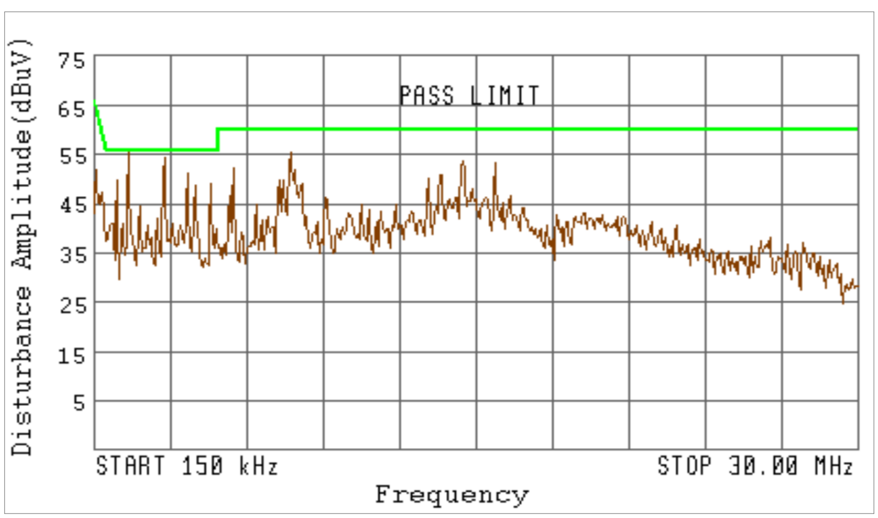

Fig. 5.13: Conducted emissions 150kHz-30MHz. No EMI filter

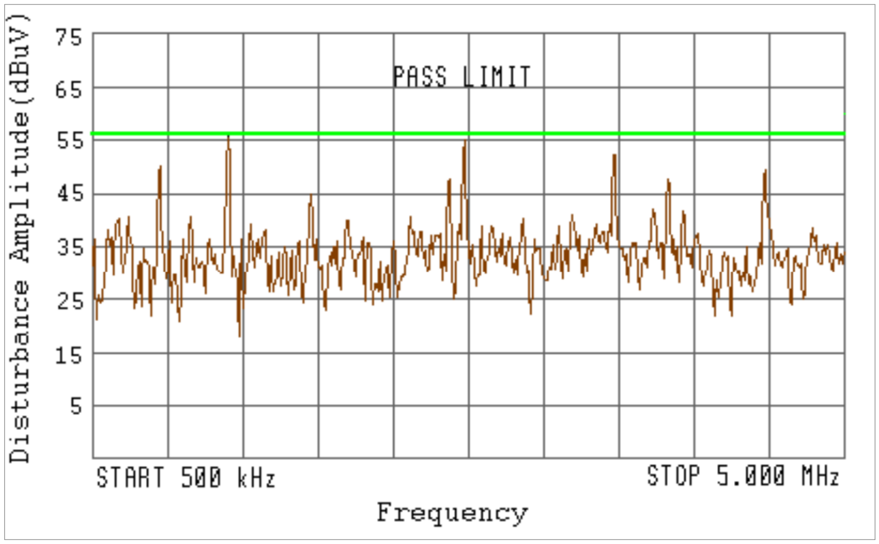

Fig. 5.14: Conducted emissions 500kHz-5MHz. No EMI filter

In this Appendix EMC safety considerations and EMC characterization of an electric wheelchair have been presented. A general overview of the EMC directives regarding electric vehicles and adjustable speed power drives has been presented. An extensive experimental test campaign has been carried out in a semi-anechoic chamber in order to evaluate the overall EMC performance of an electric vehicle. For conducted emission limits IEC 61851-21 was considered while for the radiated emissions was considered the CEI EN 61800-3 regulation. The radiated emissions were under the limits prescribed by the regulation even without the EMI filter applied to the electric vehicle. So the design of the EMI filter was focused on the attenuation of the conducted emissions. With the purpose to reduce especially the conducted emissions, an EMI filter was designed and applied to the electric vehicle. The Bode plot of the designed EMI filter was presented. The attenuation of the conducted emissions due to the EMI filter was considerable and the EMC compliance was archived.

Conclusions

In the first part of the thesis an introduction to Power Quality an most common issues related to Power Quality were given

The second part of the thesis dealed with the mimimization of the demand of the Electrical power supplied by the Grid. For this purpose a Gantry crane power drive system with a maximum capacity of 50 tons coupled with an ultracapacitors based storage system was presented. Two different criterias were taken into consideration in order to perform the sizing of the Ultracapacitors. The first one was the total energy spent during the power peaks of the whole work cycle of the Gantry crane; the second one is the energy related to the descending of the load. The Matlab-Simulink based simulation model of the system was presented and simulation results were shown. In order to have an optimization of the utilization of the Grid power, a regulation strategy was presented. A scaled esperimental model was built in order to make the validation of the simulation model. The experimental data present a good match with the simulated data. Afterwards, extensive simulation tests were performed. It is shown that by using this model, it is possible to decrease the average power suppliead by the Grid, thus it is possible to decrease the size of the power rectifier as the nominal power would be lower (less expensive). Of course, on the other hand, there will be an additional cost of the whole system, due to the Ultracapacitors storage system. An economic evaluation of costs and benefits was done for different simulation cases. It was shown that the payback time of the investment would be less than 5 years, considering a lifetime of the plant of about 15 years.

The third part of the thesis dealed with the optimization of the Power Grid at the Point of Common Coupling (PCC). This is done by an Active Front End which performs Reactive Power compensation to obtain unity Power Factor at PCC point.

First the control strategy of the Active Front End was presented. Afterwards a Matlab-Simulink model was shown. Feed–Forwar compensation was used to have a faster dynamic response of the Active front End. An extesive set of simulations was perfomed using different load conditions to simulate variable Grid conditions. From the simulations resulted that after the change in the load condition occurred, the Active Front End sets to zero the phase displacement between phase voltage and phase current, thus Power Factor = 1. This is done by trying to maintaing the reactive current to null while feeding active current to the own load.

Voltage sags and voltage notches were simulated to investigate the behavior of the Active Front End in presence of these disturbances. For both disturbance grid single phase and grid double phase were considered. In both cases, after the occurrence of the distubances, the Active Front End sets the reactive to zero (the reactive current reference remains always zero), thus resets the phase displacement back to zero,

References

[1] M. H.J. Bollen *Understanding Power Quality Problems*, :IEEE Press

[2] C. Sankaran, *Power Quality*, CRC Press, 2002

[3] "IEEE Std 1100-1999", *Powering and Grounding Electronic Equipment*, 1999

[4] Bimal K. Bose, *Power Electronics and Variable Frequency Drives*, IEEE Press

[5] D. Grahame Holmes, *Th. A. Lipo, Pulse Width Modulation for Power Converters*, IEEE Press

[6] Dugan R C etc. Electrical power systems quality. New York, McGraw2Hill,1996.

[7] Christopher J.Melhorn Sr., Arindam Maitra, Wes Sunderman, Marek Waclawiak and Ashok Sundaram, "*Distribution system power quality assessment phase II: voltage sag and interruption analysis*," Petroleum and Chemical Industry Conference, 2005. Industry Applications Society 52nd Annual12-14 Sept. 2005 Page(s):113 - 120

[8] Douglas H., and Pillay P., "*Sizing Ultracapacitors for hybrid Electric Vehicles*", Proc. IECON 2005 – 31st Annual Conference of IEEE Industrial Electronics Society, 6-10 Nov. 2005, pp 6 pages.

[9] Sen C., Usama Y., Carciumaru T., Xiaomin Lu, Kar N.C., "Design of a Novel Wavelet Based Transient Detection Unit for In-Vehicle Fault Determination and Hybrid Energy Storage Utilization", IEEE Transactions on Smart Grid, Vol.3, No 1, March 2012, pp. 422-433

[10] H. Math, J. Bollen, "*Understanding Power Quality Problems – Voltage Sags and Interruption*", 2000, New Jersey, John Wiley & Sons.

[11] Burke A., "*Ultracapacitor Technology and applications in Hybrid and Electrical vehicles*", International Journal of energy Research, Vol. 34, 2011, pp. 133-151

[12] Parvini Y., Vahidi A., *"Optimal charging of ultracapacitors during regenerative braking"*, Proc. of the 2012 IEEE International Vehicle Conference (IEVC), Greenville (USA), 4-8 march 2012, pp. 1-6.

[13] Burke A., Miller M., "The Power Capability of Ultracapacitors and Lithium Batteries for Electric and Hybrid Vehicle Applications", Journal of Power Sources, Vol. 196, 2011, pp. 514-522

[14] Schepmann S., Vahidi A., *"Heavy vehicle fuel economy improvement using ultracapacitor power assist and preview-based MPC energy management"*, Proc. of American Control Conference (ACC),San Francisco (USA), 29 june – 1 july 2011, pp. 2707-2712

[15] Shen X.J., Chen S. Zhang Y., "Configure methodology of on-board super-capacitor array for recycling regenerative braking energy of URT vehicles",Proc. of IEEE Industry Applications Society Annual Meeting (IAS), Shanghai (Ch), 7-11 Oct. 2012, pp. 1-8

[16] Iannuzzi D., Tricoli P., "Speed-based State of Charge Tracking Control for Metro-Trains with Onboard Supercapacitors", IEEE Transactions on Power Electronics Vol.27, Issue: 4, 2012 , pp.2129-2140

[17] Florescu A., Bacha S., Munteanu I, Bratcu A. I., *"Frequency-separation-based energy management control strategy of power flows within electrical vehicles using ultracapacitors"*, Proc. of IECON 2012-38th Annual Conference on IEEE Industrial Electronics, Montreal (CND), 25-28 Oct. 2012, pp. 2957-2964

[18] Camara M. B., Gualous H., Gustin F., Berthon A., and Dakyo B., *"DC/DC converter design for supercapacitor and battery power management in hybrid vehicle applications—Polynomial control strategy*", IEEE Trans. Ind. Electron., vol. 57, no. 2, pp. 587–597, Feb. 2010.

[19] A. Stepanov, I. Galkin, L. Bisenieks, "Implementation of supercapacitors in uninterruptible power supplies," in EPE 2007, 12th European Conference on Power Electronics and Applications, Aalborg, Denmark, 2-5 September 2007, [pp. 1-7].

[20] Zhou H., Bhattacharya T., Tran D., Siew T. S. T., Khambadkone A. M.,"*Composite Energy Storage System Involving Battery and Ultracapacitor With Dynamic Energy Management in Microgrid*

Applications,"IEEE Trans. on Power Electronics ,vol.26,no.3,pp.923-930,2011

[21] Steiner M., Klhor M., Pagiela S., "*Energy storage system with ultracaps on board of railway vehicle*s", EPE 2007, 12th European Conference on Power Electronics and Applications, Aalborg, Denmark, 2-5 September 2007, [pp. 1-10].

[22] Tironi E., Piagari L., Musolino V., Pagnocelli S., "Accumulo elettrico con supercondensatori nell'industria: studio disistema e valutazioni tecnico-economiche per l'applicazione ad un carro ponte", ENEA, Report RS/2009/48

[23] Camara M. B., Dakyo B., and Gualous H., "*Polynomial control method of DC/DC converters for DC/DC converters for DC-Bus voltage and currents management-battery and supercapacitors,"* IEEE Trans. Power Electron.,vol. 27, no. 3, pp. 1455–1467, Mar. 2012

[24] Bragard M., Soltau N., Thomas S. and De Doncker R. W., *"The Balance of Renewable Sources and User Demands in Grids: Power Electronics for Modular Battery Energy Storage Systems,"* Power Electronics, IEEE Transactions on, vol. 25, pp. 3049-3056, 2010

[25] Lajunen A, Suomela J., "Evaluation of Energy storage System Requirements for Hybrid Mining Loaders", Vehicular Technology, IEEE Trans. on, vol. 61, no 8, pp 3387-3393, Oct. 2012

[26] Lajunen A., "*Evaluation of the benefits of using dual-source Energy storage in hybrid electric vehicles*", Proc. IEEE Vehicle Power and Propulsion conference, Lille (FR), 1-3 Sept. 2010, pp. 1-6

[27] Da Silva V. F., Rezek A.J.J., Junior A.A.P., Da Silva L.E.B., Rosa P.C., and Reis L.O.M., "*Ultracapacitor-Based Ride-Through System for Adjustable Speed Drives Applied to Critical Process*", Proc. of the 10th International Conference on Harmonics and Quality of Power 2002, Page(s): 632 - 638 vol.2.

[28] Baalbergen F., Bauer P., Ferreira J. A., "*Energy Storage and Power Management for Typical 4Q-Load*", IEEE Trans. Ind. Electron., Vol.56, pp. 1485-1498, May 2009

[29] Pankjaj Pndit thesis, " Model And Analysis of Active Front End Induction motor Drive ", 2006

[30] Arnet B.J. and Haines L.P., October 2000, "*Combining Ultracapacitors with Lead-Acid Batteries*", 17th International Electric Vehicle Symposium, Montreal, Canada, paper 2B-2 on CD-ROM.

[31] Aklil C. R., Roboam X., Sareni B., Jeunesse A., " *Energy management and sizing of a hybrid locomotive*", The 13th Europe Power Electronics Conference, EPE 2008, Alborg, Denmark

[32] Polini, C. Crescimbini F., Di Napoli A., Lidozzi A., Solero L., "*Power Flow Analysis for Plug In Hybrid Electric Vehicles* ", International Conference on electrical Machines, ICEM 2010, Rome, Italy

[33] Grahame Holmes D., Thomas A. L., " *Pulse Width Modulation for Power Converters – Principles and practice*", IEEE Press Series on Power Engineering, ISBN: 0-471-20814-0

[34] Po-Tai Cheng, S. Bhattacharya, and D. Divan, "*Operations of thedominant harmonic active filter (DHAF) under realistic utilityconditions*", IEEE Transactions on Industry Applications, Vol. 37, Issue4, pp.1037-1044, July/Aug. 2001.

[35] Hirofumi Akagi, Edson Hirokazu Watanabe, Mauricio Aredes "*Instantaneous Power Theory and Applications to Power Conditioning*". Wiley IEEE Press, 2007.

[36] M. Kazmierkowski, L. Malesani, "Current Control Techniques for Three – Phase Voltage – Source PWM Converters: A Survey". IEEE Transactions on Industrial Electronics, Vol. 45, Nr 5, October 1998, pp. 691 – 703.

[37] K. Jalili, N. Weitendorf, S. Bernet, "*Behavior of PWM Active Front Ends in the Presence of Parallel Thyristor Converters*", IEEE Trans. on Industrial Electronics, vol. 5, issue. 3, pp.1035-1046, March 2008.

[38] J. Mazumdar, R. Harley, F. Lambert, G.K. Venayagamoorthy and M.L. Page, "*Intelligent Tool for Determining the True Harmonic Current Contribution of a Customer in a Power Distribution Network*," in Proceedings of the IEEE Industry Applications Society Annual Meeting (IAS 2006), vol. 2, pp. 664-671, Tampa, Florida, Oct 8-12, 2006.

[39] I. Zeltser and S. Ben-Yaakov, “*Modeling, analysis and simulation of "AC inductor" based converters*”, Power Electronics Specialists Conference 2007, PESC 2007, pp. 2128 – 2134, 17-21 June 2007.

[40] Mihai Ciobotaru, Remus Teodorescu and Frede Blaabjerg, “*Control of single-stage single-phase PV inverter*”, European Conference on Power Electronics and Applications 2005, pp. 1-10, 11-14 Sept. 2005.

[41] I. Zeltser, S. Ben-Yaakov, “*Modeling, analysis and simulation of "AC inductor" based converters*”, Power Electronics Specialists Conference 2007, PESC 2007, pp. 2128 – 2134, 17-21 June 2007. R. Nicole, “Title of paper with only first word capitalized,” J. Name Stand. Abbrev., in press.

[42] G.Karady, S. Saksena, B.g Shi, N. Senroy, “*Effect of Voltage Sags on Loads in a Distribution System*”, Power System Engineering Research Center, October 2005.

[43] J. G. Nielsen, F. Blaabjerg, “*A detailed comparison of system topologies for dynamic voltage restorers*”, IEEE Trans. Ind. Appl. , vol. 41, no. 5, pp. 1272-1280, Sep./Oct. 2005.

[44] Applications: a survey, *IEEE Trans. on Power Delivery*, vol. 17, pp. 668-673.IEC 61803, Amendment 1, “*Adjustable Speed Electric Power Drive Systems*”, part 3, 11-2011, 2.0 Edition

[45] CEI EN 61800-3, “*Adjustable speed electrical power drive systems*”, PART 3, EMC product standard including specific test methods

Publications

[1] Di Napoli A., Ndokaj A., “*EMC and Safety in vehicle drives*”, Proceeding of the IEEE 2011-14th European Conference on Power Electronics and Applications (EPE 2011), pp. 1-8, Aug.30-Sept.1 2011, Birmingham, UK.

[2] Ndokaj A., Di Napoli A., “*LED Power supply and EMC compliance*”, 2012 IEEE International Energy Conference and Exhibition (ENERGYCON), pp. 254-258, 9-12 Sept. 2012, Florence, IT.

[3] Di Napoli A., Ndokaj A., “*Ultracapacitor storage for a 50t capacity gantry crane*”, 2012 XXth IEEE International Conference on Electrical Machines (ICEM), pp. 2014-2018, 2-5 Sept. 2012, Marseille, FR.

[4] Di Napoli A., Ndokaj A., “*Auxiliary Power Buffer based on Ultracapacitors*”, 2012 IEEE International Symposium on Power Electronics, Electrical Drive, Automation and Motion (SPEEDAM), pp. 759-763, 20-22 June 2012, Sorrento, IT.

[5] Ndokaj A., Di Napoli A., “*Converter Simultaneously as Active Front End and as Active Filter*”, 2013 IEEE International Conference on Clean Electrical Power (ICCEP), pp. 552-556, 11-13 June 2013, Alghero, IT.

[6] Ndokaj A., Di Napoli A., “*Regulation Strategy of an Ultracapacitor Storage Model for a Gantry Crane*”, 2013-39th Annual Conference of the IEEE Industrial Electronics Society (IECON 2013), pp. 1209-12016, 10-13 Nov. 2013, Vienna, AT.

Accepted Publications:

[1] Ndokaj A., Di Napoli A., “*Behavior of an Active Front End in presece of Voltage Sags*”, 2014 IEEE International Symposium on Power Electronics, Electrical Drive, Automation and Motion (SPEEDAM), 18-20 June 2014, Ischia, IT.

[2] Ndokaj A., Di Napoli A.,”*Active Front End in Presence of Voltage Notches*”, XXIth IEEE International Conference on Electrical Machines (ICEM), 2-5 Sept. 2014, Berlin, DE.